Author/s:
Timbal, B;Fiddes, S;Brown, JR

Title:
Understanding south-east Australian rainfall projection uncertainties: the influence of patterns of projected tropical warming

Date:
2017-08-01

Citation:
Timbal, B., Fiddes, S. & Brown, J. R. (2017). Understanding south-east Australian rainfall projection uncertainties: the influence of patterns of projected tropical warming. International Journal of Climatology, 37 (S1), pp.921-939. https://doi.org/10.1002/joc.5047.

Persistent Link:
https://hdl.handle.net/11343/292789

Understanding South-east Australian rainfall projection uncertainties: the influence of patterns of projected tropical warming

Short title: **Understanding South-east Australian rainfall projection uncertainties**

B. Timbal[1], S. Fiddes[1 2] and J.R. Brown[1]

[1]: Research and Development Branch, Bureau of Meteorology, Australia

[2]: Australian-German Climate and Energy College and ARC Centre of Excellence for Climate System Science, School of Earth Sciences, University of Melbourne, Australia

Date: 28/11/2016

Key words: South-Eastern Australia; rainfall; future projections; uncertainties; tropical warming; teleconnections

Corresponding author: Bertrand Timbal, b.timbal@bom.gov.au

Phone: +61-3-9669-4697

Fax: +61-3-9669-4660

Abstract

South-Eastern Australia and, in particular the State of Victoria, has experienced record deficits of rainfall over the last 20 years, in which the cool part of the year from April to October has been most affected. This situation has created difficulties for water managers, farmers and fire services, with the need to provide more certainty about future climate trends becoming clear. The latest climate projections for South-East Australia project an overall drying in the cool part of the year with little change in the rest of the year. Although this is in line with current trends, very large uncertainties are associated with these projections. In this study, this range of projections has been investigated, first by assessing how the current suite of climate models simulate the regional rainfall as well as the tropical variability, known to be a key driver of south-eastern Australian climate. The models were found to be reasonable overall, although a number overestimate Victorian summer rainfall. Model rainfall projections are found to be related to the models' projected patterns of tropical warming, where 60% of the range in cool season rainfall projections can be explained by the range of pattern of tropical changes. In addition, the projected drying tends to be more intense in the models best able to simulate summer rainfall, thus suggesting that the upper end of the uncertainty range is less likely to be realised as it may reflect inherent model biases, rather than physical changes.

1. Introduction

South-Eastern Australia (SEA), including the state of Victoria, has experienced challenging climate variability in the last 20 years (CSIRO and BoM, 2012). This has had severe implications from water management to agriculture and natural environment agencies (Leblanc et al., 2012). Chief amongst this variability was an extended period of below average rainfall from 1997 to 2009, termed the Millennium drought. That 13-year period was by far the worst protracted drought of this duration in the instrumental record, even when that record is extended as far back as 1865 (Timbal and Fawcett, 2013). Its magnitude in comparison with previous historical low rainfall periods is even more remarkable when smaller areas with significant orography and high rainfall, generating important streamflows, are considered − such as the catchments areas to the east of the capital (and largest population centre) of Victoria, Melbourne (Timbal et al., 2015a). Soon after the Millennium drought, Australia experienced its wettest two years on record (Bureau of Meteorology, 2012) driven by a very strong La Niña in 2010 followed by a second in 2011, with additional contributions from the Indian Ocean and the Southern Annular Mode (SAM) (Lim and Hendon, 2015).

On one hand, tropical expansion due to ongoing global warming (Nguyen et al., 2015) and associated increases in the intensity of the sub-tropical ridge have been shown to partially explain the trend towards reduced rainfall during the cool part of the year (from April to October) as shown by Timbal and Drosdowsky (2013). On the other hand, naturally occurring modes of variability within the Tropics are well known to influence SEA rainfall. Many studies have reported and quantified how the Pacific Ocean El Niño Southern Oscillation (ENSO), jointly with the Indian Ocean Dipole (IOD), affects SEA and Victorian rainfall (CSIRO and BoM, 2012; and CSIRO and BoM, 2015, and reference within). Furthermore, tropical modes of variability and tropical expansion are probably related.

Combining the tropical influences of the Pacific and Indian Oceans, Timbal and Hendon (2011) developed a "Tripole index" to maximise the amount of SEA rainfall inter-annual variability captured by a simple Sea Surface Temperature (SST)-based index. Using this index, it was shown that the tropical modes of variability did not explain the rainfall reduction for the duration of the Millennium drought, although they helped contribute to the worsening of the drought at the end of the period, in particular during spring (Timbal and Hendon, 2011; Nicholls, 2010 and Smith and Timbal, 2012). On the contrary, the 2010-12 rainfall was strongly driven by tropical modes of variability, mainly occurring during the warm season. The influence of the tropics on SEA and Victoria rainfall is important for streamflows across the State: annual composite of streamflows based on the Tripole index show a sizeable difference between positive and negative years (Timbal et al., 2015a; Fiddes and Timbal, 2016).

Understanding how this mix of naturally occurring variability and human induced changes will evolve in the future is therefore particularly important to water managers. The most recent set of global climate change projections were assembled by the Climate Model Intercomparison Project Phase 5 (CMIP5; Taylor et al., 2012) in support of the 5th Assessment Report (AR5) of the Intergovernmental Panel on Climate Change (IPCC, 2013). This model dataset underpinned the latest set of national climate change projections generated by the CSIRO and the Bureau of Meteorology for the Australian continent (CSIRO and BoM, 2015).

Across SEA, the CMIP5 ensemble mean shows a mean rainfall reduction during the cool season and little change during the warm season for all RCPs by the end of the 21st century. The projections show varying magnitudes of rainfall decline during the cool season north of the Great Dividing range (Timbal et al., 2015b), south of the range (Gross et al., 2015b) and on the eastern seaboard of Australia (Dowdy et al., 2015). However, the full range of climate models indicated a wide range of possible outcomes and the reasons for this spread are not well understood.

A recent analysis (Grose et al., 2015a) focussed on future projections of the belt of high pressure controlling SEA rainfall: the sub-tropical ridge (STR), considering either its intensity (STR-I) or position (STR-P). That study was not able to relate the range of projections in rainfall to the

range of projections in changes in the STR but did show that the mean tendency toward a drier future during the cool season was primarily driven by the intensification of the sub-tropical ridge. It also suggested that since the models are not capturing the strength of the STR-rainfall relationship as observed, it is plausible that the current suite of CMIP5 models underestimate the mean future rainfall decline as they do for the historical period (Timbal et al., 2010; Nguyen et al., 2015).

Another candidate to drive SEA rainfall change is the model's projected warming in the tropics, in particular in areas which are known to influence SEA: e.g. the Western-Central Pacific and Eastern Indian Ocean. This was shown to be an important factor amongst the previous generation of climate model projections using a dipole pattern between the Indian and Pacific Oceans (Watterson, 2012), following a study which demonstrated that these two areas were important in controlling SEA rainfall in a climate model (Watterson, 2010).

In this study, we use the Tripole index of Timbal and Hendon (2011) to quantify the relationship between observed tropical SST and SEA rainfall to help explain the range of rainfall projections in the CMIP5 models. To do so, firstly we analyse the model's ability to capture the strength of the observed relationship between the Tripole index and SEA rainfall and secondly, relate the spread of tropical patterns of warming to the spread of rainfall projections across SEA. This analysis can help provide insight into the uncertainty range and help explain where these uncertainties initiate. Developing a better understanding of this teleconnection between SEA rainfall and tropical SST is also important in light of the observed multi-decadal SST variability in the last 30 years which has been linked to regional tropical expansion (Hope et al., 2015) and the global warming slowdown (England et al., 2013).

2. Data and methods

We analyse rainfall variations using the Australian Bureau of Meteorology's current operational high-resolution monthly rainfall data set, generated as part of the Australian Water

Availability Project (AWAP) (Jones et al., 2009). These analyses are at 0.05°×0.05° resolution, or approximately 5 km × 5 km. SEA rainfall is defined as the average rainfall over the main continent south of 33.5°S and east of 135.5°E (the area outlined by the grey box in the top panel of Figure 1, and shown in the bottom panel, Figure 1).

Several global SST datasets exist and Timbal and Hendon (2011) showed that when diagnosing trends over the last 30 to 40 years for the Tripole index described in their study, there is a sizeable variation depending on which dataset used. In the present study, we use the Hadley Centre/UK Meteorological Office SST (HadISST) analyses from 1870 to 2014 interpolated on a 1° by 1° grid (Rayner et al., 2003). The data was further regridded on a 1.5° by 1.5° grid as required to compare with the interpolated CMIP5 model data. The extra-tropical tele-connectivity with SEA rainfall is evaluated using the method developed by Timbal and Hendon (2011). They developed a 'tri-polar' index (Tripole) by examining the spatial distribution of the correlation of tropical SST with the time series of rainfall in SEA and observed three regions of significant correlation (in excess of ±0.2); these regions define the Tripole index. The Tripole is computed as the difference between the mean SST north of Australia (extending from the eastern Indian Ocean and across the Maritime Continent) minus the average of the SST over the central-western Indian Ocean and the central Pacific Ocean. The box boundaries are shown on Figure 1 and their coordinates are provided in Timbal and Hendon (2011). These three boxes cover most of the warm tropical SSTs (above 28°C) in the two oceanic basin influencing Australia and the index has some similarities with the Pacific–Indian Ocean dipole used in Watterson (2012)

The CMIP5 simulations provide a representation of the current climate from 1900 to 2005 using observed external forcings either anthropogenic or natural and plausible representation of the future climate based upon four Representative Concentration Pathways (RCPs) that prescribe anthropogenic greenhouse gas concentration time series which correspond to approximate end-of-century radiative forcing, from low to high of +2.6, +4.5, +6.0, and +8.5 W/m^2. RCP8.5 represents a high future emission pathway and as such produces a large warming response. It is therefore

convenient to use this RCP because the climate change signal is larger than when compared to RCPs with stronger mitigation (for example RCP2.6). To the extent that the projection signal is linear in forcing, using a higher emission scenario can increase the signal to noise in the projection relationships. Indeed, climate change projections generated for the Australian continent using the CMIP5 database (CSIRO and BoM, 2015) show that in general the climate change signal is proportional to the amount of global warming generated including SEA.

In this study we used historical climate simulations, testing each model's ability to replicate the observed climate, as well as one simulation per model of the projected climate change under RCP8.5. In total, an ensemble of 37 models were analysed out of the 48 models entered in the CMIP5 dataset due to limitations on data availability and suitability (Table 1). SEA area-averaged rainfall totals and the Tripole index were computed for each model. Monthly values were computed from 1900 to 2005 (historical climate simulations) and from 2006 to 2100 under RCP8.5. We used the largest set of simulations for which all the required data were available (NB: when several simulations were logged by modelling groups, only one was used: "run 1").

In the set of national projections delivered by CSIRO and BoM (2015), rainfall projections based on RCP8.5 use 39 models (Table 3.3.2 in CSIRO and BoM, 2015). Therefore, the present study targets a very large sample (37 out of 39 models) of the uncertainties attached to the CMIP5-based projections for rainfall (shown in Figure 12). The models used and key characteristics such as horizontal resolution are summarised in Table 1. Model data were first interpolated on a common 1.5 by 1.5 degree grid, SEA rainfall and Tripole time series were computed month by month using all the grid boxes with centres falling within the region of interest shown in Figure 1. It is worth noting that for SEA rainfall only grid boxes covering the State of Victoria are included, which is a smaller domain than the SEA box. It was noted as part of the validation of the models that the ensemble mean rainfall was biased toward too low rainfall during the wet (cool season) part of the year. This is very likely due to the difficulty of simulating rainfall over the orography of the Great Dividing Range with relatively coarse model resolution, rather than being due to model systematic biases as this is also noted for other high rainfall areas across southern Australia which also have significant orography

(South West of Western Australia, southern part of South Australia and Tasmania). Hence the SEA rainfall was better captured using model grid boxes limited to those covering the State of Victoria where rainfall is higher than further north providing a better match with observations and thus removing a key biases across most climate models.

We first report on the CMIP5 models' ability to reproduce SEA rainfall, its variability and how it relates to tropical modes of variability as captured by the Tripole index. Previous studies have already evaluated the performance of these models; in Table 1, some key evaluation metrics from previous studies relevant to this particular study are indicated (NB: 3 models considered in this study were uploaded to the CMIP5 database later than the others and hence are not included in these previous studies: CESM1-CAM5-1-FV2, FGOALS-s2 and MRI-ESM1).

Three of these metrics are based on the skill score developed by Watterson (1996) called the M-statistic. The M-statistic is a function of temperature, rainfall, and mean sea level pressure and scores are shown here for the entire Australian continent, and southern Australia (See Table 5.2.2 in CSIRO and BoM, 2015). Also shown is the M-statistic for rainfall only across Australia (See Table 5.2.4 in CSIRO and BoM, 2015). In Table 1, good performances are indicated by bold blue figures (above 690 for the M-statistics across Australia, and 540 for Southern Australia and 560 for precipitation across Australia) and poor performance by bold red figures (respectively below 600, 460 and 440). As part of the complete model evaluation performed to deliver Australia-wide projections (CSIRO and BoM, 2015), several other evaluation tests were utilized. A summary of the number of tests for which individual models performed poorly (See Table 5.6.1 in CSIRO and BoM, 2014) is also provided for the models selected in this study. Models that did not fail any test are shown in bold blue while models that failed three tests or more are shown in bold red.

Besides examining the influence of tropical SSTs on SEA rainfall as a way to interpret the range of uncertainties in rainfall projections, we are also interested in the global model warming response. This is captured by providing the linear global mean warming for each model under the RCP 8.5 scenario (last column in Table 1 in degrees Celsius multiply by 100 years). In most instances

211 across the Australian climate change projections generated from the CMIP5 data base, it was found
212 that the strength of the climate change signal for any variable, but in particular rainfall, is proportional
213 to the amount of global warming (See section 6.2.3 in CSIRO and BoM 2015; Watterson and Whetton
214 (2011 and 2013)) and is commonly used to compare signals between various emissions scenarios and
215 for different time-slices in the future. Here we will use it to evaluate if the range of SEA rainfall
216 projections is linked to the range of warming trends over the century projected by individual models.

217 Another relevant metric of model performance is the model's ability to reproduce the position
218 of the STR across Eastern Australia which has a well-established annual cycle (Drosdowsky, 2005)
219 and relationship with SEA rainfall (Timbal and Drosdowsky, 2013). This was evaluated by Grose et
220 al., (2015b); using their results we classified the CMIP5 models here into three categories: 1) the
221 model was able to capture the signature of the regional STR in the same longitudinal band as the
222 reanalysis (shown in blue, Table 1), or 2) within an overlapping band no wider than 30 degree or 3) a
223 longitude band which did not overlap the reanalyses band or was larger than 30 degree (shown in red,
224 Table 1).

225 The various evaluations considered in Table 1 show that of the 37 models, quite a spread in
226 performance exists. Only one model is amongst the better performer for all the statistics considered
227 (CNRM-CM5), but many are for several criteria; in total 17 models are amongst the better models for
228 at least one statistic and never amongst the poorest performer for any statistics. Amongst poor
229 performers, only one model is amongst the poorest performer for all statistics (MIROC-ESM-CHEM)
230 but many are for several criteria. In total 12 models are amongst the poorest group for at least one
231 statistic and never amongst the better performers for any statistics. Overall, based on past studies there
232 is a group of 17 models which are "better" performers 12 models which are "poorer" performers and 8
233 models in between. However, this evaluation, while relevant, is preliminary and needs to be
234 confirmed by looking at these models' ability to reproduce specifically SEA rainfall, its variability
235 and how it relates to tropical modes of variability as captured by the Tripole index. An updated
236 classification of models, based on this wider set of criteria, is provided in the next Section.

3. Results:

3.1 Validation of the current climate simulations

3.1.1 South-Eastern Australia Rainfall

Model simulation of SEA rainfall is analysed by looking at the mean, variability and trends as well as the relationship between the SEA rainfall and the Tripole index amongst the 37 CMIP5 models available. The model ensemble mean computed using the grid boxes within the State of Victoria is compared to both observed rainfall for Victoria (dashed line) and for the entire SEA box (full line in Figure 2). Climate averages are computed for the 1900 to 2005 period for every month. Due to a general dry bias inherent to coarse climate model resolution, the modelled rainfall for the grid boxes contained within the boundary of the State of Victoria is the best proxy for SEA rainfall and is used for the rest of the study. This full ensemble mean is within 3 mm of the observed SEA rainfall during the cool season from April to October. However, it has a relatively flat annual cycle with December and January rainfall being too high. The models are ranked according to the Euclidean distance between the individual model annual cycle and the observations, the models with the 10 smallest (largest) Euclidean distances are classified as best (worst) (see Table 2 for full results). The ensemble mean of the “best” 10 models for this metric is very close to the observed rainfall for the entire year. The ensemble mean of the 10 “worst” models is generally too wet throughout the year, but the largest bias is observed during the warm months (November to March). This contributes to the wet bias in summer observed in the full ensemble mean.

The overestimation of summer rainfall mean also impacts the computation of the standard deviation (Figure 2, lower panel). As per the mean, this affects only some of the CMIP5 models; the ensemble mean of the "best" 10 models is close to the observations. The summertime rainfall overestimation amongst some models appears to be the most significant discrepancy in the CMIP5 models’ ability to capture the SEA rainfall. Models which have largest mean summer rainfall have also largest standard deviation for summer rainfall, which is expected (Figure 3, upper panel).

However, once the coefficients of variation are used (i.e. standard deviations normalised by the mean), a strong opposite linear relationship emerges (Figure 3, lower panel). This suggests that generally, models with high summer rainfall tend to have comparatively lower year-to-year variability implying more consistent summer rainfall.

In particular 15 models (green symbols in Figure 3) were identified as being too wet in summer, with a number having a reversed annual cycle (e.g. a summer peak for rainfall). These 15 models are: CCSM4, CESM1-BGC, CESM1-CAM5, CESM1-CAM5-1-FV2, CNRM-CM5, GISS-E2-H, GISS-E2-H-CC, GISS-E2-R, GISS-E2-R-CC, inmcm4, MIROC5, MIROC-ESM, MIROC-ESM-CHEM, NorESM1-M and NorESM1-ME. From a global perspective, these models tend to have too strong Inter-Tropical Convergence Zone (ITCZ) with excess rainfall and have a notably weak or absent South Pacific Convergence Zone (SPCZ) and a strong dry bias across the Indonesian archipelago (Figure 4). While both groups of models simulate too much rainfall across Australia in summer, the errors are larger and affect the entire continent, in the group of models identified as having a too wet (south-east) summer. Thus, the very wet SEA summer simulated by this group of models does not appear to be a local error but rather a large-scale problem linked to the way that tropical precipitation is represented in these models. This casts doubt on the ability of this group of models to capture the relationship between SEA rainfall and tropical SST variability, which is being investigated. We will therefore aim to quantify the impact of including these models in the ensemble mean.

Finally, linear trends were computed for each CMIP5 model for the last 30 years from 1985 to 2014 (including the end of the historical simulation of the current climate, which ends in 2005 and the start of the RCP8.5 future emission scenario from 2006). During this period, observed SEA rainfall has experienced a marked reduction during the cool season (from April to October) with serious hydro-climatic consequences (CSIRO and BoM, 2012). This cool season decline is counteracted somewhat by a small warm season increase, resulting in a negligible annual decline (Figure 5). Individual climate models simulate monthly rainfall trends that are at times as large as observed, but

292 are highly variable from one month to the next with very little consistent behaviour. Indeed, the
293 ensemble mean indicates no systematic 30-year trends of either dry or wet throughout the year. Even
294 the 10 “best” models, which best match the observed annual cycle have little trend. Only one model
295 (IPSL-CM5B-LR) has a negative rainfall trend, which is of similar magnitude to the observed
296 (indicated in Figure 5).
297
298 **3.1.2 Tropical Tripole index**
299 Moving to the evaluation of the CMIP5 models’ performances in the tropics that are of
300 relevance to SEA rainfall, the mean Tripole index has a clear annual cycle with negative values from
301 May to October and positive values during the warm season (Figure 6, upper panel). The CMIP5
302 models largely reproduce the annual cycle but with a general bias leading to more positive values (i.e.
303 warmer central box SSTs) from December to August. This tendency is seen across nearly all CMIP5
304 models including when the “best” models for that metric are considered. More importantly, since the
305 Tripole has been constructed to capture inter-annual variability in the tropics, the annual cycle of the
306 standard deviation computed from 1900 to 2005 (Figure 6, lower panel) is of great interest. In the
307 observations, the largest variability is seen in late winter and spring (July to November). Whilst the
308 CMIP5 models give a range of annual cycles, the ensemble mean mimics the observed one well,
309 although with somewhat too large variability in summer. There are a number of models which have
310 too much variability all year around, as can be seen from the ensemble mean of the 10 “worst”
311 models.
312
313 In the last 30 years, there has been a large annual mean warming trend across the Indian
314 Ocean, the Maritime Continent and Western Pacific, with opposite cooling in the Central and Eastern
315 Pacific (Figure 1). As per rainfall, linear trends in the Tripole index from 1985 to 2014 were
316 computed for both observations and the CMIP5 models (Figure 7). These Tripole trends are not very
317 large (due to the two negative poles having opposite trends: cooling in the Central Pacific box and
318 warming in the Indian Ocean box against a warming trend in the Maritime Continent box). The annual

cycle of the observed trend shows a small increase in most months apart from June and August. In contrast to the observations, the ensemble mean of CMIP5 models shows a consistent cooling trend for all months in the vicinity of -0.05°C for the 1985-2014 period. There is considerable range across the 37 models considered (grey lines in Figure 7); within that range it is possible to identify 10 models (their mean is labelled "best" models in Figure 7) that have very similar trends to the observed.

3.1.3 Tripole-rainfall relationship

Having evaluated the tropical SST variability and SEA rainfall separately, the ability of the models to capture the observed relationship between the two is now evaluated, as well as the role this relationship might play in explaining the range of behaviour displayed by the CMIP5 models. Overall, the CMIP5 models ability to simulate this tropical-extratropical teleconnection is convincing (Figure 8). Although the largest observed correlation coefficients in July to November (around 0.4) are underestimated by the ensemble mean (around 0.3), the annual cycle and the peak in late winter-spring is well captured. The ensemble mean of the “best” 10 models is similar to the observations. One aspect of the Tripole-SEA rainfall relationship is its fluctuations on decadal times-scales. This was shown by Timbal and Hendon (2012) and arises from well-known decadal variability such as the Inter-decadal Pacific Oscillation (IPO) and its impact on Australian rainfall (Power et al., 1999). Computing the correlation coefficients for the July to November averaged SEA rainfall and Tripole in 50 years periods (Figure 9) shows a marked difference between 1900-1949 (0.50) and 1956-2005 (0.65). These differences are even larger when annual values are considered (0.33 and 0.66, not shown). Some individual CMIP5 models do reproduce differences between 50 year periods of similar magnitude either positive or negative (individual models in Figure 9), but as far as the ensemble mean is concerned, there is no indication of a systematic shift either in the past century for the last 50 years or the two 50-year periods of the 21st century under RCP8.5 pathways. Thus it appears that shifts in the strength of the relationship between tropical variability and SEA rainfall are possible due to internally generated decadal variability (reproducible by climate models) as occurred in the 20th century and are also possible in the future (i.e. individual models do have changes of this magnitude

346 between future 50 year periods). But based on these results, any such shift towards a reduction or an
347 increase in the strength of the relationship during the 21st century cannot be ascribed to anthropogenic
348 forcing as there is no indication of such a change in the ensemble mean.
349
350 Since the CMIP5 models (or at least a subset thereof) appear to have a realistic relationship
351 between tropical SSTs and SEA rainfall, it is worth investigating if some of the observed differences
352 amongst model climatologies in SEA rainfall may be related to how the models behave in the tropics.
353 Moderate (around 0.5) and significant (99% level) relationships were found between the magnitude of
354 year-to-year variability in July to November of both rainfall and the Tripole. This was measured using
355 standard deviation of the two quantities computed for each individual model for the period 1956 to
356 2005 (Figure 10, top panel, r=0.50). The strength of the relationship varies if different months are
357 considered (Table 3). That relationship is moderate in spring, for the July to November and the cool
358 season (April to October) period, but is non-existent for the summer months, thus giving only a weak
359 relationship for the annual means (Table 3).
360
361 As a way to investigate the cause of model SEA rainfall variability, the relationship between
362 the model scatter of SEA rainfall variability and the strength of the SEA rainfall-Tripole correlation in
363 models was investigated. The relationship was found to be strong over the 1956-2005 period (Figure
364 10, bottom panel, R=0.60) accounting for more than a third of the range of rainfall inter-annual
365 variability in the July to November period indicating that climate models' ability to capture the
366 observed inter-annual variability in SEA rainfall is driven by the strength of the teleconnections
367 between the tropics and SEA within each model. The figure shows that some models are clear outliers
368 (these are the four models from the NASA/GISS research centre in the U.S.A.); without these models
369 the relationship increases to R=0.77 explaining 60% of the range. The same seasonality is observed
370 as per the previous relationship: strongest relationship in spring or July-November, also strong in
371 April to October and non-existent in summer, limiting the strength of the relationship for the annual
372 means.
373

In the case of SEA rainfall trends, a weaker and less significant relationship is found amongst the model scatter between SEA rainfall trends and Tripole trends across the CMIP5 models over the 1985-2014 period. Although this period is when most of the cool season rainfall decline has been observed (Table 3), the relationship is stronger when the full historical simulations are considered. The strongest relationship is observed in the cool season April to October (R=0.58), explaining about a third of the range of rainfall trends amongst models. This result indicates that, as expected from the inter-annual relationship, models that exhibit a trend in tropical SST, which project positively (negatively) on the Tripole tend to deliver a positive (negative) rainfall trend in SEA. However, it is worth remembering that these trends are small in comparison to the observed one (see earlier section and Figures 4 and 6).

3.2 Analysis of the future climate simulations

We now turn to investigate whether the SEA rainfall-Tripole relationship can help to better understand the range of future projections of SEA rainfall generated by the CMIP5 models. The first part of this investigation considers the projected changes in tropical SSTs generated by the CMIP5 models. The CMIP5 multi-model mean tends to display global warming with the strongest tropical warming located in the Eastern Equatorial Pacific. However, projected changes in the Tripole index are small (Figure 11). There is, however, a large range of responses across the models, with some displaying trends as large as 1 °C for particular months, either positive or negative. This is shown in particular in the key part of the annual cycle most strongly relating to SEA rainfall, April to October. Many of the models indicating large positive trends in the Tripole index are amongst the group of models with very wet summer identified earlier, leading to the ensemble mean of these models indicating a small positive trend for the Tripole index, especially for the months from April to November. Excluding these models (to produce the ensemble mean labelled “other models” in Figure 11) leads to a larger negative trend for the Tripole index for that critical part of the year (April to November). Beside the differences in trends in the Tripole index annual cycle, it is noteworthy that

overall the ensemble of models with very wet summer have less warming in the Tripole index than the "other" group for which the tropical warming is stronger in the Eastern Pacific. In addition, at high latitudes in the Southern Hemisphere where the warming is less than further equatorward, it is weaker in the "other" group of models. Therefore the "other" group have a warming pattern that will cause a greater increase of the climatological SST gradient between equator and pole in the Southern Hemisphere.

The ensemble mean SEA rainfall projections show a drying trend from May to November and a small positive trend during the warm season (Figure 12, top panel). It bears some resemblance to the observed trends over the last 30 years (shown in Figure 4), with the difference that the projected future rainfall decreases are greatest in austral spring (SON) while the observed cool season decline is greatest in austral autumn (MAM). That seasonality of the future projections is depicted further for SEA as well as sub-regions within that box (lower panels in Figure 12, N.B. in percentage change while the top panel is in absolute change), showing slight differences in the mean projected change south or north of the Great Dividing range across southern Victoria.

As can be seen in Figure 12, the spread of SEA rainfall projections amongst the CMIP5 models is very large. Of interest is the behaviour of the group of 15 models that simulate a very wet summer for the current climate. The "very wet model" ensemble mean displays an annual cycle of trends similar to the full ensemble mean, but on the wetter side (Figure 12: larger positive trends in the warm season and smaller negative trends in the cool season), leading to negligible trends in the annual mean (Table 4). As a result the ensemble mean of the "other models" projects stronger rainfall declines all year round (Figure 12). The difference from the full ensemble mean leads to a mean signal in excess of 50% greater reduction in rainfall across the entire cool season and spring (Table 4). The difference in the rainfall projections between these two groups of models is not limited to the SEA. A global perspective (Figure 13) shows sizeable differences in projected rainfall changes by the end of the 21st century compared to the end of the 20th century including a very large rainfall increase in the ITCZ in the "other models" group, larger than for the "very wet summer" group. This difference exists in both

austral summer (DJF) and winter (JJA), but in winter it is coupled with a reduction of rainfall in the sub-tropical band of the Southern Hemisphere and in particular across the Australian continent including SEA. In the "other models" group, that reduction is much larger than the "very wet summer" group, leading to the sizeable differences in ensemble mean reported in Table 4.

There is a general expectation that the projected rainfall decline in the cool season is proportional to the emission pathways used to force the models and the subsequent global warming projected for each pathway (CSIRO and BoM, 2015). We do find evidence of this in the magnitude of the projected rainfall decline for SEA and sub-regions in Victoria, as the magnitude of the austral winter and spring decline increases with the severity of the emission pathways (bottom panel in Figure 12 from RCP 2.6 to RCP 8.5). However, there is only a weak relationship amongst the 37 CMIP5 models considered here between global warming and SEA rainfall changes (R=-0.34, significant at the 95% level). The two quantities used are a proxy for the sensitivity of the models, expressed as the amount of global warming simulated during the 21st century under the RCP 8.5 pathways, and the magnitude of the rainfall decline (in the cool season). The relationship is non-existent for austral summer and non-significant for the annual mean (Table 5).

The scatter in projected rainfall trends amongst models was evaluated further by relating it to the Tripole trends projected by the same model (Figure 14 and Table 5). A very strong and highly significant relationship was found for the annual mean (R=0.65). The correlations are higher for the critical time of the year where the relationship is known to peak (July to November) reaching R=0.75, and equally very high for the key season in term of SEA rainfall (April to October). In contrast, the relationship is almost non-existent in austral summer (DJF: R=0.23). With such a small sample, correlation coefficients can be affected by a single case. In Figure 14 for both July to November and Austral summer a single model is a clear outlier (CSIRO-mk3.6). Without this model, the picture is even clearer, with a stronger relationship in the cool season and July to November and a correlation below 0.1 in summer (Table 5). It is worth noting that although the "very wet summer" models are clustered towards the more positive rainfall trend, as expected from ensemble mean results (Table 4),

457 removing them only marginally reduces the overall range of projections as both groups of models are
458 widely scattered.
459
460
461 **Discussion and conclusions**
462
463 37 CMIP5 global climate models are examined for this study. They were assessed for their
464 ability to reproduce both observed SEA rainfall and the relationship between rainfall and a tropical
465 Tripole index. The model means, inter-annual variability and trends as well as the relationship
466 between the two quantities were investigated and found to match observations sufficiently well to
467 warrant using this relationship as a tool to analyse future projections. Indeed some of the range of
468 model simulations of SEA rainfall appears to be related to the way they capture the relationship
469 between SEA rainfall and tropical SST or how the tropical SSTs behave in the climate models and in
470 turn affect the SEA rainfall.
471
472 In terms of model assessment and the ability to identify a group of better performing models, all the
473 metrics evaluated were measured between individual models and observations using Euclidean
474 distance across the annual cycle. A group of ten models emerged that were never amongst the worst
475 performers for any statistics. Of these ten, nine were already identified from earlier studies (CSIRO
476 and BoM, 2015) amongst the 17 better performers: ACCESS1.0, CESM1-CAM5, CMCC-CM, CMC-
477 CMS, FGOAL-g2, HadGem2-CC, MPI-ESM-LR, MPI-ESM-MR and MRI-GCM3. At the other end
478 of the spectrum, seven models are amongst the worst performers for at least one statistic and never
479 amongst the better one for any statistics. Amongst these seven models, five were also identified from
480 previous studies (CSIRO and BoM 2015) as being amongst the poorest performers: CAN-ESM2,
481 GISS-E2-H, GISS-E2-H-CC, GISS-E2-R and NorESM1-ME. Outside these two groups, most model
482 performances vary across the range of metrics considered, underlining the difficulties in model
483 ranking.

A group of models was identified as having a very wet summer, with low relative inter-annual variability and in most cases a reversal of the annual cycle with more rain in the warm rather than cool season. These 15 “very wet summer” models are consistent with the other evaluation metrics: i.e. the entire group of seven worst performers was included in that group, and only one from the group of ten better performers was included (CNRM-CM5). Overall, the contrast between the two groups of models is significant in terms of the various metrics considered: while the “very wet summer” group has metrics in the bottom 10 performances 50% of the time, with 32% in the average and 18% in the top performances, the “other” group has 11% of metrics in the bottom 10 performances, with 56% in the average and 33% in the top performances.

It was noted that representing the spatial maximum in rainfall at the very southern edge of the Australian continent (SEA in particular) does pose a challenge to coarse resolution climate models as the higher rainfall in SEA compared to further inland is due to the interaction between moisture fluxes and coastal and orographic features. This was dealt with by using only a limited number of grid box from models (those covering Victoria) to represent the entire SEA. However, that overall limitation, due to resolution, does not explain how models could get more rainfall than observed as it is unlikely to be due to model resolution (Figure 2 shows that Victoria rainfall is not higher than SEA rainfall in summer) thus casting doubt on these models with very wet summers. We speculate that the source of the excess summer rainfall in these models is overly frequent tropical moisture inflow across the continent but further examination of the mechanisms operating in these models is beyond the scope of the current study.

There is a general expectation that the projected rainfall decline in the cool season increases with emissions and warming. We do find evidence of this in the magnitude of the projected rainfall decline for SEA region and sub-regions within Victoria. However the model temperature sensitivity to emissions does not appear to relate significantly to the strength of the projected rainfall response.

In contrast, the relationship between the projected rainfall decline and the pattern of tropical warming are related. We find that up to 60% of the range in SEA cool season rainfall projections is explained in terms of how the individual model's tropical warming projects on the Tripole. Therefore, this Tripole index is a relevant tool to monitor future SST warming in the near future, and in future projection work and how it may impact on future SEA rainfall trends. The spatial pattern of SST warming in the tropical Pacific was also found to be an important influence on northern Australian rainfall projections (Brown et al., 2016). It confirms the importance of patterns of tropical warming in driving range of rainfall projections across Australia from climate models as was noted by Watterson (2012) for the CMIP3 generation of models. Furthermore, it is worth noting that this approach of mapping range of future projections on established modes of variability for a particular regional climate is also likely to provide useful insights for other parts of the world.

It was also noted that while the observed teleconnection between tropical modes of variability and SEA rainfall has marked multi-decadal variability during the 20th century, similar multi-decadal variability exist and are internally generated by models. However, the ensemble mean shows a stable picture for past and future centuries, suggesting no change in the magnitude of this relationship is to be expected in response to anthropogenic forcing and the observed changes in the last 100 years is not in response to external forcings. This is consistent with many studies about the influence of natural multi-decadal variability on regional rainfall (IPCC, 2013).

Finally, it appears that the current range of model projections is influenced by a group of models which were found to have a poorer simulation of the rainfall annual cycle in SEA with very wet summers. These models also performed notably worse on a range of metrics considered in this study and previously. Excluding this group of models significantly increases the mean model rainfall decline projections (by about 50%) in Victoria and more broadly across SEA. Although based on different criteria of models evaluation, this conclusion is supported by recent findings by Grose et al. (2016). It is unclear why such a difference exists between the two groups of models - one hint comes from the pattern of future warming, which appears to have a larger temperature gradient between the

tropics and high latitudes for the "other" group of models. This is likely to impact changes in the mean meridional circulation, which have been shown to be important for SEA rainfall (Nguyen et al., 2013). While the mean signal is markedly different, the range of projections is not affected significantly by the omissions of that group of models, indicating that weaker future rainfall reductions cannot be entirely ruled out.

Acknowledgments:

We acknowledge the World Climate Research Programme's Working Group on Coupled Modelling, which is responsible for CMIP, and we thank the climate modelling groups (listed in Table 1) for producing and making available their model output. BT and SF contribution to this work was supported by the Victorian Climate Initiative (VicCI). JRB was supported by the Australian Climate Change Science Programme, jointly funded by the Department of the Environment, the Bureau of Meteorology and CSIRO. D. Jones and R. Colman (Bureau of Meteorology) provided useful comments on an earlier draft of this manuscript.

557 **References**

558

559 Brown JR, Moise AF, Colman R, Zhang H (2016) Will a warmer world mean a wetter or drier
560 Australian monsoon? J. Climate, doi:10.1175/JCLI-D-15-0695.1
561 Bureau of Meteorology (2012) Australia's wettest two-year period on record; 2010-11, Special
562 Climate Statement No. 38, National Climate Centre, Bureau of Meteorology,
563 www.bom.gov.au/climate/current/statements/scs38.pdf
564 CSIRO and Bureau of Meteorology (2012) Climate Change and water availability in south-eastern
565 Australia: A synthesis of findings from Phase 2 of the South Eastern Australian Climate
566 Initiative (SEACI), CSIRO, Australia
567 CSIRO and Bureau of Meteorology (2015) Climate Change in Australia Information for Australia's
568 Natural Resource Management Regions: Technical Report, CSIRO and Bureau of
569 Meteorology, Australia
570 Dowdy A, et al (2015) East Coast Cluster Report, Climate Change in Australia Projections for
571 Australia's Natural Resource Management Regions: Cluster Reports", eds. Ekström, M. et
572 al.,, CSIRO and Bureau of Meteorology, Australia
573 Drosdowsky W, (2005) The latitude of the subtropical ridge over eastern Australia: the L index
574 revisited. Int. J. Climatol. 25 1291-1299
575 England MH, McGregor S, Spence P, Meehl GA, Timmermann A, Cai W, Sen Gupta A, McPhaden
576 MJ, Purich A, Santoso A (2014) Recent intensification of wind-driven circulation in the
577 Pacific and the ongoing warming hiatus. Nature Climate Change, 4 222–227,
578 doi:10.1038/nclimate2106
579 Fiddes S, Timbal B (2016) Assessment and reconstruction of catchment streamflow trends and
580 variability in response to rainfall across Victoria, Australia. Clim. Res., 67, 43-60,
581 doi:10.3354/cr01355

582 Grose M, Timbal B, Wilson L, Bathols J, Kent D (2015a) The subtropical ridge in CMIP5, and
583 implications for projections of rainfall in southeast Australia. Aust. Met. & Ocean. J., 65, 90-
584 106
585 Grose M, et al (2015b) Southern Slopes Cluster Report, Climate Change in Australia Projections for
586 Australia's Natural Resource Management Regions: Cluster Reports, eds. Ekström, M. et
587 al.,,CSIRO and Bureau of Meteorology, Australia
588 Grose, M., J. Risbey, A. Moise, S. Osbrough, C. Heady, L. Wilson, and T. Erwin, 2016: Constraints
589 on southern Australian rainfall change based on atmospheric circulation in CMIP5
590 simulations. J. Climate. doi:10.1175/JCLI-D-16-0142.1, in press.
591 Hope P, Timbal B, Hendon H, Ekström M (eds.) (2015) Victorian Climate Initiative annual report
592 2014-15, Bureau Research Report, 5 128pp
593 IPCC (2013) Climate Change 2013: The Physical Science Basis. Contribution of Working Group I to
594 the Fifth Assessment Report of the Intergovernmental Panel on Climate Change. In:
595 STOCKER, T. F., D. QIN, G.-K. PLATTNER, M. TIGNOR, S. K. ALLEN, J. BOSCHUNG,
596 A. NAUELS, Y. XIA, V. BEX AND P. M. MIDGLEY (ed.)
597 Jones DA, Wang W, Fawcett R (2009) High-quality spatial climate data-sets for Australia. Aust.
598 Meteorol. Ocean. J. 58 233-248
599 Kent DM, Kirono D, Timbal B, Chiew FHS (2011) Representation of the Australian sub-tropical
600 ridge in the CMIP3 model. Int. J. of Clim., 33(1), 48-57, DOI: 10.1002/joc.3406
601 Leblanc M, Tweed S, Van Dijk A, Timbal B (2012) A review of historic and future hydrological
602 changes in the Murray-Darling Basin. Global Planetary Change, 80 226-246
603 doi:10.1016/j.gloplacha.2011.10.012
604 Lim E-P, Hendon HH (2015) Understanding and predicting the strong Southern Annular Mode and its
605 impact on the record wet east Australian spring 2010. Climate Dynamics, 44 2807-2824,
606 DOI:10.1007/s00382-014-2400-5
607 Nicholls N (2010) Local and remote causes of the southern Australian autumn−winter rainfall decline
608 1958−2007. Clim. Dyn., 34, 835–845

609 Nguyen H, Evans A, Lucas C, Smith I, Timbal B (2013) The Hadley Circulation in Reanalyses:
610 climatology, variability and expansion, J. Climate 26(10), 3357-3376
611 Nguyen H, Lucas C, Evans A, Timbal B, Hanson L (2015) Expansion of the Southern Hemisphere
612 Hadley Cell in response to greenhouse gas forcing. J. Climate 28, 8067-8077
613 Power S, Casey T, Folland C, Colman R, Mehta V (1999) Inter-decadal modulation of the impact of
614 ENSO on Australia. Clim. Dyn. 15, 319-324
615 Rayner NA, Parker DE, Horton EB, Folland CK, Alexander LV, Rowell DP, Kent EC, Kaplan A
616 (2003) Global analyses of sea surface temperature, sea ice, and night marine air temperature
617 since the late nineteenth century. J. Geophys. Res. 108 (D14), 4407,
618 DOI:10.1029/2002JD002670
619 Reynolds RW, Smith TM, Liu C, Chelton DB, Casey KS, Schlax MG (2007) Daily high-resolution
620 blended analyses for sea surface temperature. J. Climate 20, 5473-5496
621 Smith I, Timbal B (2012) Links between tropical indices and southern Australia rainfall. Int. J. of
622 Clim., 32(1), 33-40, DOI: 10.1002/joc.2251
623 Taylor KE, et al (2012) An Overview of CMIP5 and the Experiment Design. Bull. Amer. Meteor.
624 Soc., 93(4), 485-498
625 Timbal B, Arblaster J, Braganza K, Fernandez E, Hendon H, Murphy B, Raupach M, Rakich C, Smith
626 I, Whan K, Wheeler M (2010) Understanding the anthropogenic nature of the observed
627 rainfall decline across south-eastern Australia. CAWCR Technical Report 26 180pp, ISSN:
628 1835-9884
629 Timbal B, Drosdowsky W (2013) The relationship between the decline of South Eastern Australia
630 rainfall and the strengthening of the sub-tropical ridge, Int. J. of Clim., 33(4) 1021-1034,
631 DOI: 10.1002/joc.3492
632 Timbal B, Fawcett R (2013) An historical perspective on South Eastern Australia rainfall since 1865.
633 J. Climate 26(4) 1112-1129
634 Timbal B, Hendon H (2011) The role of tropical modes of variability in recent rainfall deficits across
635 the Murray-Darling basin. Water Res. Res., 47(12), W00G09. ZOI:10.1029/2010WR009834

636 Timbal B, Griffith M, Tan KS (2015a) Rainfall and streamflow in Greater Melbourne catchment
637 areas: variability and recent anomalies. Clim. Res., 63 215-232, doi:10.3354/cr01296
638 Timbal B, et al (2015b) Murray Basin Cluster Report, Climate Change in Australia Projections for
639 Australia's Natural Resource Management Regions: Cluster Reports, eds. Ekström, M. et al.,,
640 CSIRO and Bureau of Meteorology, Australia
641 Van Vuuren D P, Edmonds J, Kainuma M, Riahi K, Thomson A, Hibbard K, Hurtt GC, Kram T, Krey
642 V, Lamarque J-L (2011) The representative concentration pathways: an overview. Clim.
643 Change 109, 5-31
644 Watterson I (1996) Non-dimensional measures of climate model performance. Int. J. of Clim. 16, 379-
645 391
646 Watterson I (2010) Relationships between south-eastern Australian rainfall and sea surface
647 temperatures examined using a climate model. J. Geophys. Res. 115, D10108,
648 doi:10.1029/2009JD012120
649 Watterson I (2012) Understanding and partitioning future climates for Australian regions from
650 CMIP3 using ocean warming indices. Clim. Change 111(3-4), 903-922,
651 DOI:10.1007/s10584-011-0166-x
652 Watterson IG and Whetton PH (2011) Distributions of decadal means of temperature and precipitation
653 change under global warming. J. of Geo. Res.: Atmospheres 116 1984–2012
654 Watterson IG and Whetton PH (2013) Probabilistic projections of regional temperature and
655 precipitation extending from observed time series. Clim. Change 1-15
656

Table 1: The 37 *CMIP5 climate models used in this study; model name; institution; atmospheric resolutions (size of a single grid cell in km); results of previous evaluations of these models relevant to South-Eastern Australian climate: skill score (M-statistic, Watterson, 1996) averaged across temperature, rainfall and mean sea level pressure for the entire Australian continent and southern Australia (See Table 5.2.2 in CSIRO and BoM, 2015) and for rainfall alone across Australia (See Table 5.2.4 in CSIRO and BoM, 2015); a summary of the number of tests for which individual models performed poorly (See Table 5.6.1 in CSIRO and BoM, 2015); and an evaluation of the model ability to reproduce the sub-tropical ridge at the correct longitude above eastern Australia (see Grose et al.,, 2015). The last column indicates the global warming trends for the RCP8.5 emission pathway. See data section of this study for additional details. NB: score in bold blue (red) indicates good (poor) performance.*

Model	Institution Name and country	Lat. grid size (km)	Lon. grid size (km)	M-Stat. Aus.	M-Stat. Sou. Aus.	M-Stat Prec. Aus.	Poor Perf.	STR	RCP 8.5 GW
ACCESS1-0	CSIRO-BOM, Australia	210	130	**727**	**575**	552	1	2	4.63
ACCESS1-.3	CSIRO-BOM, Australia	210	130	**691**	492	544	2	2	4.58
bcc-csm1-1	BCC, CMA, China	310	310	684	464	499	**0**	**1**	3.86
bcc-csm1-1-m	BCC, CMA, China	120	120	**711**	**573**	525	**0**	2	3.44
BNU-ESM	BNU, China	310	310	**564**	**388**	451	**3**	**3**	4.85
CanESM2	CCCMA, Canada	310	310	**706**	**542**	492	1	2	4.90
CCSM4	NCAR, USA	130	100	642	519	**379**	1	2	3.97
CESM1-BGC	NSF-DOE-NCAR, USA	130	100	653	518	**400**	1	2	3.92
CESM1-CAM5	NSF-DOE-NCAR, USA	130	100	659	**589**	493	**0**	2	4.70
CESM1-CAM5-1-FV2	NSF-DOE-NCAR, USA	275	210						
CMCC-CESM	CMCC, Italy	410	410	**549**	**355**	479	1	**3**	4.25
CMCC-CM	CMCC, Italy	78	78	663	**583**	486	**0**	**1**	4.85
CMCC-CMS	CMCC, Italy	210	210	672	471	**564**	1	**1**	4.99
CNRM-CM5	CNRM-CERFACS, France	155	155	**706**	**587**	**602**	**0**	**1**	3.98
CSIRO-mk3.6	CSIRO-QCCCE, Australia	210	210	613	**431**	**482**	2	**3**	4.67
FGOAL-g2	LASG-CESS, China	310	310	653	518	535	**0**		3.43
FGOALS-s2	LASG-CESS, China	190	310						
GFDL-CM3	NOAA, GFDL, USA	275	220	676	**546**	**564**	1	2	5.17
GFDL-ESM2G	NOAA, GFDL, USA	275	220	638	467	472	**3**	2	3.13
GFDL-ESM2M	NOAA, GFDL, USA	275	220	607	**383**	469	**0**	2	3.01
GISS-E2-H	NASA/GISS, NY, USA	275	220	**586**	458	490	**4**	2	3.21
GISS-E2-H-CC	NASA/GISS, NY, USA	110	110	**581**	473	501	**3**	2	3.12
GISS-E2-R	NASA/GISS, NY, USA	275	220	**575**	516	461	**3**	**3**	2.72
GISS-E2-R-CC	NASA/GISS, NY, USA	110	110	614	**543**	472	**0**	2	2.76
HadGEM2-CC	MOHC, UK	210	130	**698**	533	541	**0**	**1**	5.30
HadGEM2-ES	MOHC, UK	210	130	**720**	**556**	**561**	1	2	5.19
INMCM4	INM, Russia	220	165	657	**455**	524	**3**	2	3.09
IPSL-CM5B-LR	IPSL, France	410	210	625	**424**	**596**	1	**3**	3.87
MIROC5	JAMSTEC, Japan	155	155	644	488	**432**	**0**	2	3.69
MIROC-ESM	JAMSTEC, Japan	310	310	**549**	**434**	**342**	**0**	**3**	5.35
MIROC-ESM-CHEM	JAMSTEC, Japan	310	310	**561**	**450**	**333**	**4**	**3**	5.60
MPI-ESM-LR	MPI-N, Germany	210	210	**720**	**542**	**593**	1	2	4.01
MPI-ESM-MR	MPI-N, Germany	210	210	**705**	513	**640**	1	**1**	4.02
MRI-CGCM3	MRI, Japan	120	120	659	511	**599**	1	**1**	3.84
MRI-ESM1	MRI, Japan	120	120						
NorESM1-M	NCC, Norway	275	210	604	480	**347**	1	2	3.62
NorESM1-ME	NCC, Norway	275	210	**594**	475	**343**	1	2	3.78

672 **Table 2**: *Evaluation of the reproduction of the annual cycle of some key quantities by the 37 CMIP5*
673 *models considered using Euclidean distance between the model values and the observations. See*
674 *results section for additional details. NB: score in bold blue (red) indicate the top (bottom) 10*
675 *performances.*

	Rainfall			Rain-Tripole
	Mean	STD	Trend	Correlation
	1900-2005		1985-2014	1900-2005
ACCESS1-0	6	9	17	18
ACCESS1-3	11	25	30	3
bcc-csm1-1	18	16	27	20
bcc-csm1-1-m	5	2	29	9
BNU-ESM	21	21	13	11
CanESM2	12	18	31	16
CCSM4	34	35	25	8
CESM1-BGC	29	29	24	2
CESM1-CAM5	15	7	18	4
CESM1-CAM5-1-FV2	20	8	32	28
CMCC-CESM	27	17	5	15
CMCC-CM	17	10	26	17
CMCC-CMS	22	12	12	1
CNRM-CM5	23	34	37	5
CSIRO-Mk3.6	24	23	14	19
FGOAL-g2	7	15	10	25
FGOAL-s2	25	33	3	21
GFDL-CM3	1	6	23	32
GFDL-ESM2G	3	13	35	13
GFDL-ESM2M	8	24	19	23
GISS-E2-H	36	37	36	37
GISS-E2-H-CC	33	36	33	29
GISS-E2-R	28	30	11	26
GISS-E2-R-CC	26	26	9	35
HadGEM2-CC	19	14	2	27
HadGEM2-ES	16	19	7	36
inmcm4	14	20	34	6
IPSL-CM5B-LR	9	28	22	34
MIROC5	31	31	21	24
MIROC-ESM	37	11	15	31
MIROC-ESM-CHEM	35	1	6	30
MPI-ESM-LR	13	22	1	10
MPI-ESM-MR	10	4	20	12
MRI-CGCM3	4	3	16	7
MRI-ESM1	2	5	4	33
NorESM1-M	32	32	8	22
NorESM1-ME	30	27	28	14

676
677

678 **Table 3***: Correlation coefficients computed across the 37 individual CMIP5 model quantities*
679 *(indicated in the two left columns) averaged over a period of time indicated in the third column and*
680 *for different seasons (columns 4 to 8). Correlation coefficients above 0.33 (0.42) are significant at the*
681 *95% (99%) level and are indicated in italics (bold). Numbers in brackets are obtained with some*
682 *individual models removed (see text for details).*
683

Correlated quantities:							
Variable 1	Variable 2	Period considered	Annual	JASON	AMJJASO	SON	DJF
Standard Deviation of SEA Rainfall	Standard deviation of Tropical Tripole	1900-2005	*0.38*	**0.44**	**0.44**	**0.46**	0.04
		1956-2005	**0.41**	**0.50**	**0.43**	**0.50**	0.09
		1985-2014	*0.36*	**0.56**	*0.40*	**0.58**	0.02
	Corr. Coef. Victoria rainfall vs. Tropical Tripole	1900-2005	*0.39*	*0.35*	**0.44**	0.25	0.07
		1956-2005	*0.39* **(0.60)**	**0.60 (0.77)**	**0.59 (0.67)**	**0.52 (0.60)**	-0.16 (-0.04)
		1985-2014	0.19	**0.43**	0.24	**0.52**	0.00
SEA Rainfall trends	Tropical Tripole trends	1900-2005	**0.49**	**0.52**	**0.58**	**0.54**	0.18
		1956-2005	0.14	0.27	*0.33*	0.29	-0.23
		1985-2014	**0.52**	*0.38*	**0.44**	0.31	*0.36*

684
685

686 **Table 4***: Projected rainfall changes (in %) for the last 20 years of the RCP8.5 simulations (2080-*
687 *2099) compared to the last 20 years of the historical simulations (1986-2005) for different seasons*
688 *(columns 3 to 7) showing all CMIP5 models together and separated in two groups, one being the*
689 *models with "very wet summers" in the simulations of the current climate and the "other" being the*
690 *remainder of the models.*
691

		Annual	JASON	AMJJASO	SON	DJF
Mean rainfall changes (percent)	All models	-8.4	-15.8	-12.1	-19.7	1.2
	Very wet summer models	-0.1	-6.1	-3.9	-5.6	5.7
	Other models	-14.1	-22.5	-17.7	-29.4	-1.8

692
693
694

695 **Table 5***: Correlation coefficients computed across the 37 individual CMIP5 model quantities*
696 *(indicated in the two left columns) averaged over a period of time indicated in the third column and*
697 *for different seasons (columns 4 to 8). Correlation coefficients significant at the 95% (99%) level are*
698 *indicated in italics (bold)). Numbers in brackets are obtained with some individual models removed*
699 *(see text for details).*

Correlated quantities							
Variable 1	Variable 2	Period considered	Annual	JASON	AMJJASO	SON	DJF
SEA Rainfall Trend	Tripole trend	2006-2099	**0.65 (0.63)**	**0.75 (0.78)**	**0.74 (0.77)**	**0.70 (0.72)**	0.23 (0.09)
	Global Warming	2006-2099	-0.30	-0.32	*-0.34*	-0.19	-0.07

700

List of Figures:

Figure 1: *Global map of mean Sea Surface Temperature linear trends from 1986 to 2014 (in °C) (top) with overlay the area used to construct the Tripole index, (central box minus the average of the other two boxes); also shown and enlarged in the lower panel is the State of Victoria and the model grid boxes considered to construct the South-Eastern Australia average rainfall time series with the red box showing the area considered when observations are used (values are from January 2006 from Access1.0).*

Figure 2:
Annual cycle of monthly mean (top) and standard deviation (bottom) of South-Eastern Australia rainfall (in mm) averaged from 1900 to 2005 for the observations (BoM operational 0.05 degree gridded rainfall), the ensemble mean of the 37 CMIP5 models considered; a selection of the 10 "best" and "worst" CMIP5 GCMs (defined using Euclidean distance), and all individual models. NB: on the top diagram "Victoria only" observed rainfall show the observed rainfall when only gridded data within the boundary of the State of Victoria are used in contrast with SEA rainfall which cover a wider box (displayed in Figure 1b).

Figure 3:
R*elationship between each model's DJF (austral summer) mean rainfall and its year-to-year variability (top panel), computed using values from 1900 to 2005 across the 37 CMIP5 models (the ensemble mean is shown with a red symbol and the observations with a black symbol), lines of best fit and explained variance are displayed. The bottom panel shows the relationship with the coefficient of variation.*

F**igure 4**: *Maps of global DJF (austral summer) rainfall climatologies (top row) from the 2 groups of CMIP5 models ("very wet summer" on the left, "other" on the right) in mm.day^{-1} and anomalies from the CMAP climatology averaged from 1980-2005 period (bottom row also in mm.day^{-1}).* N.B. scales differ between top and bottom rows.

Figure 5: *Annual cycle of linear trends of SEA rainfall (in mm) from 1985 to 2014, for the observations (BoM operational 0.05 degree gridded rainfall), the ensemble mean of the 37 CMIP5 models considered, a selection of the 10 "best" models (defined using Euclidean distance from the black line), all individual models, including the model identified as the closest to the observations (green line). N.B: for the CMIP5 simulations, the historical simulations are used until 2005 and the simulations forced with the RCP 8.5 concentration pathways from 2006.*

Figure 6: *Annual cycle of the tropical Tripole index mean (top) and year to year variability (standard deviation, bottom) computed from 1900 to 2005 for the observations (HadISST dataset), the ensemble mean of the 37 CMIP5 models considered; a selection of the 10 "best" and "worst" models (defined using Euclidean distance) and all individual model.*

Figure 7: *Annual cycle of linear trends of the tropical Tripole index (in degree Celsius per 30 years) from 1985 to 2014, for the observations (HadISST dataset), the ensemble mean of the 37 CMIP5 models considered, a selection of the 10 "best" and "worst" models (defined using Euclidean distance) and all individual models.*

Figure 8: *Annual cycle of the correlation coefficients between the tropical Tripole index and SEA rainfall, computed form 1900 to 2005: for the observations, the ensemble mean of the 37 CMIP5 models considered; a selection of the 10 "best" and "worst" models (defined using Euclidean distance) and all individual models. Correlations above the dashed line are significant at the 95% confidence level.*

Figure 9: Correlation coefficients between July to November mean Tripole index and SEA rainfall computed on 50-year periods for the observations (past climate only), the ensemble mean of the 37 CMIP5 models considered and the individual models.

Figure 10: *Scatter plots across metrics computed for 37 individual CMIP5 models: standard deviation of July to November of SEA rainfall versus tropical Tripole index (top panel) and standard deviation of July to November SEA rainfall versus the strength of the SEA rainfall-Tripole relationship (lower panel). All quantities are computed on the last 50 years of the current climate simulations (1956-2005). In all panels, the ensemble mean is shown with a red symbol and the observations with a black symbol, models with very wet summer are identified as green symbols; lines of best fit and square correlation for the whole ensemble are displayed. The four models from the GISS family are outlined by a red box.*

Figure 11: *Maps of global surface temperature change (in °C, annual mean) from the 2 groups of CMIP5 models ("very wet summer" on the left, other on the right). Anomalies are computed between the last 30 years of the 21st century (RCP 8.5) and 20th century (historical) simulations***.** *Bottom panel shows the annual cycles of the mean monthly trends in Tripole index computed from 2006 to 2099: for the ensemble mean of the 37 CMIP5 models considered and the individual model; ensemble mean of the 15 models with "very wet summer" as well as the ensemble mean of the other 22 models are identified.*

Figure 12: Annual cycle of the *projected rainfall trends in mm over 2006-2099 for the entire South-Eastern Australia box following the RCP8.5 pathway for the ensemble mean of the 37 CMIP5 models considered and individual models (top panel); comparison between various sub-regions across SEA (lower panels): (top left, continental point within the red rectangular in the top right map) and for three Victorian sub-region (South-West, bottom left, Murray basin side of Victoria, bottom middle panel, and South-East Victoria, bottom right panel). Rainfall anomalies are given in per cent with respect to the 1986-2005 mean, for the four calendar seasons, under RCP 2.6 (green), RCP 4.5 (blue) and RCP 8.5 (purple) for 2090. Natural climate variability is represented by the grey bars. For each bar plot, the box shows the median, 10th and 90th percentiles of the 20-year average while line segments indicates changes in the 20-year average of the 10th and 90th percentile, as calculated from individual years.*

Figure 13: *Maps of Pacific/Indian region change in precipitation (%) in DJF (austral summer: top row) and JJA (austral winter: bottom row) from the 2 groups of CMIP5 models (very wet summer models on the left, other models on the right). Anomalies are computed between the last 30 years of the 21st century (RCP 8.5) and 20th century (historical) simulations.*

Figure 14: *Scatter plots across metrics computed for 37 individual CMIP5 models: trends in July to November SEA rainfall from 2006 to 2099 using the RCP8.5 pathway versus the tropical Tripole index for the same seasons (top panel); same quantities for the austral summer (DJF: lower panel). In all panels, the ensemble mean is shown with a red symbol and models with very wet summer are shown as green symbols, lines of best fit and square correlation are displayed.*

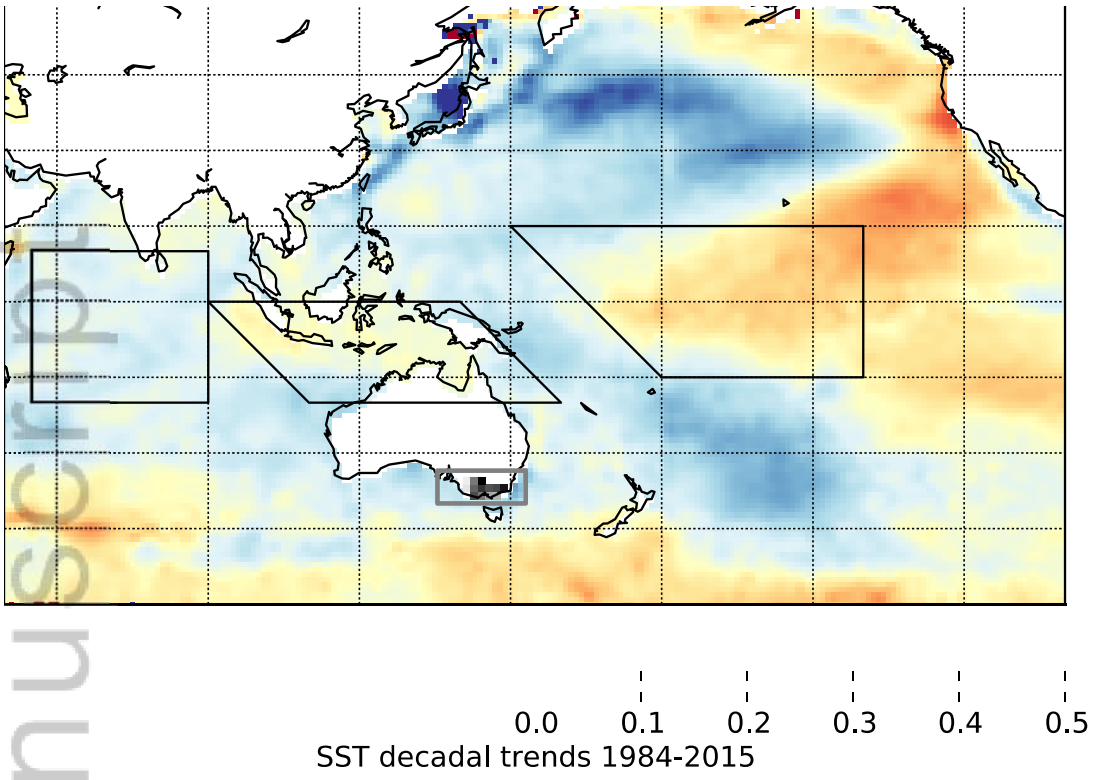

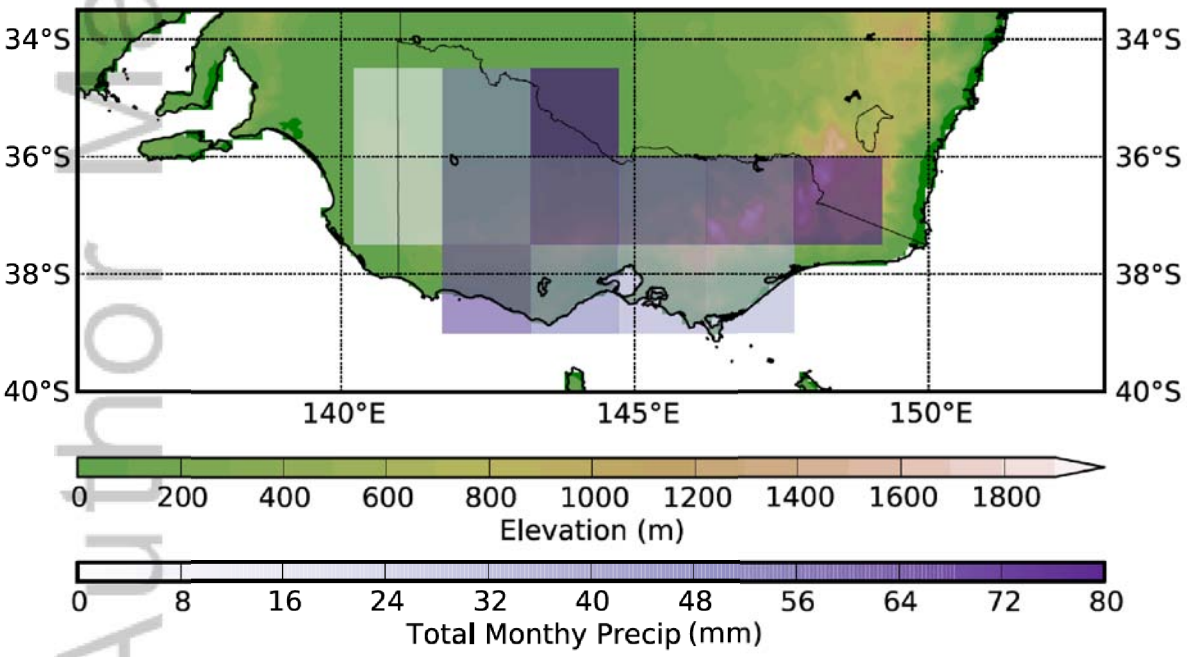

Figure 1: *Global map of mean Sea Surface Temperature linear trends from 1986 to 2014 (in °C) (top) with overlay the area used to construct the Tripole index, (central box minus the average of the other two boxes); also shown by the grey box and enlarged in the lower panel is the area considered as South-East Australia used to define observed rainfall and the model grid boxes considered to construct the South-Eastern Australia average rainfall. The topography of South East Australia is also shown in the lower panel.*

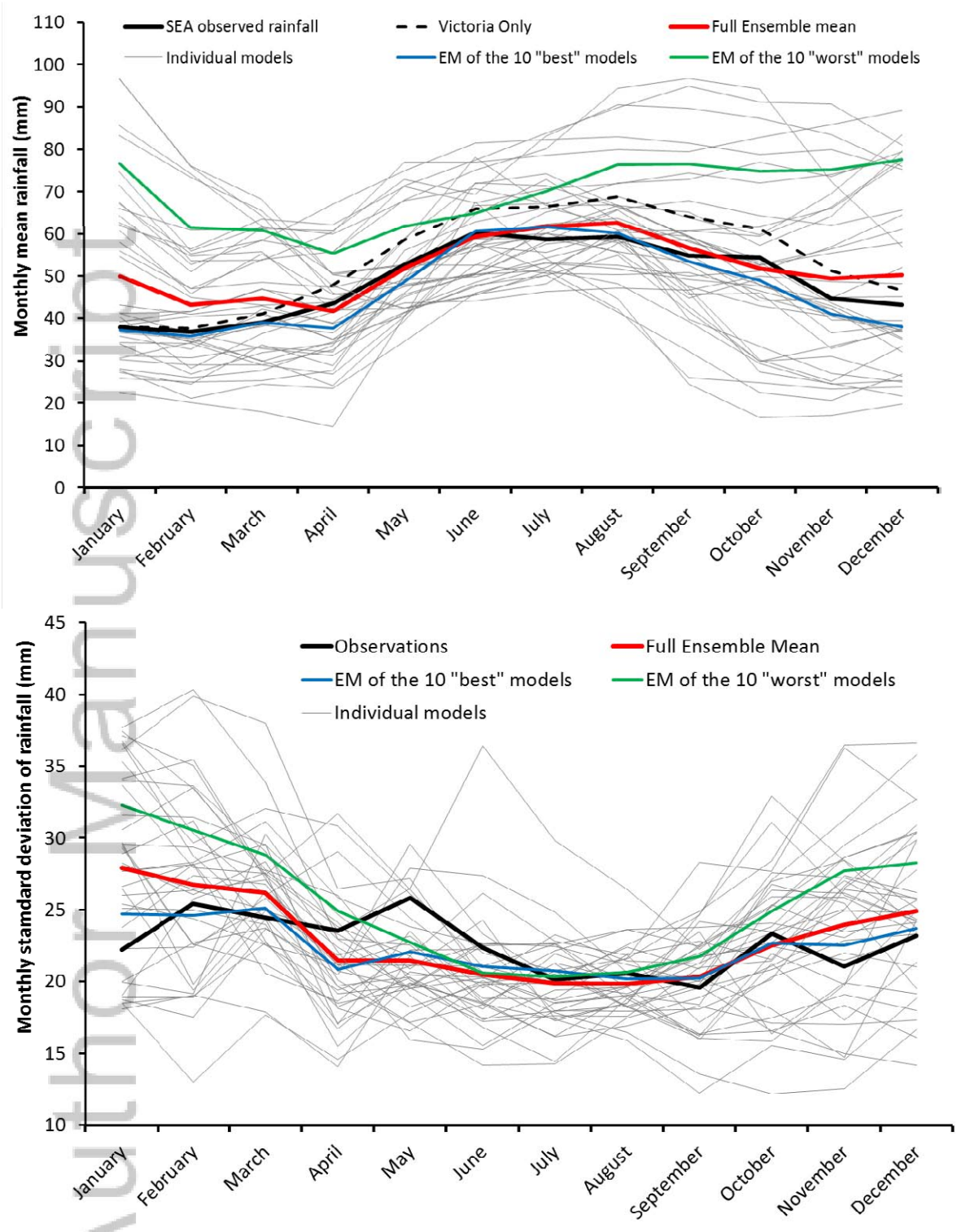

Figure 2: *Annual cycle of monthly mean (top) and standard deviation (bottom) of South-Eastern Australia rainfall (in mm) averaged from 1900 to 2005 for the observations (BoM operational 0.05 degree gridded rainfall), the ensemble mean of the 37 CMIP5 models considered; a selection of the 10 "best" and "worst" CMIP5 GCMs (defined using Euclidean distance), and all individual models. NB: on the top diagram "Victoria only" observed rainfall show the observed rainfall when only gridded data within the boundary of the State of Victoria are used in contrast with SEA rainfall which cover a wider box (displayed in Figure 1b).*

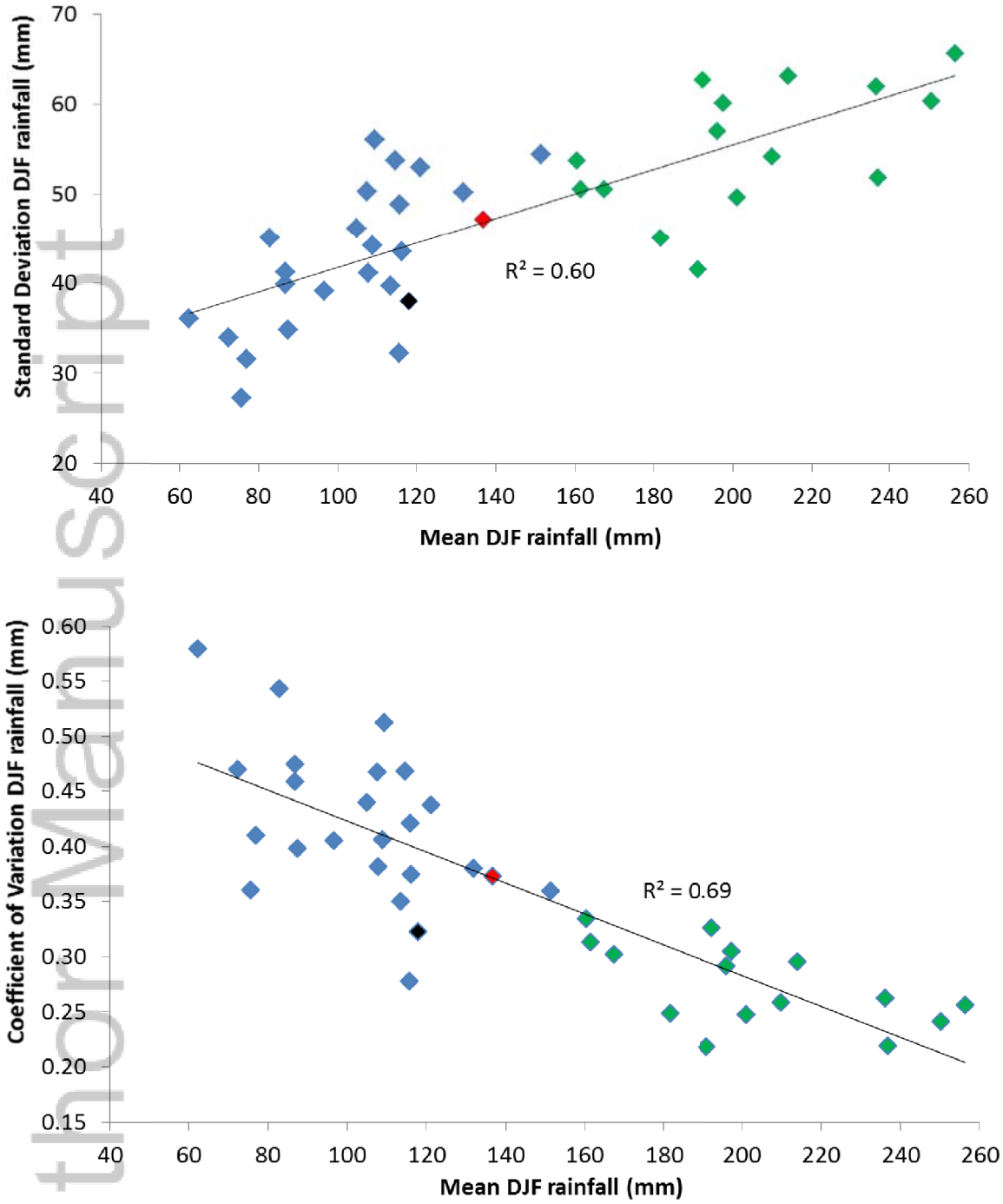

Figure 3: *Relationship between each model's DJF (austral summer) mean rainfall and its year-to-year variability (top panel), computed using values from 1900 to 2005 across the 37 CMIP5 models (the ensemble mean is shown with a red symbol and the observations with a black symbol), lines of best fit and explained variance are displayed. The bottom panel shows the relationship with the coefficient of variation.*

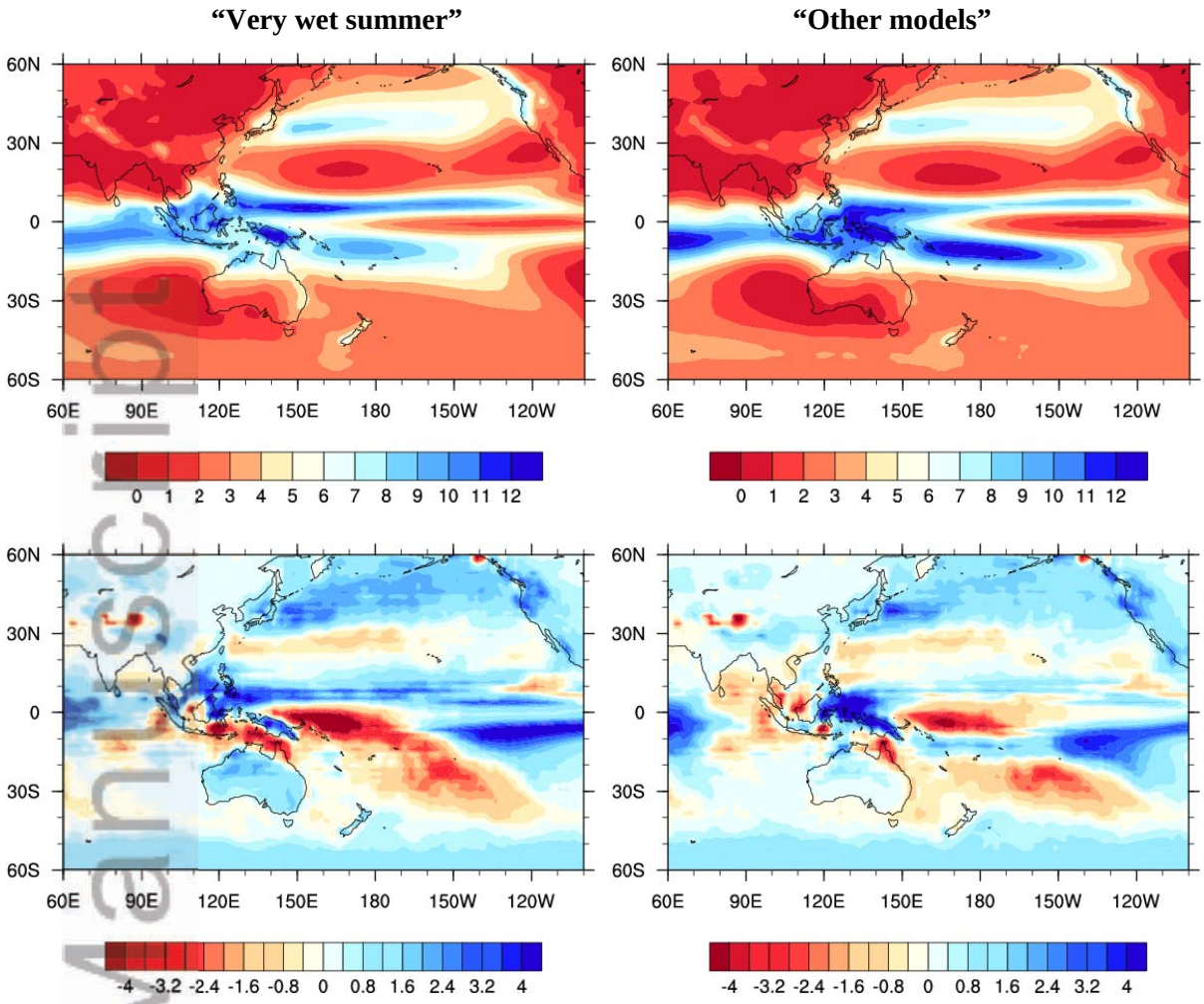

Figure 4: *Maps of global DJF (austral summer) rainfall climatologies (top row) from the 2 groups of CMIP5 models ("very wet summer" on the left, "other" on the right) in mm.day^{-1} and anomalies from the CMAP climatology averaged from 1980-2005 period (bottom row also in mm.day^{-1}).* N.B. scales differ between top and bottom rows.

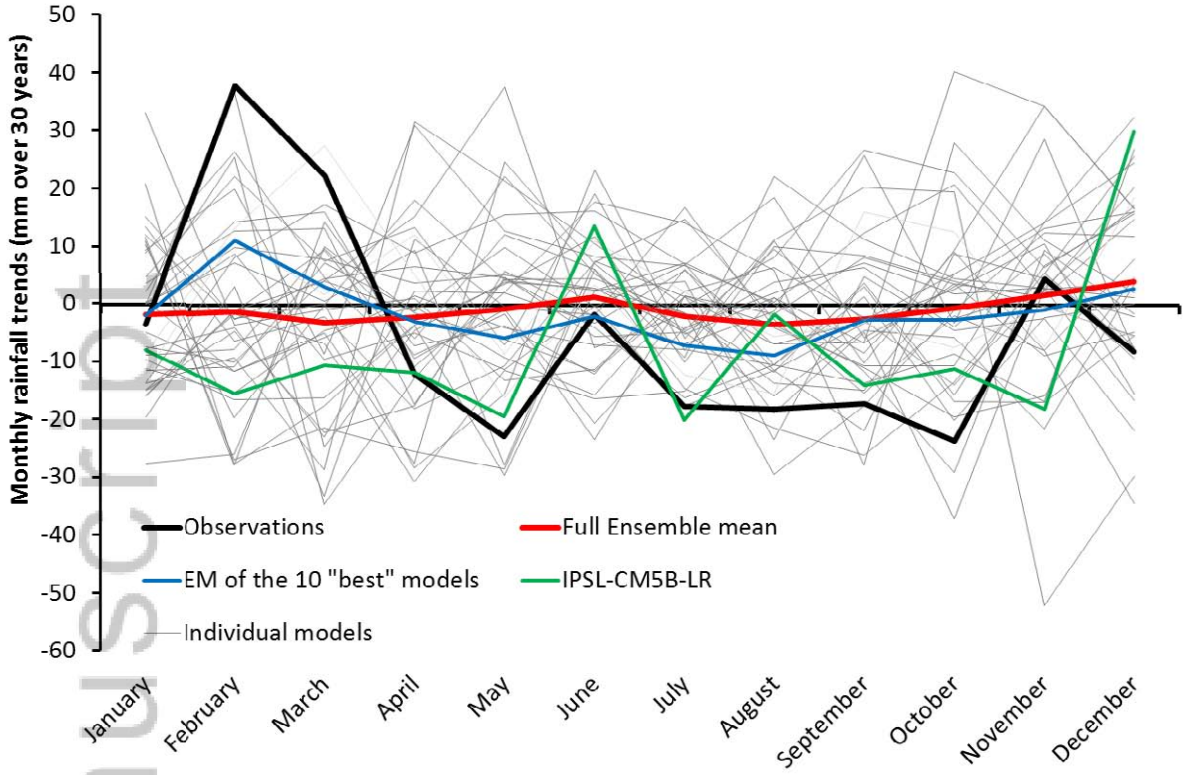

Figure 5: *Annual cycle of linear trends of SEA rainfall (in mm) from 1985 to 2014, for the observations (BoM operational 0.05 degree gridded rainfall), the ensemble mean of the 37 CMIP5 models considered, a selection of the 10 "best" models (defined using Euclidean distance from the black line), all individual models, including the model identified as the closest to the observations (green line). N.B: for the CMIP5 simulations, the historical simulations are used until 2005 and the simulations forced with the RCP 8.5 concentration pathways from 2006.*

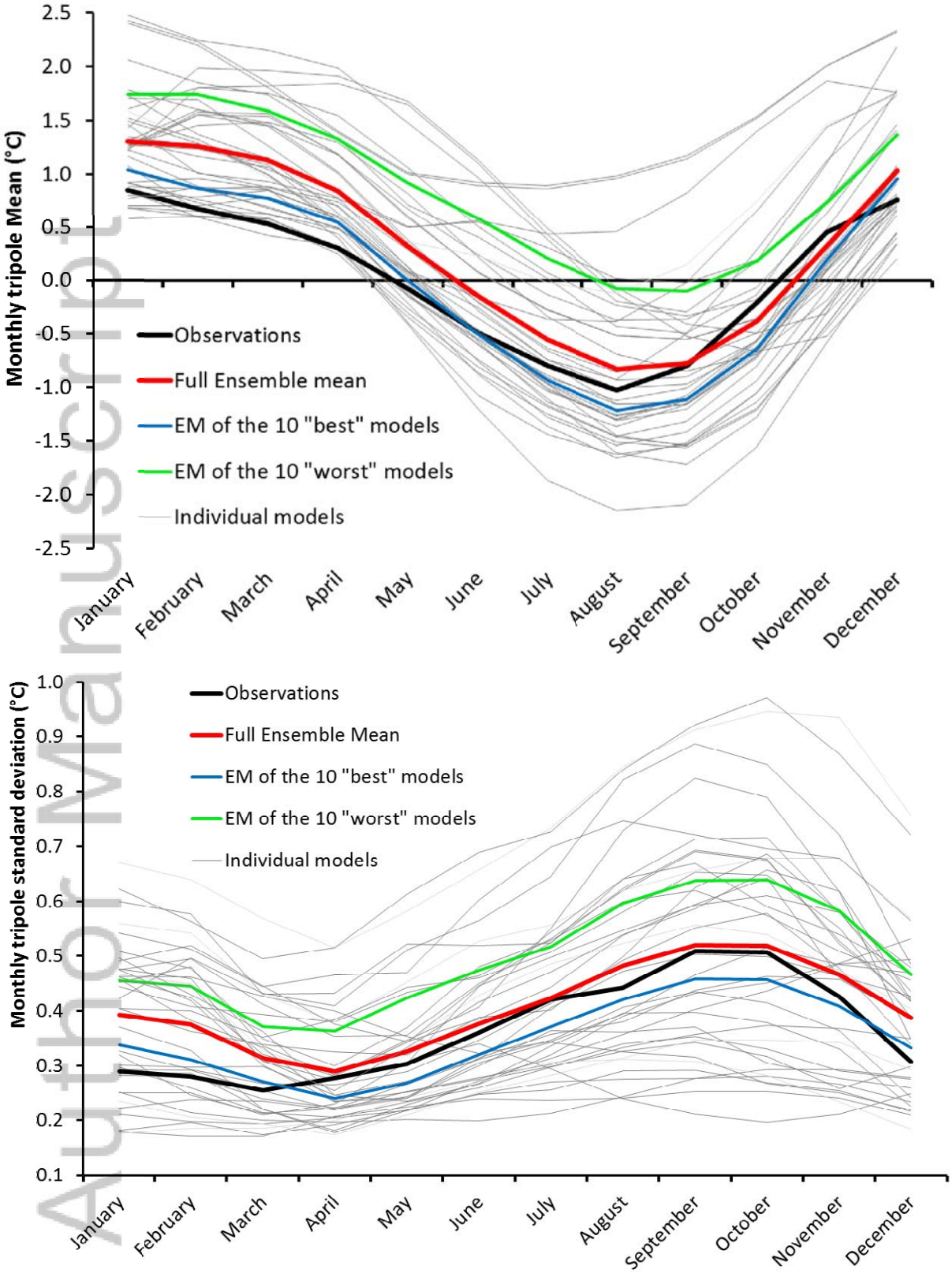

Figure 6: *Annual cycle of the tropical Tripole index mean (top) and year to year variability (standard deviation, bottom) computed from 1900 to 2005 for the observations (HadISST dataset), the ensemble mean of the 37 CMIP5 models considered; a selection of the 10 "best" and "worst" models (defined using Euclidean distance) and all individual model.*

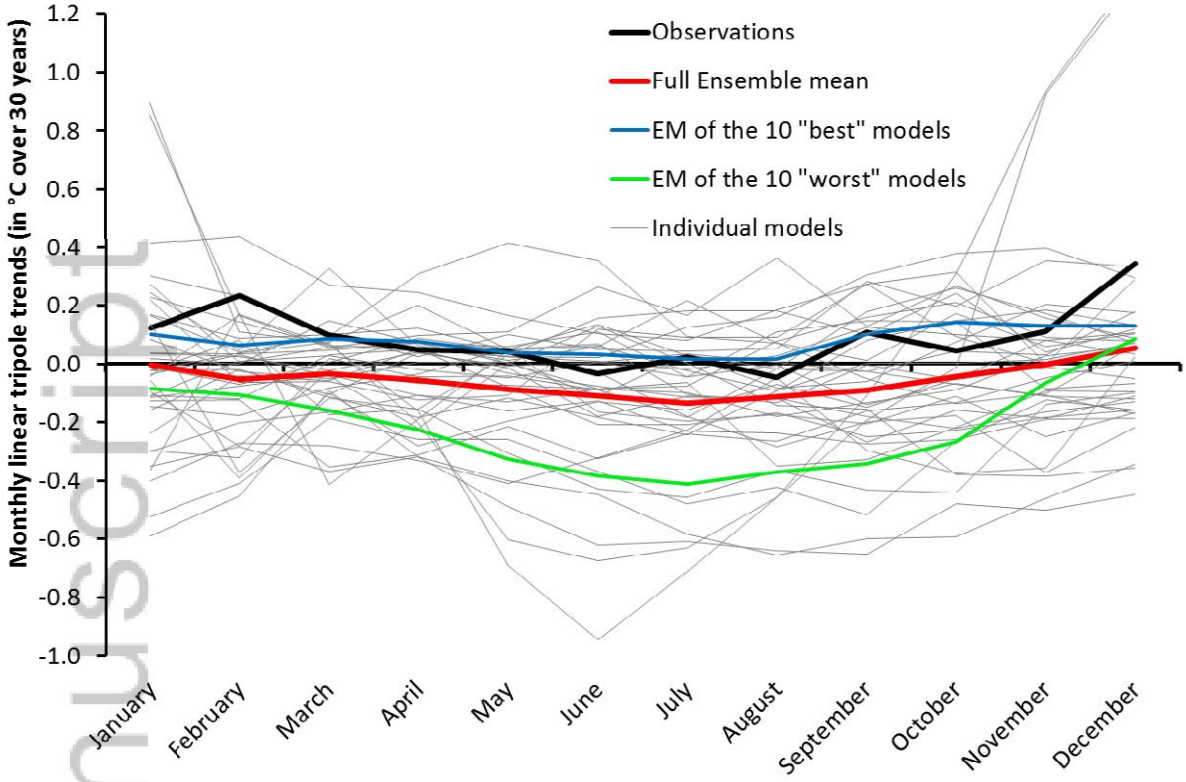

Figure 7: *Annual cycle of linear trends of the tropical Tripole index (in degree Celsius per 30 years) from 1985 to 2014, for the observations (HadISST dataset), the ensemble mean of the 37 CMIP5 models considered, a selection of the 10 "best" and "worst" models (defined using Euclidean distance) and all individual models.*

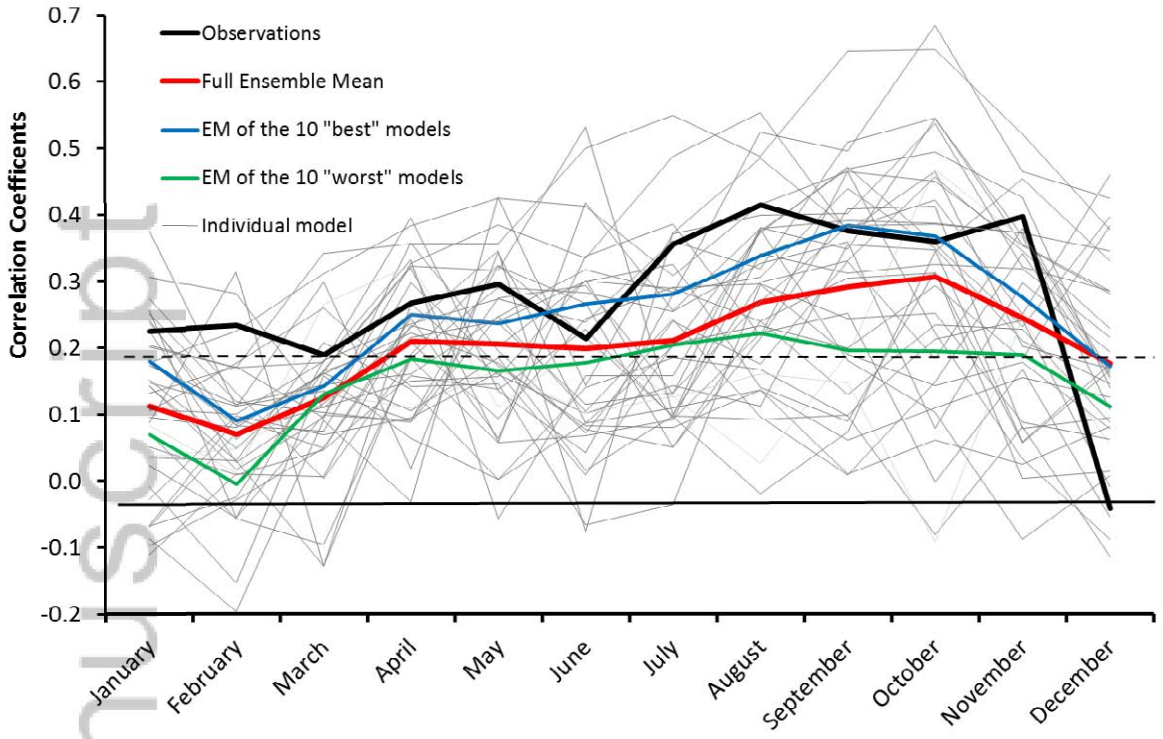

Figure 8: *Annual cycle of the correlation coefficients between the tropical Tripole index and SEA rainfall, computed form 1900 to 2005: for the observations, the ensemble mean of the 37 CMIP5 models considered; a selection of the 10 "best" and "worst" models (defined using Euclidean distance) and all individual models. Correlation above the dashed line are significant at the 95% confidence level.*

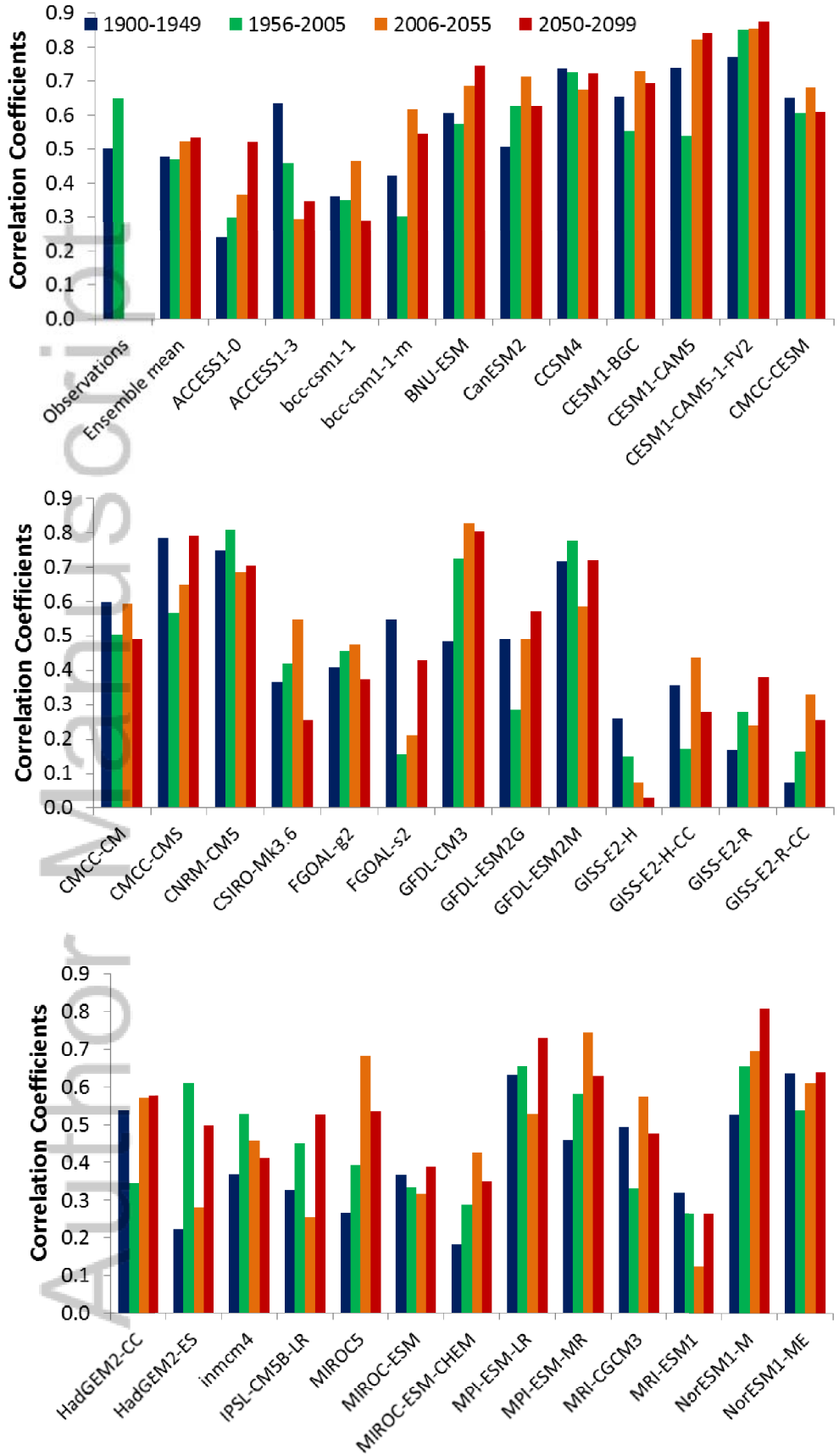

Figure 9: Correlation coefficients between July to November mean Tripole index and SEA rainfall computed on 50-year periods for the observations (past climate only), the ensemble mean of the 37 CMIP5 models considered and the individual models.

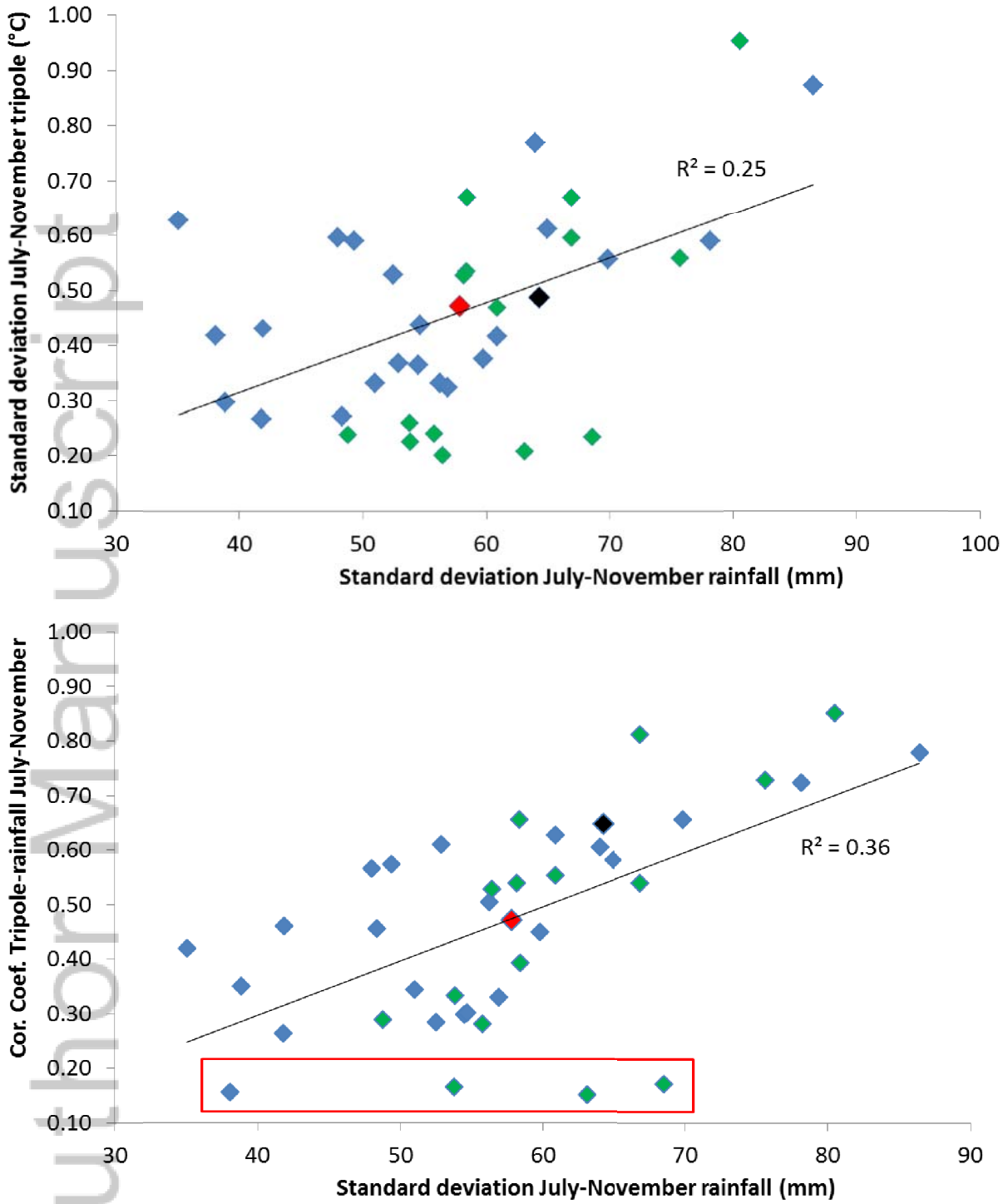

Figure 10: *Scatter plots across metrics computed for 37 individual CMIP5 models: standard deviation of July to November of SEA rainfall versus tropical Tripole index (top panel) and standard deviation of July to November SEA rainfall versus the strength of the SEA rainfall-Tripole relationship (lower panel). All quantities are computed on the last 50 years of the current climate simulations (1956-2005). In all panels, the ensemble mean is shown with a red symbol and the observations with a black symbol, models with very wet summer are identified as green symbols; lines of best fit and square correlation for the whole ensemble are displayed. The four models from the GISS family are outlined by a red box.*

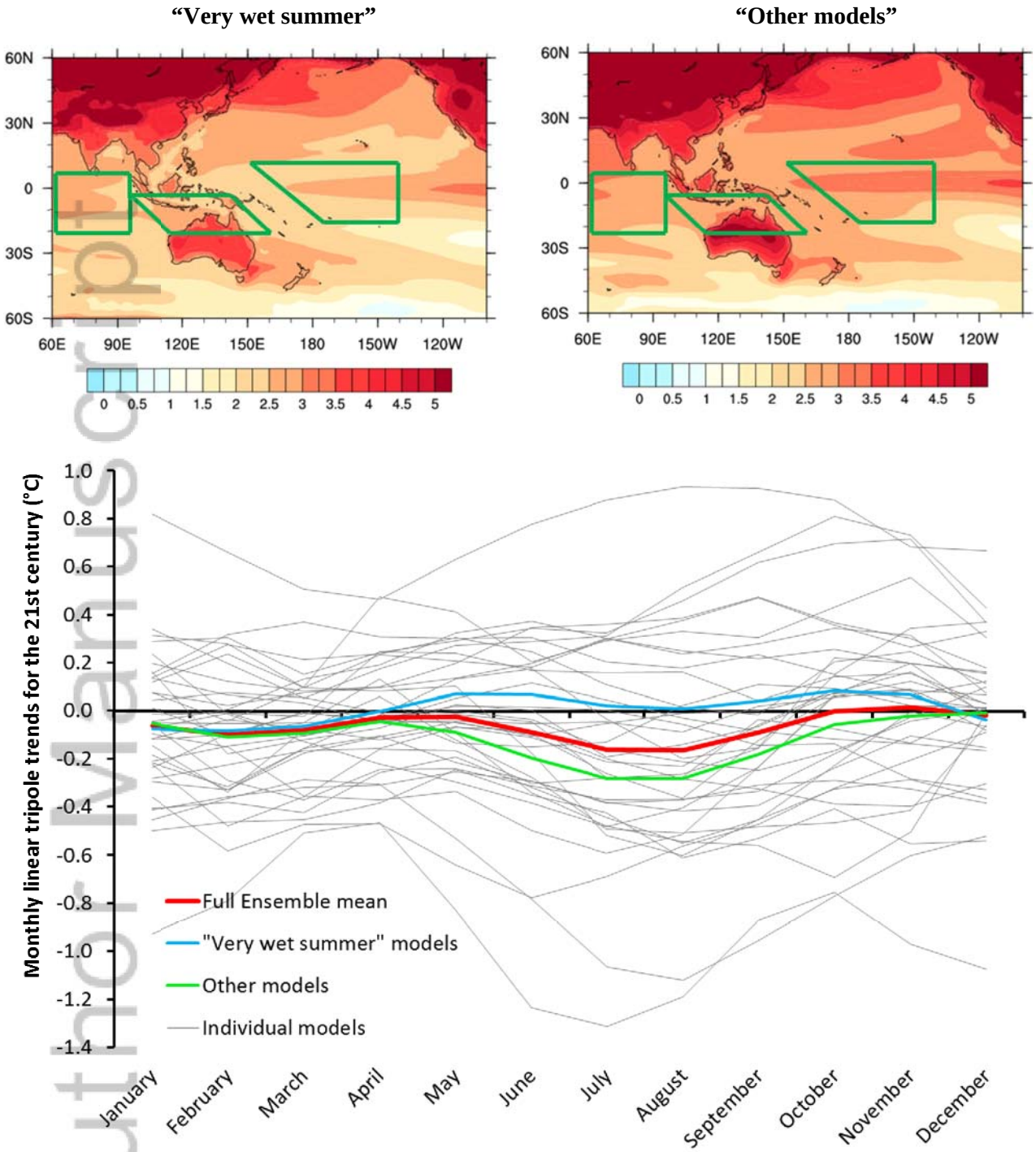

Figure 11: *Maps of global surface temperature change (in °C, annual mean) from the 2 groups of CMIP5 models ("very wet summer" on the left, other on the right). Anomalies are computed between the last 30 years of the 21st century (RCP 8.5) and 20th century (historical) simulations. Bottom panel shows the annual cycles of the mean monthly trends in Tripole index computed from 2006 to 2099: for the ensemble mean of the 37 CMIP5 models considered and the individual model; ensemble mean of the 15 models with "very wet summer" as well as the ensemble mean of the other 22 models are identified.*

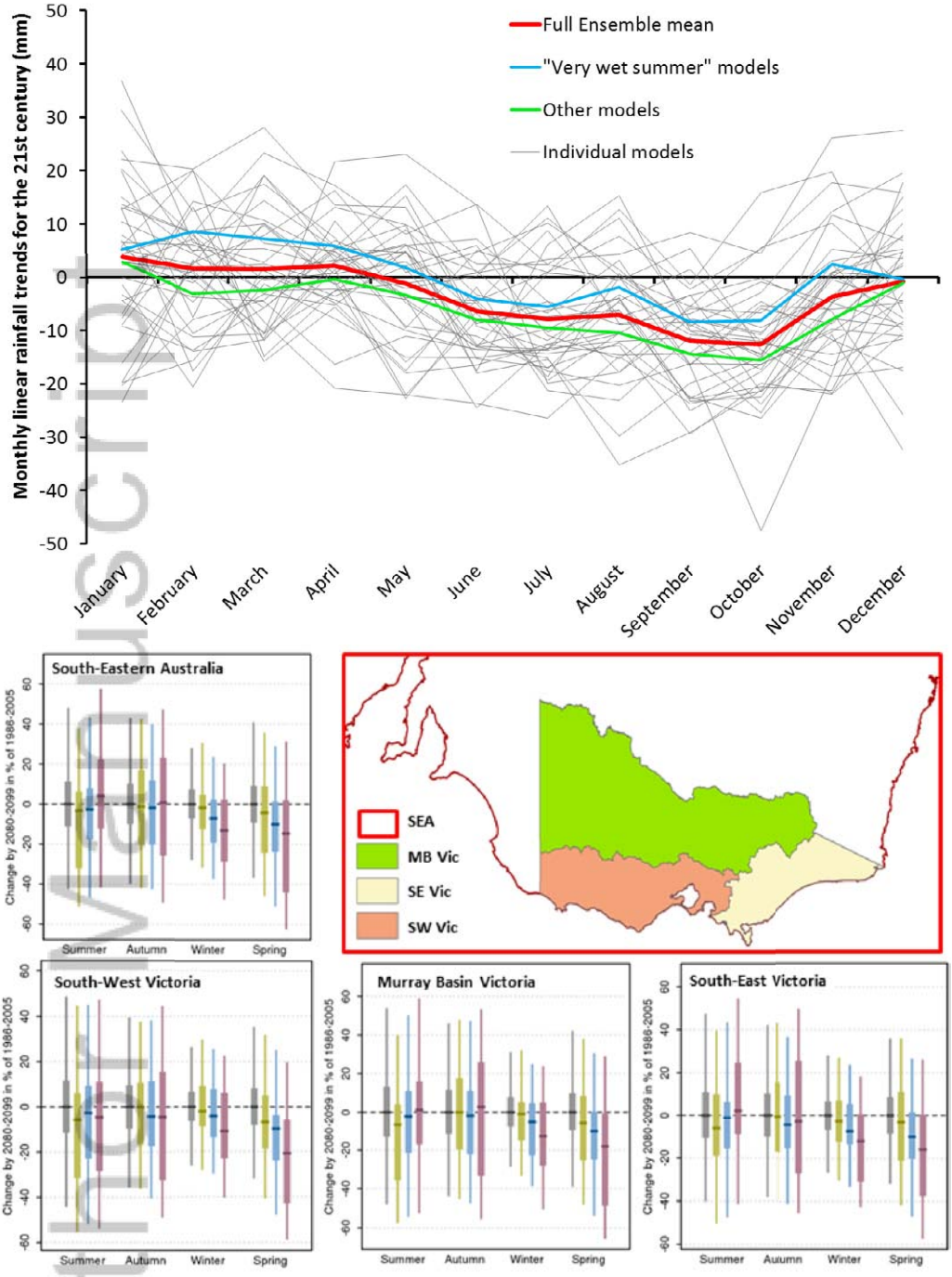

Figure 12: Annual cycle of the *projected rainfall trends in mm over 2006-2099 for the entire South-Eastern Australia box following the RCP8.5 pathway for the ensemble mean of the 37 CMIP5 models considered and individual models (top panel); comparison between various sub-regions across SEA (lower panels): (top left, continental point within the red rectangular in the top right map) and for three Victorian sub-region (South-West, bottom left, Murray basin side of Victoria, bottom middle panel, and South-East Victoria, bottom right panel). Rainfall anomalies are given in per cent with respect to the 1986-2005 mean, for the four calendar seasons, under RCP 2.6 (green), RCP 4.5 (blue) and RCP 8.5 (purple) for 2090. Natural climate variability is represented by the grey bars. For each bar plot, the box shows the median, 10th and 90th percentiles of the 20-year average while line segments indicates changes in the 20-year average of the 10th and 90th percentile, as calculated from individual years.*

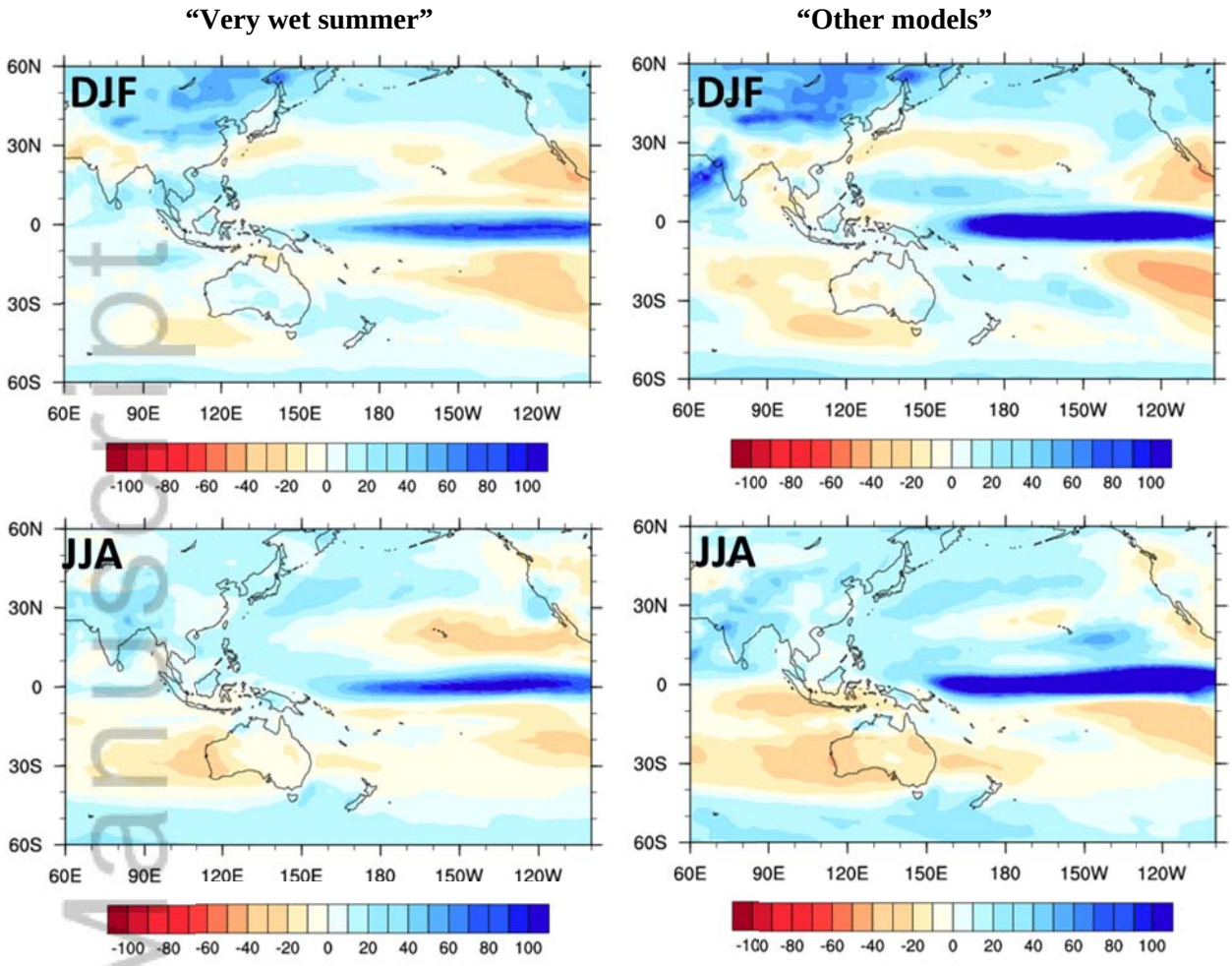

Figure 13: *Maps of Pacific/Indian region change in precipitation (%) in DJF (austral summer: top row) and JJA (austral winter: bottom row) from the 2 groups of CMIP5 models (very wet summer models on the left, other models on the right). Anomalies are computed between the last 30 years of the 21st century (RCP 8.5) and 20th century (historical) simulations.*

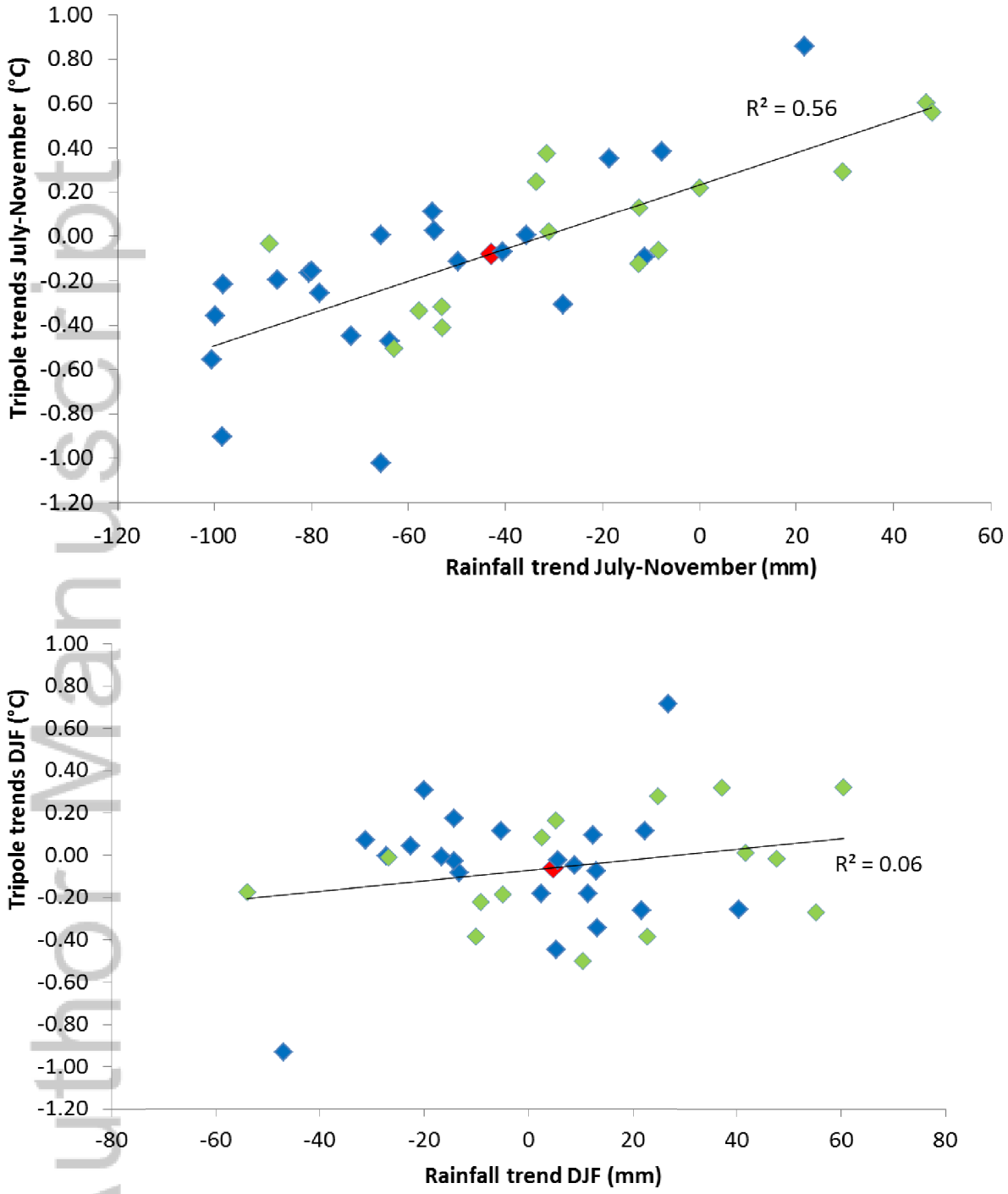

Figure 14: *Scatter plots across metrics computed for 37 individual CMIP5 models: trends in July to November SEA rainfall from 2006 to 2099 using the RCP8.5 pathway versus the tropical Tripole index for the same seasons (top panel); same quantities for the austral summer (DJF: lower panel). In all panels, the ensemble mean is shown with a red symbol and models with very wet summer are shown as green symbols, lines of best fit and square correlation are displayed.*

Understanding South-east Australian rainfall projection uncertainties: the influence of patterns of projected tropical warming

Short title: **Understanding South-east Australian rainfall projection uncertainties**

B. Timbal[1], S. Fiddes[1 2] and J.R. Brown[1]

[1]: Research and Development Branch, Bureau of Meteorology, Australia

[2]: Australian-German Climate and Energy College and ARC Centre of Excellence for Climate System Science, School of Earth Sciences, University of Melbourne, Australia

Date: 28/11/2016

Key words: South-Eastern Australia; rainfall; future projections; uncertainties; tropical warming; teleconnections

Corresponding author: Bertrand Timbal, b.timbal@bom.gov.au

Phone: +61-3-9669-4697

Fax: +61-3-9669-4660

Abstract

South-Eastern Australia and, in particular the State of Victoria, has experienced record deficits of rainfall over the last 20 years, in which the cool part of the year from April to October has been most affected. This situation has created difficulties for water managers, farmers and fire services, with the need to provide more certainty about future climate trends becoming clear. The latest climate projections for South-East Australia project an overall drying in the cool part of the year with little change in the rest of the year. Although this is in line with current trends, very large uncertainties are associated with these projections. In this study, this range of projections has been investigated, first by assessing how the current suite of climate models simulate the regional rainfall as well as the tropical variability, known to be a key driver of south-eastern Australian climate. The models were found to be reasonable overall, although a number overestimate Victorian summer rainfall. Model rainfall projections are found to be related to the models' projected patterns of tropical warming, where 60% of the range in cool season rainfall projections can be explained by the range of pattern of tropical changes. In addition, the projected drying tends to be more intense in the models best able to simulate summer rainfall, thus suggesting that the upper end of the uncertainty range is less likely to be realised as it may reflect inherent model biases, rather than physical changes.

1. Introduction

South-Eastern Australia (SEA), including the state of Victoria, has experienced challenging climate variability in the last 20 years (CSIRO and BoM, 2012). This has had severe implications from water management to agriculture and natural environment agencies (Leblanc et al., 2012). Chief amongst this variability was an extended period of below average rainfall from 1997 to 2009, termed the Millennium drought. That 13-year period was by far the worst protracted drought of this duration in the instrumental record, even when that record is extended as far back as 1865 (Timbal and Fawcett, 2013). Its magnitude in comparison with previous historical low rainfall periods is even more remarkable when smaller areas with significant orography and high rainfall, generating important streamflows, are considered − such as the catchments areas to the east of the capital (and largest population centre) of Victoria, Melbourne (Timbal et al., 2015a). Soon after the Millennium drought, Australia experienced its wettest two years on record (Bureau of Meteorology, 2012) driven by a very strong La Niña in 2010 followed by a second in 2011, with additional contributions from the Indian Ocean and the Southern Annular Mode (SAM) (Lim and Hendon, 2015).

On one hand, tropical expansion due to ongoing global warming (Nguyen et al., 2015) and associated increases in the intensity of the sub-tropical ridge have been shown to partially explain the trend towards reduced rainfall during the cool part of the year (from April to October) as shown by Timbal and Drosdowsky (2013). On the other hand, naturally occurring modes of variability within the Tropics are well known to influence SEA rainfall. Many studies have reported and quantified how the Pacific Ocean El Niño Southern Oscillation (ENSO), jointly with the Indian Ocean Dipole (IOD), affects SEA and Victorian rainfall (CSIRO and BoM, 2012; and CSIRO and BoM, 2015, and reference within). Furthermore, tropical modes of variability and tropical expansion are probably related.

Combining the tropical influences of the Pacific and Indian Oceans, Timbal and Hendon (2011) developed a "Tripole index" to maximise the amount of SEA rainfall inter-annual variability captured by a simple Sea Surface Temperature (SST)-based index. Using this index, it was shown that the tropical modes of variability did not explain the rainfall reduction for the duration of the Millennium drought, although they helped contribute to the worsening of the drought at the end of the period, in particular during spring (Timbal and Hendon, 2011; Nicholls, 2010 and Smith and Timbal, 2012). On the contrary, the 2010-12 rainfall was strongly driven by tropical modes of variability, mainly occurring during the warm season. The influence of the tropics on SEA and Victoria rainfall is important for streamflows across the State: annual composite of streamflows based on the Tripole index show a sizeable difference between positive and negative years (Timbal et al., 2015a; Fiddes and Timbal, 2016).

Understanding how this mix of naturally occurring variability and human induced changes will evolve in the future is therefore particularly important to water managers. The most recent set of global climate change projections were assembled by the Climate Model Intercomparison Project Phase 5 (CMIP5; Taylor et al., 2012) in support of the 5th Assessment Report (AR5) of the Intergovernmental Panel on Climate Change (IPCC, 2013). This model dataset underpinned the latest set of national climate change projections generated by the CSIRO and the Bureau of Meteorology for the Australian continent (CSIRO and BoM, 2015).

Across SEA, the CMIP5 ensemble mean shows a mean rainfall reduction during the cool season and little change during the warm season for all RCPs by the end of the 21st century. The projections show varying magnitudes of rainfall decline during the cool season north of the Great Dividing range (Timbal et al., 2015b), south of the range (Gross et al., 2015b) and on the eastern seaboard of Australia (Dowdy et al., 2015). However, the full range of climate models indicated a wide range of possible outcomes and the reasons for this spread are not well understood.

A recent analysis (Grose et al., 2015a) focussed on future projections of the belt of high pressure controlling SEA rainfall: the sub-tropical ridge (STR), considering either its intensity (STR-I) or position (STR-P). That study was not able to relate the range of projections in rainfall to the

range of projections in changes in the STR but did show that the mean tendency toward a drier future during the cool season was primarily driven by the intensification of the sub-tropical ridge. It also suggested that since the models are not capturing the strength of the STR-rainfall relationship as observed, it is plausible that the current suite of CMIP5 models underestimate the mean future rainfall decline as they do for the historical period (Timbal et al., 2010; Nguyen et al., 2015).

Another candidate to drive SEA rainfall change is the model's projected warming in the tropics, in particular in areas which are known to influence SEA: e.g. the Western-Central Pacific and Eastern Indian Ocean. This was shown to be an important factor amongst the previous generation of climate model projections using a dipole pattern between the Indian and Pacific Oceans (Watterson, 2012), following a study which demonstrated that these two areas were important in controlling SEA rainfall in a climate model (Watterson, 2010).

In this study, we use the Tripole index of Timbal and Hendon (2011) to quantify the relationship between observed tropical SST and SEA rainfall to help explain the range of rainfall projections in the CMIP5 models. To do so, firstly we analyse the model's ability to capture the strength of the observed relationship between the Tripole index and SEA rainfall and secondly, relate the spread of tropical patterns of warming to the spread of rainfall projections across SEA. This analysis can help provide insight into the uncertainty range and help explain where these uncertainties initiate. Developing a better understanding of this teleconnection between SEA rainfall and tropical SST is also important in light of the observed multi-decadal SST variability in the last 30 years which has been linked to regional tropical expansion (Hope et al., 2015) and the global warming slowdown (England et al., 2013).

2. Data and methods

We analyse rainfall variations using the Australian Bureau of Meteorology's current operational high-resolution monthly rainfall data set, generated as part of the Australian Water

Availability Project (AWAP) (Jones et al., 2009). These analyses are at 0.05°×0.05° resolution, or approximately 5 km × 5 km. SEA rainfall is defined as the average rainfall over the main continent south of 33.5°S and east of 135.5°E (the area outlined by the grey box in the top panel of Figure 1, and shown in the bottom panel, Figure 1).

Several global SST datasets exist and Timbal and Hendon (2011) showed that when diagnosing trends over the last 30 to 40 years for the Tripole index described in their study, there is a sizeable variation depending on which dataset used. In the present study, we use the Hadley Centre/UK Meteorological Office SST (HadISST) analyses from 1870 to 2014 interpolated on a 1° by 1° grid (Rayner et al., 2003). The data was further regridded on a 1.5° by 1.5° grid as required to compare with the interpolated CMIP5 model data. The extra-tropical tele-connectivity with SEA rainfall is evaluated using the method developed by Timbal and Hendon (2011). They developed a 'tri-polar' index (Tripole) by examining the spatial distribution of the correlation of tropical SST with the time series of rainfall in SEA and observed three regions of significant correlation (in excess of ±0.2); these regions define the Tripole index. The Tripole is computed as the difference between the mean SST north of Australia (extending from the eastern Indian Ocean and across the Maritime Continent) minus the average of the SST over the central-western Indian Ocean and the central Pacific Ocean. The box boundaries are shown on Figure 1 and their coordinates are provided in Timbal and Hendon (2011). These three boxes cover most of the warm tropical SSTs (above 28°C) in the two oceanic basin influencing Australia and the index has some similarities with the Pacific–Indian Ocean dipole used in Watterson (2012)

The CMIP5 simulations provide a representation of the current climate from 1900 to 2005 using observed external forcings either anthropogenic or natural and plausible representation of the future climate based upon four Representative Concentration Pathways (RCPs) that prescribe anthropogenic greenhouse gas concentration time series which correspond to approximate end-of-century radiative forcing, from low to high of +2.6, +4.5, +6.0, and +8.5 W/m^2. RCP8.5 represents a high future emission pathway and as such produces a large warming response. It is therefore

convenient to use this RCP because the climate change signal is larger than when compared to RCPs with stronger mitigation (for example RCP2.6). To the extent that the projection signal is linear in forcing, using a higher emission scenario can increase the signal to noise in the projection relationships. Indeed, climate change projections generated for the Australian continent using the CMIP5 database (CSIRO and BoM, 2015) show that in general the climate change signal is proportional to the amount of global warming generated including SEA.

In this study we used historical climate simulations, testing each model's ability to replicate the observed climate, as well as one simulation per model of the projected climate change under RCP8.5. In total, an ensemble of 37 models were analysed out of the 48 models entered in the CMIP5 dataset due to limitations on data availability and suitability (Table 1). SEA area-averaged rainfall totals and the Tripole index were computed for each model. Monthly values were computed from 1900 to 2005 (historical climate simulations) and from 2006 to 2100 under RCP8.5. We used the largest set of simulations for which all the required data were available (NB: when several simulations were logged by modelling groups, only one was used: "run 1").

In the set of national projections delivered by CSIRO and BoM (2015), rainfall projections based on RCP8.5 use 39 models (Table 3.3.2 in CSIRO and BoM, 2015). Therefore, the present study targets a very large sample (37 out of 39 models) of the uncertainties attached to the CMIP5-based projections for rainfall (shown in Figure 12). The models used and key characteristics such as horizontal resolution are summarised in Table 1. Model data were first interpolated on a common 1.5 by 1.5 degree grid, SEA rainfall and Tripole time series were computed month by month using all the grid boxes with centres falling within the region of interest shown in Figure 1. It is worth noting that for SEA rainfall only grid boxes covering the State of Victoria are included, which is a smaller domain than the SEA box. It was noted as part of the validation of the models that the ensemble mean rainfall was biased toward too low rainfall during the wet (cool season) part of the year. This is very likely due to the difficulty of simulating rainfall over the orography of the Great Dividing Range with relatively coarse model resolution, rather than being due to model systematic biases as this is also noted for other high rainfall areas across southern Australia which also have significant orography

(South West of Western Australia, southern part of South Australia and Tasmania). Hence the SEA rainfall was better captured using model grid boxes limited to those covering the State of Victoria where rainfall is higher than further north providing a better match with observations and thus removing a key biases across most climate models.

We first report on the CMIP5 models' ability to reproduce SEA rainfall, its variability and how it relates to tropical modes of variability as captured by the Tripole index. Previous studies have already evaluated the performance of these models; in Table 1, some key evaluation metrics from previous studies relevant to this particular study are indicated (NB: 3 models considered in this study were uploaded to the CMIP5 database later than the others and hence are not included in these previous studies: CESM1-CAM5-1-FV2, FGOALS-s2 and MRI-ESM1).

Three of these metrics are based on the skill score developed by Watterson (1996) called the M-statistic. The M-statistic is a function of temperature, rainfall, and mean sea level pressure and scores are shown here for the entire Australian continent, and southern Australia (See Table 5.2.2 in CSIRO and BoM, 2015). Also shown is the M-statistic for rainfall only across Australia (See Table 5.2.4 in CSIRO and BoM, 2015). In Table 1, good performances are indicated by bold blue figures (above 690 for the M-statistics across Australia, and 540 for Southern Australia and 560 for precipitation across Australia) and poor performance by bold red figures (respectively below 600, 460 and 440). As part of the complete model evaluation performed to deliver Australia-wide projections (CSIRO and BoM, 2015), several other evaluation tests were utilized. A summary of the number of tests for which individual models performed poorly (See Table 5.6.1 in CSIRO and BoM, 2014) is also provided for the models selected in this study. Models that did not fail any test are shown in bold blue while models that failed three tests or more are shown in bold red.

Besides examining the influence of tropical SSTs on SEA rainfall as a way to interpret the range of uncertainties in rainfall projections, we are also interested in the global model warming response. This is captured by providing the linear global mean warming for each model under the RCP 8.5 scenario (last column in Table 1 in degrees Celsius multiply by 100 years). In most instances

211 across the Australian climate change projections generated from the CMIP5 data base, it was found
212 that the strength of the climate change signal for any variable, but in particular rainfall, is proportional
213 to the amount of global warming (See section 6.2.3 in CSIRO and BoM 2015; Watterson and Whetton
214 (2011 and 2013)) and is commonly used to compare signals between various emissions scenarios and
215 for different time-slices in the future. Here we will use it to evaluate if the range of SEA rainfall
216 projections is linked to the range of warming trends over the century projected by individual models.

217 Another relevant metric of model performance is the model's ability to reproduce the position
218 of the STR across Eastern Australia which has a well-established annual cycle (Drosdowsky, 2005)
219 and relationship with SEA rainfall (Timbal and Drosdowsky, 2013). This was evaluated by Grose et
220 al., (2015b); using their results we classified the CMIP5 models here into three categories: 1) the
221 model was able to capture the signature of the regional STR in the same longitudinal band as the
222 reanalysis (shown in blue, Table 1), or 2) within an overlapping band no wider than 30 degree or 3) a
223 longitude band which did not overlap the reanalyses band or was larger than 30 degree (shown in red,
224 Table 1).

225 The various evaluations considered in Table 1 show that of the 37 models, quite a spread in
226 performance exists. Only one model is amongst the better performer for all the statistics considered
227 (CNRM-CM5), but many are for several criteria; in total 17 models are amongst the better models for
228 at least one statistic and never amongst the poorest performer for any statistics. Amongst poor
229 performers, only one model is amongst the poorest performer for all statistics (MIROC-ESM-CHEM)
230 but many are for several criteria. In total 12 models are amongst the poorest group for at least one
231 statistic and never amongst the better performers for any statistics. Overall, based on past studies there
232 is a group of 17 models which are "better" performers 12 models which are "poorer" performers and 8
233 models in between. However, this evaluation, while relevant, is preliminary and needs to be
234 confirmed by looking at these models' ability to reproduce specifically SEA rainfall, its variability
235 and how it relates to tropical modes of variability as captured by the Tripole index. An updated
236 classification of models, based on this wider set of criteria, is provided in the next Section.

3. Results:

3.1 Validation of the current climate simulations

3.1.1 South-Eastern Australia Rainfall

Model simulation of SEA rainfall is analysed by looking at the mean, variability and trends as well as the relationship between the SEA rainfall and the Tripole index amongst the 37 CMIP5 models available. The model ensemble mean computed using the grid boxes within the State of Victoria is compared to both observed rainfall for Victoria (dashed line) and for the entire SEA box (full line in Figure 2). Climate averages are computed for the 1900 to 2005 period for every month. Due to a general dry bias inherent to coarse climate model resolution, the modelled rainfall for the grid boxes contained within the boundary of the State of Victoria is the best proxy for SEA rainfall and is used for the rest of the study. This full ensemble mean is within 3 mm of the observed SEA rainfall during the cool season from April to October. However, it has a relatively flat annual cycle with December and January rainfall being too high. The models are ranked according to the Euclidean distance between the individual model annual cycle and the observations, the models with the 10 smallest (largest) Euclidean distances are classified as best (worst) (see Table 2 for full results). The ensemble mean of the “best” 10 models for this metric is very close to the observed rainfall for the entire year. The ensemble mean of the 10 “worst” models is generally too wet throughout the year, but the largest bias is observed during the warm months (November to March). This contributes to the wet bias in summer observed in the full ensemble mean.

The overestimation of summer rainfall mean also impacts the computation of the standard deviation (Figure 2, lower panel). As per the mean, this affects only some of the CMIP5 models; the ensemble mean of the "best" 10 models is close to the observations. The summertime rainfall overestimation amongst some models appears to be the most significant discrepancy in the CMIP5 models’ ability to capture the SEA rainfall. Models which have largest mean summer rainfall have also largest standard deviation for summer rainfall, which is expected (Figure 3, upper panel).

However, once the coefficients of variation are used (i.e. standard deviations normalised by the mean), a strong opposite linear relationship emerges (Figure 3, lower panel). This suggests that generally, models with high summer rainfall tend to have comparatively lower year-to-year variability implying more consistent summer rainfall.

In particular 15 models (green symbols in Figure 3) were identified as being too wet in summer, with a number having a reversed annual cycle (e.g. a summer peak for rainfall). These 15 models are: CCSM4, CESM1-BGC, CESM1-CAM5, CESM1-CAM5-1-FV2, CNRM-CM5, GISS-E2-H, GISS-E2-H-CC, GISS-E2-R, GISS-E2-R-CC, inmcm4, MIROC5, MIROC-ESM, MIROC-ESM-CHEM, NorESM1-M and NorESM1-ME. From a global perspective, these models tend to have too strong Inter-Tropical Convergence Zone (ITCZ) with excess rainfall and have a notably weak or absent South Pacific Convergence Zone (SPCZ) and a strong dry bias across the Indonesian archipelago (Figure 4). While both groups of models simulate too much rainfall across Australia in summer, the errors are larger and affect the entire continent, in the group of models identified as having a too wet (south-east) summer. Thus, the very wet SEA summer simulated by this group of models does not appear to be a local error but rather a large-scale problem linked to the way that tropical precipitation is represented in these models. This casts doubt on the ability of this group of models to capture the relationship between SEA rainfall and tropical SST variability, which is being investigated. We will therefore aim to quantify the impact of including these models in the ensemble mean.

Finally, linear trends were computed for each CMIP5 model for the last 30 years from 1985 to 2014 (including the end of the historical simulation of the current climate, which ends in 2005 and the start of the RCP8.5 future emission scenario from 2006). During this period, observed SEA rainfall has experienced a marked reduction during the cool season (from April to October) with serious hydro-climatic consequences (CSIRO and BoM, 2012). This cool season decline is counteracted somewhat by a small warm season increase, resulting in a negligible annual decline (Figure 5). Individual climate models simulate monthly rainfall trends that are at times as large as observed, but

292 are highly variable from one month to the next with very little consistent behaviour. Indeed, the
293 ensemble mean indicates no systematic 30-year trends of either dry or wet throughout the year. Even
294 the 10 “best” models, which best match the observed annual cycle have little trend. Only one model
295 (IPSL-CM5B-LR) has a negative rainfall trend, which is of similar magnitude to the observed
296 (indicated in Figure 5).
297
298 **3.1.2 Tropical Tripole index**
299 Moving to the evaluation of the CMIP5 models’ performances in the tropics that are of
300 relevance to SEA rainfall, the mean Tripole index has a clear annual cycle with negative values from
301 May to October and positive values during the warm season (Figure 6, upper panel). The CMIP5
302 models largely reproduce the annual cycle but with a general bias leading to more positive values (i.e.
303 warmer central box SSTs) from December to August. This tendency is seen across nearly all CMIP5
304 models including when the “best” models for that metric are considered. More importantly, since the
305 Tripole has been constructed to capture inter-annual variability in the tropics, the annual cycle of the
306 standard deviation computed from 1900 to 2005 (Figure 6, lower panel) is of great interest. In the
307 observations, the largest variability is seen in late winter and spring (July to November). Whilst the
308 CMIP5 models give a range of annual cycles, the ensemble mean mimics the observed one well,
309 although with somewhat too large variability in summer. There are a number of models which have
310 too much variability all year around, as can be seen from the ensemble mean of the 10 “worst”
311 models.
312
313 In the last 30 years, there has been a large annual mean warming trend across the Indian
314 Ocean, the Maritime Continent and Western Pacific, with opposite cooling in the Central and Eastern
315 Pacific (Figure 1). As per rainfall, linear trends in the Tripole index from 1985 to 2014 were
316 computed for both observations and the CMIP5 models (Figure 7). These Tripole trends are not very
317 large (due to the two negative poles having opposite trends: cooling in the Central Pacific box and
318 warming in the Indian Ocean box against a warming trend in the Maritime Continent box). The annual

cycle of the observed trend shows a small increase in most months apart from June and August. In contrast to the observations, the ensemble mean of CMIP5 models shows a consistent cooling trend for all months in the vicinity of -0.05°C for the 1985-2014 period. There is considerable range across the 37 models considered (grey lines in Figure 7); within that range it is possible to identify 10 models (their mean is labelled "best" models in Figure 7) that have very similar trends to the observed.

3.1.3 Tripole-rainfall relationship

Having evaluated the tropical SST variability and SEA rainfall separately, the ability of the models to capture the observed relationship between the two is now evaluated, as well as the role this relationship might play in explaining the range of behaviour displayed by the CMIP5 models. Overall, the CMIP5 models ability to simulate this tropical-extratropical teleconnection is convincing (Figure 8). Although the largest observed correlation coefficients in July to November (around 0.4) are underestimated by the ensemble mean (around 0.3), the annual cycle and the peak in late winter-spring is well captured. The ensemble mean of the “best” 10 models is similar to the observations. One aspect of the Tripole-SEA rainfall relationship is its fluctuations on decadal times-scales. This was shown by Timbal and Hendon (2012) and arises from well-known decadal variability such as the Inter-decadal Pacific Oscillation (IPO) and its impact on Australian rainfall (Power et al., 1999). Computing the correlation coefficients for the July to November averaged SEA rainfall and Tripole in 50 years periods (Figure 9) shows a marked difference between 1900-1949 (0.50) and 1956-2005 (0.65). These differences are even larger when annual values are considered (0.33 and 0.66, not shown). Some individual CMIP5 models do reproduce differences between 50 year periods of similar magnitude either positive or negative (individual models in Figure 9), but as far as the ensemble mean is concerned, there is no indication of a systematic shift either in the past century for the last 50 years or the two 50-year periods of the 21st century under RCP8.5 pathways. Thus it appears that shifts in the strength of the relationship between tropical variability and SEA rainfall are possible due to internally generated decadal variability (reproducible by climate models) as occurred in the 20th century and are also possible in the future (i.e. individual models do have changes of this magnitude

346 between future 50 year periods). But based on these results, any such shift towards a reduction or an
347 increase in the strength of the relationship during the 21st century cannot be ascribed to anthropogenic
348 forcing as there is no indication of such a change in the ensemble mean.
349
350 Since the CMIP5 models (or at least a subset thereof) appear to have a realistic relationship
351 between tropical SSTs and SEA rainfall, it is worth investigating if some of the observed differences
352 amongst model climatologies in SEA rainfall may be related to how the models behave in the tropics.
353 Moderate (around 0.5) and significant (99% level) relationships were found between the magnitude of
354 year-to-year variability in July to November of both rainfall and the Tripole. This was measured using
355 standard deviation of the two quantities computed for each individual model for the period 1956 to
356 2005 (Figure 10, top panel, r=0.50). The strength of the relationship varies if different months are
357 considered (Table 3). That relationship is moderate in spring, for the July to November and the cool
358 season (April to October) period, but is non-existent for the summer months, thus giving only a weak
359 relationship for the annual means (Table 3).
360
361 As a way to investigate the cause of model SEA rainfall variability, the relationship between
362 the model scatter of SEA rainfall variability and the strength of the SEA rainfall-Tripole correlation in
363 models was investigated. The relationship was found to be strong over the 1956-2005 period (Figure
364 10, bottom panel, R=0.60) accounting for more than a third of the range of rainfall inter-annual
365 variability in the July to November period indicating that climate models' ability to capture the
366 observed inter-annual variability in SEA rainfall is driven by the strength of the teleconnections
367 between the tropics and SEA within each model. The figure shows that some models are clear outliers
368 (these are the four models from the NASA/GISS research centre in the U.S.A.); without these models
369 the relationship increases to R=0.77 explaining 60% of the range. The same seasonality is observed
370 as per the previous relationship: strongest relationship in spring or July-November, also strong in
371 April to October and non-existent in summer, limiting the strength of the relationship for the annual
372 means.
373

In the case of SEA rainfall trends, a weaker and less significant relationship is found amongst the model scatter between SEA rainfall trends and Tripole trends across the CMIP5 models over the 1985-2014 period. Although this period is when most of the cool season rainfall decline has been observed (Table 3), the relationship is stronger when the full historical simulations are considered. The strongest relationship is observed in the cool season April to October (R=0.58), explaining about a third of the range of rainfall trends amongst models. This result indicates that, as expected from the inter-annual relationship, models that exhibit a trend in tropical SST, which project positively (negatively) on the Tripole tend to deliver a positive (negative) rainfall trend in SEA. However, it is worth remembering that these trends are small in comparison to the observed one (see earlier section and Figures 4 and 6).

3.2 Analysis of the future climate simulations

We now turn to investigate whether the SEA rainfall-Tripole relationship can help to better understand the range of future projections of SEA rainfall generated by the CMIP5 models. The first part of this investigation considers the projected changes in tropical SSTs generated by the CMIP5 models. The CMIP5 multi-model mean tends to display global warming with the strongest tropical warming located in the Eastern Equatorial Pacific. However, projected changes in the Tripole index are small (Figure 11). There is, however, a large range of responses across the models, with some displaying trends as large as 1 °C for particular months, either positive or negative. This is shown in particular in the key part of the annual cycle most strongly relating to SEA rainfall, April to October. Many of the models indicating large positive trends in the Tripole index are amongst the group of models with very wet summer identified earlier, leading to the ensemble mean of these models indicating a small positive trend for the Tripole index, especially for the months from April to November. Excluding these models (to produce the ensemble mean labelled “other models” in Figure 11) leads to a larger negative trend for the Tripole index for that critical part of the year (April to November). Beside the differences in trends in the Tripole index annual cycle, it is noteworthy that

overall the ensemble of models with very wet summer have less warming in the Tripole index than the "other" group for which the tropical warming is stronger in the Eastern Pacific. In addition, at high latitudes in the Southern Hemisphere where the warming is less than further equatorward, it is weaker in the "other" group of models. Therefore the "other" group have a warming pattern that will cause a greater increase of the climatological SST gradient between equator and pole in the Southern Hemisphere.

The ensemble mean SEA rainfall projections show a drying trend from May to November and a small positive trend during the warm season (Figure 12, top panel). It bears some resemblance to the observed trends over the last 30 years (shown in Figure 4), with the difference that the projected future rainfall decreases are greatest in austral spring (SON) while the observed cool season decline is greatest in austral autumn (MAM). That seasonality of the future projections is depicted further for SEA as well as sub-regions within that box (lower panels in Figure 12, N.B. in percentage change while the top panel is in absolute change), showing slight differences in the mean projected change south or north of the Great Dividing range across southern Victoria.

As can be seen in Figure 12, the spread of SEA rainfall projections amongst the CMIP5 models is very large. Of interest is the behaviour of the group of 15 models that simulate a very wet summer for the current climate. The "very wet model" ensemble mean displays an annual cycle of trends similar to the full ensemble mean, but on the wetter side (Figure 12: larger positive trends in the warm season and smaller negative trends in the cool season), leading to negligible trends in the annual mean (Table 4). As a result the ensemble mean of the "other models" projects stronger rainfall declines all year round (Figure 12). The difference from the full ensemble mean leads to a mean signal in excess of 50% greater reduction in rainfall across the entire cool season and spring (Table 4). The difference in the rainfall projections between these two groups of models is not limited to the SEA. A global perspective (Figure 13) shows sizeable differences in projected rainfall changes by the end of the 21st century compared to the end of the 20th century including a very large rainfall increase in the ITCZ in the "other models" group, larger than for the "very wet summer" group. This difference exists in both

austral summer (DJF) and winter (JJA), but in winter it is coupled with a reduction of rainfall in the sub-tropical band of the Southern Hemisphere and in particular across the Australian continent including SEA. In the "other models" group, that reduction is much larger than the "very wet summer" group, leading to the sizeable differences in ensemble mean reported in Table 4.

There is a general expectation that the projected rainfall decline in the cool season is proportional to the emission pathways used to force the models and the subsequent global warming projected for each pathway (CSIRO and BoM, 2015). We do find evidence of this in the magnitude of the projected rainfall decline for SEA and sub-regions in Victoria, as the magnitude of the austral winter and spring decline increases with the severity of the emission pathways (bottom panel in Figure 12 from RCP 2.6 to RCP 8.5). However, there is only a weak relationship amongst the 37 CMIP5 models considered here between global warming and SEA rainfall changes (R=-0.34, significant at the 95% level). The two quantities used are a proxy for the sensitivity of the models, expressed as the amount of global warming simulated during the 21st century under the RCP 8.5 pathways, and the magnitude of the rainfall decline (in the cool season). The relationship is non-existent for austral summer and non-significant for the annual mean (Table 5).

The scatter in projected rainfall trends amongst models was evaluated further by relating it to the Tripole trends projected by the same model (Figure 14 and Table 5). A very strong and highly significant relationship was found for the annual mean (R=0.65). The correlations are higher for the critical time of the year where the relationship is known to peak (July to November) reaching R=0.75, and equally very high for the key season in term of SEA rainfall (April to October). In contrast, the relationship is almost non-existent in austral summer (DJF: R=0.23). With such a small sample, correlation coefficients can be affected by a single case. In Figure 14 for both July to November and Austral summer a single model is a clear outlier (CSIRO-mk3.6). Without this model, the picture is even clearer, with a stronger relationship in the cool season and July to November and a correlation below 0.1 in summer (Table 5). It is worth noting that although the "very wet summer" models are clustered towards the more positive rainfall trend, as expected from ensemble mean results (Table 4),

457 removing them only marginally reduces the overall range of projections as both groups of models are
458 widely scattered.
459
460
461 **Discussion and conclusions**
462
463 37 CMIP5 global climate models are examined for this study. They were assessed for their
464 ability to reproduce both observed SEA rainfall and the relationship between rainfall and a tropical
465 Tripole index. The model means, inter-annual variability and trends as well as the relationship
466 between the two quantities were investigated and found to match observations sufficiently well to
467 warrant using this relationship as a tool to analyse future projections. Indeed some of the range of
468 model simulations of SEA rainfall appears to be related to the way they capture the relationship
469 between SEA rainfall and tropical SST or how the tropical SSTs behave in the climate models and in
470 turn affect the SEA rainfall.
471
472 In terms of model assessment and the ability to identify a group of better performing models, all the
473 metrics evaluated were measured between individual models and observations using Euclidean
474 distance across the annual cycle. A group of ten models emerged that were never amongst the worst
475 performers for any statistics. Of these ten, nine were already identified from earlier studies (CSIRO
476 and BoM, 2015) amongst the 17 better performers: ACCESS1.0, CESM1-CAM5, CMCC-CM, CMC-
477 CMS, FGOAL-g2, HadGem2-CC, MPI-ESM-LR, MPI-ESM-MR and MRI-GCM3. At the other end
478 of the spectrum, seven models are amongst the worst performers for at least one statistic and never
479 amongst the better one for any statistics. Amongst these seven models, five were also identified from
480 previous studies (CSIRO and BoM 2015) as being amongst the poorest performers: CAN-ESM2,
481 GISS-E2-H, GISS-E2-H-CC, GISS-E2-R and NorESM1-ME. Outside these two groups, most model
482 performances vary across the range of metrics considered, underlining the difficulties in model
483 ranking.

A group of models was identified as having a very wet summer, with low relative inter-annual variability and in most cases a reversal of the annual cycle with more rain in the warm rather than cool season. These 15 “very wet summer” models are consistent with the other evaluation metrics: i.e. the entire group of seven worst performers was included in that group, and only one from the group of ten better performers was included (CNRM-CM5). Overall, the contrast between the two groups of models is significant in terms of the various metrics considered: while the “very wet summer” group has metrics in the bottom 10 performances 50% of the time, with 32% in the average and 18% in the top performances, the “other” group has 11% of metrics in the bottom 10 performances, with 56% in the average and 33% in the top performances.

It was noted that representing the spatial maximum in rainfall at the very southern edge of the Australian continent (SEA in particular) does pose a challenge to coarse resolution climate models as the higher rainfall in SEA compared to further inland is due to the interaction between moisture fluxes and coastal and orographic features. This was dealt with by using only a limited number of grid box from models (those covering Victoria) to represent the entire SEA. However, that overall limitation, due to resolution, does not explain how models could get more rainfall than observed as it is unlikely to be due to model resolution (Figure 2 shows that Victoria rainfall is not higher than SEA rainfall in summer) thus casting doubt on these models with very wet summers. We speculate that the source of the excess summer rainfall in these models is overly frequent tropical moisture inflow across the continent but further examination of the mechanisms operating in these models is beyond the scope of the current study.

There is a general expectation that the projected rainfall decline in the cool season increases with emissions and warming. We do find evidence of this in the magnitude of the projected rainfall decline for SEA region and sub-regions within Victoria. However the model temperature sensitivity to emissions does not appear to relate significantly to the strength of the projected rainfall response.

In contrast, the relationship between the projected rainfall decline and the pattern of tropical warming are related. We find that up to 60% of the range in SEA cool season rainfall projections is explained in terms of how the individual model's tropical warming projects on the Tripole. Therefore, this Tripole index is a relevant tool to monitor future SST warming in the near future, and in future projection work and how it may impact on future SEA rainfall trends. The spatial pattern of SST warming in the tropical Pacific was also found to be an important influence on northern Australian rainfall projections (Brown et al., 2016). It confirms the importance of patterns of tropical warming in driving range of rainfall projections across Australia from climate models as was noted by Watterson (2012) for the CMIP3 generation of models. Furthermore, it is worth noting that this approach of mapping range of future projections on established modes of variability for a particular regional climate is also likely to provide useful insights for other parts of the world.

It was also noted that while the observed teleconnection between tropical modes of variability and SEA rainfall has marked multi-decadal variability during the 20th century, similar multi-decadal variability exist and are internally generated by models. However, the ensemble mean shows a stable picture for past and future centuries, suggesting no change in the magnitude of this relationship is to be expected in response to anthropogenic forcing and the observed changes in the last 100 years is not in response to external forcings. This is consistent with many studies about the influence of natural multi-decadal variability on regional rainfall (IPCC, 2013).

Finally, it appears that the current range of model projections is influenced by a group of models which were found to have a poorer simulation of the rainfall annual cycle in SEA with very wet summers. These models also performed notably worse on a range of metrics considered in this study and previously. Excluding this group of models significantly increases the mean model rainfall decline projections (by about 50%) in Victoria and more broadly across SEA. Although based on different criteria of models evaluation, this conclusion is supported by recent findings by Grose et al. (2016). It is unclear why such a difference exists between the two groups of models - one hint comes from the pattern of future warming, which appears to have a larger temperature gradient between the

tropics and high latitudes for the "other" group of models. This is likely to impact changes in the mean meridional circulation, which have been shown to be important for SEA rainfall (Nguyen et al., 2013). While the mean signal is markedly different, the range of projections is not affected significantly by the omissions of that group of models, indicating that weaker future rainfall reductions cannot be entirely ruled out.

Acknowledgments:

We acknowledge the World Climate Research Programme's Working Group on Coupled Modelling, which is responsible for CMIP, and we thank the climate modelling groups (listed in Table 1) for producing and making available their model output. BT and SF contribution to this work was supported by the Victorian Climate Initiative (VicCI). JRB was supported by the Australian Climate Change Science Programme, jointly funded by the Department of the Environment, the Bureau of Meteorology and CSIRO. D. Jones and R. Colman (Bureau of Meteorology) provided useful comments on an earlier draft of this manuscript.

557 **References**

558

559 Brown JR, Moise AF, Colman R, Zhang H (2016) Will a warmer world mean a wetter or drier
560 Australian monsoon? J. Climate, doi:10.1175/JCLI-D-15-0695.1
561 Bureau of Meteorology (2012) Australia's wettest two-year period on record; 2010-11, Special
562 Climate Statement No. 38, National Climate Centre, Bureau of Meteorology,
563 www.bom.gov.au/climate/current/statements/scs38.pdf
564 CSIRO and Bureau of Meteorology (2012) Climate Change and water availability in south-eastern
565 Australia: A synthesis of findings from Phase 2 of the South Eastern Australian Climate
566 Initiative (SEACI), CSIRO, Australia
567 CSIRO and Bureau of Meteorology (2015) Climate Change in Australia Information for Australia's
568 Natural Resource Management Regions: Technical Report, CSIRO and Bureau of
569 Meteorology, Australia
570 Dowdy A, et al (2015) East Coast Cluster Report, Climate Change in Australia Projections for
571 Australia's Natural Resource Management Regions: Cluster Reports", eds. Ekström, M. et
572 al.,, CSIRO and Bureau of Meteorology, Australia
573 Drosdowsky W, (2005) The latitude of the subtropical ridge over eastern Australia: the L index
574 revisited. Int. J. Climatol. 25 1291-1299
575 England MH, McGregor S, Spence P, Meehl GA, Timmermann A, Cai W, Sen Gupta A, McPhaden
576 MJ, Purich A, Santoso A (2014) Recent intensification of wind-driven circulation in the
577 Pacific and the ongoing warming hiatus. Nature Climate Change, 4 222–227,
578 doi:10.1038/nclimate2106
579 Fiddes S, Timbal B (2016) Assessment and reconstruction of catchment streamflow trends and
580 variability in response to rainfall across Victoria, Australia. Clim. Res., 67, 43-60,
581 doi:10.3354/cr01355

582 Grose M, Timbal B, Wilson L, Bathols J, Kent D (2015a) The subtropical ridge in CMIP5, and
583 implications for projections of rainfall in southeast Australia. Aust. Met. & Ocean. J., 65, 90-
584 106
585 Grose M, et al (2015b) Southern Slopes Cluster Report, Climate Change in Australia Projections for
586 Australia's Natural Resource Management Regions: Cluster Reports, eds. Ekström, M. et
587 al.,,CSIRO and Bureau of Meteorology, Australia
588 Grose, M., J. Risbey, A. Moise, S. Osbrough, C. Heady, L. Wilson, and T. Erwin, 2016: Constraints
589 on southern Australian rainfall change based on atmospheric circulation in CMIP5
590 simulations. J. Climate. doi:10.1175/JCLI-D-16-0142.1, in press.
591 Hope P, Timbal B, Hendon H, Ekström M (eds.) (2015) Victorian Climate Initiative annual report
592 2014-15, Bureau Research Report, 5 128pp
593 IPCC (2013) Climate Change 2013: The Physical Science Basis. Contribution of Working Group I to
594 the Fifth Assessment Report of the Intergovernmental Panel on Climate Change. In:
595 STOCKER, T. F., D. QIN, G.-K. PLATTNER, M. TIGNOR, S. K. ALLEN, J. BOSCHUNG,
596 A. NAUELS, Y. XIA, V. BEX AND P. M. MIDGLEY (ed.)
597 Jones DA, Wang W, Fawcett R (2009) High-quality spatial climate data-sets for Australia. Aust.
598 Meteorol. Ocean. J. 58 233-248
599 Kent DM, Kirono D, Timbal B, Chiew FHS (2011) Representation of the Australian sub-tropical
600 ridge in the CMIP3 model. Int. J. of Clim., 33(1), 48-57, DOI: 10.1002/joc.3406
601 Leblanc M, Tweed S, Van Dijk A, Timbal B (2012) A review of historic and future hydrological
602 changes in the Murray-Darling Basin. Global Planetary Change, 80 226-246
603 doi:10.1016/j.gloplacha.2011.10.012
604 Lim E-P, Hendon HH (2015) Understanding and predicting the strong Southern Annular Mode and its
605 impact on the record wet east Australian spring 2010. Climate Dynamics, 44 2807-2824,
606 DOI:10.1007/s00382-014-2400-5
607 Nicholls N (2010) Local and remote causes of the southern Australian autumn−winter rainfall decline
608 1958−2007. Clim. Dyn., 34, 835–845

609 Nguyen H, Evans A, Lucas C, Smith I, Timbal B (2013) The Hadley Circulation in Reanalyses:
610 climatology, variability and expansion, J. Climate 26(10), 3357-3376
611 Nguyen H, Lucas C, Evans A, Timbal B, Hanson L (2015) Expansion of the Southern Hemisphere
612 Hadley Cell in response to greenhouse gas forcing. J. Climate 28, 8067-8077
613 Power S, Casey T, Folland C, Colman R, Mehta V (1999) Inter-decadal modulation of the impact of
614 ENSO on Australia. Clim. Dyn. 15, 319-324
615 Rayner NA, Parker DE, Horton EB, Folland CK, Alexander LV, Rowell DP, Kent EC, Kaplan A
616 (2003) Global analyses of sea surface temperature, sea ice, and night marine air temperature
617 since the late nineteenth century. J. Geophys. Res. 108 (D14), 4407,
618 DOI:10.1029/2002JD002670
619 Reynolds RW, Smith TM, Liu C, Chelton DB, Casey KS, Schlax MG (2007) Daily high-resolution
620 blended analyses for sea surface temperature. J. Climate 20, 5473-5496
621 Smith I, Timbal B (2012) Links between tropical indices and southern Australia rainfall. Int. J. of
622 Clim., 32(1), 33-40, DOI: 10.1002/joc.2251
623 Taylor KE, et al (2012) An Overview of CMIP5 and the Experiment Design. Bull. Amer. Meteor.
624 Soc., 93(4), 485-498
625 Timbal B, Arblaster J, Braganza K, Fernandez E, Hendon H, Murphy B, Raupach M, Rakich C, Smith
626 I, Whan K, Wheeler M (2010) Understanding the anthropogenic nature of the observed
627 rainfall decline across south-eastern Australia. CAWCR Technical Report 26 180pp, ISSN:
628 1835-9884
629 Timbal B, Drosdowsky W (2013) The relationship between the decline of South Eastern Australia
630 rainfall and the strengthening of the sub-tropical ridge, Int. J. of Clim., 33(4) 1021-1034,
631 DOI: 10.1002/joc.3492
632 Timbal B, Fawcett R (2013) An historical perspective on South Eastern Australia rainfall since 1865.
633 J. Climate 26(4) 1112-1129
634 Timbal B, Hendon H (2011) The role of tropical modes of variability in recent rainfall deficits across
635 the Murray-Darling basin. Water Res. Res., 47(12), W00G09. ZOI:10.1029/2010WR009834

636 Timbal B, Griffith M, Tan KS (2015a) Rainfall and streamflow in Greater Melbourne catchment
637 areas: variability and recent anomalies. Clim. Res., 63 215-232, doi:10.3354/cr01296
638 Timbal B, et al (2015b) Murray Basin Cluster Report, Climate Change in Australia Projections for
639 Australia's Natural Resource Management Regions: Cluster Reports, eds. Ekström, M. et al.,,
640 CSIRO and Bureau of Meteorology, Australia
641 Van Vuuren D P, Edmonds J, Kainuma M, Riahi K, Thomson A, Hibbard K, Hurtt GC, Kram T, Krey
642 V, Lamarque J-L (2011) The representative concentration pathways: an overview. Clim.
643 Change 109, 5-31
644 Watterson I (1996) Non-dimensional measures of climate model performance. Int. J. of Clim. 16, 379-
645 391
646 Watterson I (2010) Relationships between south-eastern Australian rainfall and sea surface
647 temperatures examined using a climate model. J. Geophys. Res. 115, D10108,
648 doi:10.1029/2009JD012120
649 Watterson I (2012) Understanding and partitioning future climates for Australian regions from
650 CMIP3 using ocean warming indices. Clim. Change 111(3-4), 903-922,
651 DOI:10.1007/s10584-011-0166-x
652 Watterson IG and Whetton PH (2011) Distributions of decadal means of temperature and precipitation
653 change under global warming. J. of Geo. Res.: Atmospheres 116 1984–2012
654 Watterson IG and Whetton PH (2013) Probabilistic projections of regional temperature and
655 precipitation extending from observed time series. Clim. Change 1-15
656

Table 1: The 37 *CMIP5 climate models used in this study; model name; institution; atmospheric resolutions (size of a single grid cell in km); results of previous evaluations of these models relevant to South-Eastern Australian climate: skill score (M-statistic, Watterson, 1996) averaged across temperature, rainfall and mean sea level pressure for the entire Australian continent and southern Australia (See Table 5.2.2 in CSIRO and BoM, 2015) and for rainfall alone across Australia (See Table 5.2.4 in CSIRO and BoM, 2015); a summary of the number of tests for which individual models performed poorly (See Table 5.6.1 in CSIRO and BoM, 2015); and an evaluation of the model ability to reproduce the sub-tropical ridge at the correct longitude above eastern Australia (see Grose et al.,, 2015). The last column indicates the global warming trends for the RCP8.5 emission pathway. See data section of this study for additional details. NB: score in bold blue (red) indicates good (poor) performance.*

Model	Institution Name and country	Lat. grid size (km)	Lon. grid size (km)	M-Stat. Aus.	M-Stat. Sou. Aus.	M-Stat Prec. Aus.	Poor Perf.	STR	RCP 8.5 GW
ACCESS1-0	CSIRO-BOM, Australia	210	130	**727**	**575**	552	1	2	4.63
ACCESS1-.3	CSIRO-BOM, Australia	210	130	**691**	492	544	2	2	4.58
bcc-csm1-1	BCC, CMA, China	310	310	684	464	499	**0**	**1**	3.86
bcc-csm1-1-m	BCC, CMA, China	120	120	**711**	**573**	525	**0**	2	3.44
BNU-ESM	BNU, China	310	310	**564**	**388**	451	**3**	**3**	4.85
CanESM2	CCCMA, Canada	310	310	**706**	**542**	492	1	2	4.90
CCSM4	NCAR, USA	130	100	642	519	**379**	1	2	3.97
CESM1-BGC	NSF-DOE-NCAR, USA	130	100	653	518	**400**	1	2	3.92
CESM1-CAM5	NSF-DOE-NCAR, USA	130	100	659	**589**	493	**0**	2	4.70
CESM1-CAM5-1-FV2	NSF-DOE-NCAR, USA	275	210						
CMCC-CESM	CMCC, Italy	410	410	**549**	**355**	479	1	**3**	4.25
CMCC-CM	CMCC, Italy	78	78	663	**583**	486	**0**	**1**	4.85
CMCC-CMS	CMCC, Italy	210	210	672	471	**564**	1	**1**	4.99
CNRM-CM5	CNRM-CERFACS, France	155	155	**706**	**587**	**602**	**0**	**1**	3.98
CSIRO-mk3.6	CSIRO-QCCCE, Australia	210	210	613	**431**	**482**	2	**3**	4.67
FGOAL-g2	LASG-CESS, China	310	310	653	518	535	**0**		3.43
FGOALS-s2	LASG-CESS, China	190	310						
GFDL-CM3	NOAA, GFDL, USA	275	220	676	**546**	**564**	1	2	5.17
GFDL-ESM2G	NOAA, GFDL, USA	275	220	638	467	472	**3**	2	3.13
GFDL-ESM2M	NOAA, GFDL, USA	275	220	607	**383**	469	**0**	2	3.01
GISS-E2-H	NASA/GISS, NY, USA	275	220	**586**	458	490	**4**	2	3.21
GISS-E2-H-CC	NASA/GISS, NY, USA	110	110	**581**	473	501	**3**	2	3.12
GISS-E2-R	NASA/GISS, NY, USA	275	220	**575**	516	461	**3**	**3**	2.72
GISS-E2-R-CC	NASA/GISS, NY, USA	110	110	614	**543**	472	**0**	2	2.76
HadGEM2-CC	MOHC, UK	210	130	**698**	533	541	**0**	**1**	5.30
HadGEM2-ES	MOHC, UK	210	130	**720**	**556**	**561**	1	2	5.19
INMCM4	INM, Russia	220	165	657	**455**	524	**3**	2	3.09
IPSL-CM5B-LR	IPSL, France	410	210	625	**424**	**596**	1	**3**	3.87
MIROC5	JAMSTEC, Japan	155	155	644	488	**432**	**0**	2	3.69
MIROC-ESM	JAMSTEC, Japan	310	310	**549**	**434**	**342**	**0**	**3**	5.35
MIROC-ESM-CHEM	JAMSTEC, Japan	310	310	**561**	**450**	**333**	**4**	**3**	5.60
MPI-ESM-LR	MPI-N, Germany	210	210	**720**	**542**	**593**	1	2	4.01
MPI-ESM-MR	MPI-N, Germany	210	210	**705**	513	**640**	1	**1**	4.02
MRI-CGCM3	MRI, Japan	120	120	659	511	**599**	1	**1**	3.84
MRI-ESM1	MRI, Japan	120	120						
NorESM1-M	NCC, Norway	275	210	604	480	**347**	1	2	3.62
NorESM1-ME	NCC, Norway	275	210	**594**	475	**343**	1	2	3.78

Table 2: *Evaluation of the reproduction of the annual cycle of some key quantities by the 37 CMIP5 models considered using Euclidean distance between the model values and the observations. See results section for additional details. NB: score in bold blue (red) indicate the top (bottom) 10 performances.*

	Rainfall			Rain-Tripole
	Mean	STD	Trend	Correlation
	1900-2005		1985-2014	1900-2005
ACCESS1-0	6	9	17	18
ACCESS1-3	11	25	30	3
bcc-csm1-1	18	16	27	20
bcc-csm1-1-m	5	2	29	9
BNU-ESM	21	21	13	11
CanESM2	12	18	31	16
CCSM4	34	35	25	8
CESM1-BGC	29	29	24	2
CESM1-CAM5	15	7	18	4
CESM1-CAM5-1-FV2	20	8	32	28
CMCC-CESM	27	17	5	15
CMCC-CM	17	10	26	17
CMCC-CMS	22	12	12	1
CNRM-CM5	23	34	37	5
CSIRO-Mk3.6	24	23	14	19
FGOAL-g2	7	15	10	25
FGOAL-s2	25	33	3	21
GFDL-CM3	1	6	23	32
GFDL-ESM2G	3	13	35	13
GFDL-ESM2M	8	24	19	23
GISS-E2-H	36	37	36	37
GISS-E2-H-CC	33	36	33	29
GISS-E2-R	28	30	11	26
GISS-E2-R-CC	26	26	9	35
HadGEM2-CC	19	14	2	27
HadGEM2-ES	16	19	7	36
inmcm4	14	20	34	6
IPSL-CM5B-LR	9	28	22	34
MIROC5	31	31	21	24
MIROC-ESM	37	11	15	31
MIROC-ESM-CHEM	35	1	6	30
MPI-ESM-LR	13	22	1	10
MPI-ESM-MR	10	4	20	12
MRI-CGCM3	4	3	16	7
MRI-ESM1	2	5	4	33
NorESM1-M	32	32	8	22
NorESM1-ME	30	27	28	14

678 **Table 3***: Correlation coefficients computed across the 37 individual CMIP5 model quantities*
679 *(indicated in the two left columns) averaged over a period of time indicated in the third column and*
680 *for different seasons (columns 4 to 8). Correlation coefficients above 0.33 (0.42) are significant at the*
681 *95% (99%) level and are indicated in italics (bold). Numbers in brackets are obtained with some*
682 *individual models removed (see text for details).*
683

Correlated quantities:							
Variable 1	Variable 2	Period considered	Annual	JASON	AMJJASO	SON	DJF
Standard Deviation of SEA Rainfall	Standard deviation of Tropical Tripole	1900-2005	*0.38*	**0.44**	**0.44**	**0.46**	0.04
		1956-2005	**0.41**	**0.50**	**0.43**	**0.50**	0.09
		1985-2014	*0.36*	**0.56**	*0.40*	**0.58**	0.02
	Corr. Coef. Victoria rainfall vs. Tropical Tripole	1900-2005	*0.39*	*0.35*	**0.44**	0.25	0.07
		1956-2005	*0.39* **(0.60)**	**0.60 (0.77)**	**0.59 (0.67)**	**0.52 (0.60)**	-0.16 (-0.04)
		1985-2014	0.19	**0.43**	0.24	**0.52**	0.00
SEA Rainfall trends	Tropical Tripole trends	1900-2005	**0.49**	**0.52**	**0.58**	**0.54**	0.18
		1956-2005	0.14	0.27	*0.33*	0.29	-0.23
		1985-2014	**0.52**	*0.38*	**0.44**	0.31	*0.36*

684
685

686 **Table 4***: Projected rainfall changes (in %) for the last 20 years of the RCP8.5 simulations (2080-*
687 *2099) compared to the last 20 years of the historical simulations (1986-2005) for different seasons*
688 *(columns 3 to 7) showing all CMIP5 models together and separated in two groups, one being the*
689 *models with "very wet summers" in the simulations of the current climate and the "other" being the*
690 *remainder of the models.*
691

		Annual	JASON	AMJJASO	SON	DJF
Mean rainfall changes (percent)	All models	-8.4	-15.8	-12.1	-19.7	1.2
	Very wet summer models	-0.1	-6.1	-3.9	-5.6	5.7
	Other models	-14.1	-22.5	-17.7	-29.4	-1.8

692
693
694

695 **Table 5***: Correlation coefficients computed across the 37 individual CMIP5 model quantities*
696 *(indicated in the two left columns) averaged over a period of time indicated in the third column and*
697 *for different seasons (columns 4 to 8). Correlation coefficients significant at the 95% (99%) level are*
698 *indicated in italics (bold)). Numbers in brackets are obtained with some individual models removed*
699 *(see text for details).*

Correlated quantities							
Variable 1	Variable 2	Period considered	Annual	JASON	AMJJASO	SON	DJF
SEA Rainfall Trend	Tripole trend	2006-2099	**0.65 (0.63)**	**0.75 (0.78)**	**0.74 (0.77)**	**0.70 (0.72)**	0.23 (0.09)
	Global Warming	2006-2099	-0.30	-0.32	*-0.34*	-0.19	-0.07

700

List of Figures:

Figure 1: *Global map of mean Sea Surface Temperature linear trends from 1986 to 2014 (in °C) (top) with overlay the area used to construct the Tripole index, (central box minus the average of the other two boxes); also shown and enlarged in the lower panel is the State of Victoria and the model grid boxes considered to construct the South-Eastern Australia average rainfall time series with the red box showing the area considered when observations are used (values are from January 2006 from Access1.0).*

Figure 2:
Annual cycle of monthly mean (top) and standard deviation (bottom) of South-Eastern Australia rainfall (in mm) averaged from 1900 to 2005 for the observations (BoM operational 0.05 degree gridded rainfall), the ensemble mean of the 37 CMIP5 models considered; a selection of the 10 "best" and "worst" CMIP5 GCMs (defined using Euclidean distance), and all individual models. NB: on the top diagram "Victoria only" observed rainfall show the observed rainfall when only gridded data within the boundary of the State of Victoria are used in contrast with SEA rainfall which cover a wider box (displayed in Figure 1b).

Figure 3:
R*elationship between each model's DJF (austral summer) mean rainfall and its year-to-year variability (top panel), computed using values from 1900 to 2005 across the 37 CMIP5 models (the ensemble mean is shown with a red symbol and the observations with a black symbol), lines of best fit and explained variance are displayed. The bottom panel shows the relationship with the coefficient of variation.*

F**igure 4**: *Maps of global DJF (austral summer) rainfall climatologies (top row) from the 2 groups of CMIP5 models ("very wet summer" on the left, "other" on the right) in mm.day^{-1} and anomalies from the CMAP climatology averaged from 1980-2005 period (bottom row also in mm.day^{-1}).* N.B. scales differ between top and bottom rows.

Figure 5: *Annual cycle of linear trends of SEA rainfall (in mm) from 1985 to 2014, for the observations (BoM operational 0.05 degree gridded rainfall), the ensemble mean of the 37 CMIP5 models considered, a selection of the 10 "best" models (defined using Euclidean distance from the black line), all individual models, including the model identified as the closest to the observations (green line). N.B: for the CMIP5 simulations, the historical simulations are used until 2005 and the simulations forced with the RCP 8.5 concentration pathways from 2006.*

Figure 6: *Annual cycle of the tropical Tripole index mean (top) and year to year variability (standard deviation, bottom) computed from 1900 to 2005 for the observations (HadISST dataset), the ensemble mean of the 37 CMIP5 models considered; a selection of the 10 "best" and "worst" models (defined using Euclidean distance) and all individual model.*

Figure 7: *Annual cycle of linear trends of the tropical Tripole index (in degree Celsius per 30 years) from 1985 to 2014, for the observations (HadISST dataset), the ensemble mean of the 37 CMIP5 models considered, a selection of the 10 "best" and "worst" models (defined using Euclidean distance) and all individual models.*

Figure 8: *Annual cycle of the correlation coefficients between the tropical Tripole index and SEA rainfall, computed form 1900 to 2005: for the observations, the ensemble mean of the 37 CMIP5 models considered; a selection of the 10 "best" and "worst" models (defined using Euclidean distance) and all individual models. Correlations above the dashed line are significant at the 95% confidence level.*

Figure 9: Correlation coefficients between July to November mean Tripole index and SEA rainfall computed on 50-year periods for the observations (past climate only), the ensemble mean of the 37 CMIP5 models considered and the individual models.

Figure 10: *Scatter plots across metrics computed for 37 individual CMIP5 models: standard deviation of July to November of SEA rainfall versus tropical Tripole index (top panel) and standard deviation of July to November SEA rainfall versus the strength of the SEA rainfall-Tripole relationship (lower panel). All quantities are computed on the last 50 years of the current climate simulations (1956-2005). In all panels, the ensemble mean is shown with a red symbol and the observations with a black symbol, models with very wet summer are identified as green symbols; lines of best fit and square correlation for the whole ensemble are displayed. The four models from the GISS family are outlined by a red box.*

Figure 11: *Maps of global surface temperature change (in °C, annual mean) from the 2 groups of CMIP5 models ("very wet summer" on the left, other on the right). Anomalies are computed between the last 30 years of the 21st century (RCP 8.5) and 20th century (historical) simulations***.** *Bottom panel shows the annual cycles of the mean monthly trends in Tripole index computed from 2006 to 2099: for the ensemble mean of the 37 CMIP5 models considered and the individual model; ensemble mean of the 15 models with "very wet summer" as well as the ensemble mean of the other 22 models are identified.*

Figure 12: Annual cycle of the *projected rainfall trends in mm over 2006-2099 for the entire South-Eastern Australia box following the RCP8.5 pathway for the ensemble mean of the 37 CMIP5 models considered and individual models (top panel); comparison between various sub-regions across SEA (lower panels): (top left, continental point within the red rectangular in the top right map) and for three Victorian sub-region (South-West, bottom left, Murray basin side of Victoria, bottom middle panel, and South-East Victoria, bottom right panel). Rainfall anomalies are given in per cent with respect to the 1986-2005 mean, for the four calendar seasons, under RCP 2.6 (green), RCP 4.5 (blue) and RCP 8.5 (purple) for 2090. Natural climate variability is represented by the grey bars. For each bar plot, the box shows the median, 10th and 90th percentiles of the 20-year average while line segments indicates changes in the 20-year average of the 10th and 90th percentile, as calculated from individual years.*

Figure 13: *Maps of Pacific/Indian region change in precipitation (%) in DJF (austral summer: top row) and JJA (austral winter: bottom row) from the 2 groups of CMIP5 models (very wet summer models on the left, other models on the right). Anomalies are computed between the last 30 years of the 21st century (RCP 8.5) and 20th century (historical) simulations.*

Figure 14: *Scatter plots across metrics computed for 37 individual CMIP5 models: trends in July to November SEA rainfall from 2006 to 2099 using the RCP8.5 pathway versus the tropical Tripole index for the same seasons (top panel); same quantities for the austral summer (DJF: lower panel). In all panels, the ensemble mean is shown with a red symbol and models with very wet summer are shown as green symbols, lines of best fit and square correlation are displayed.*

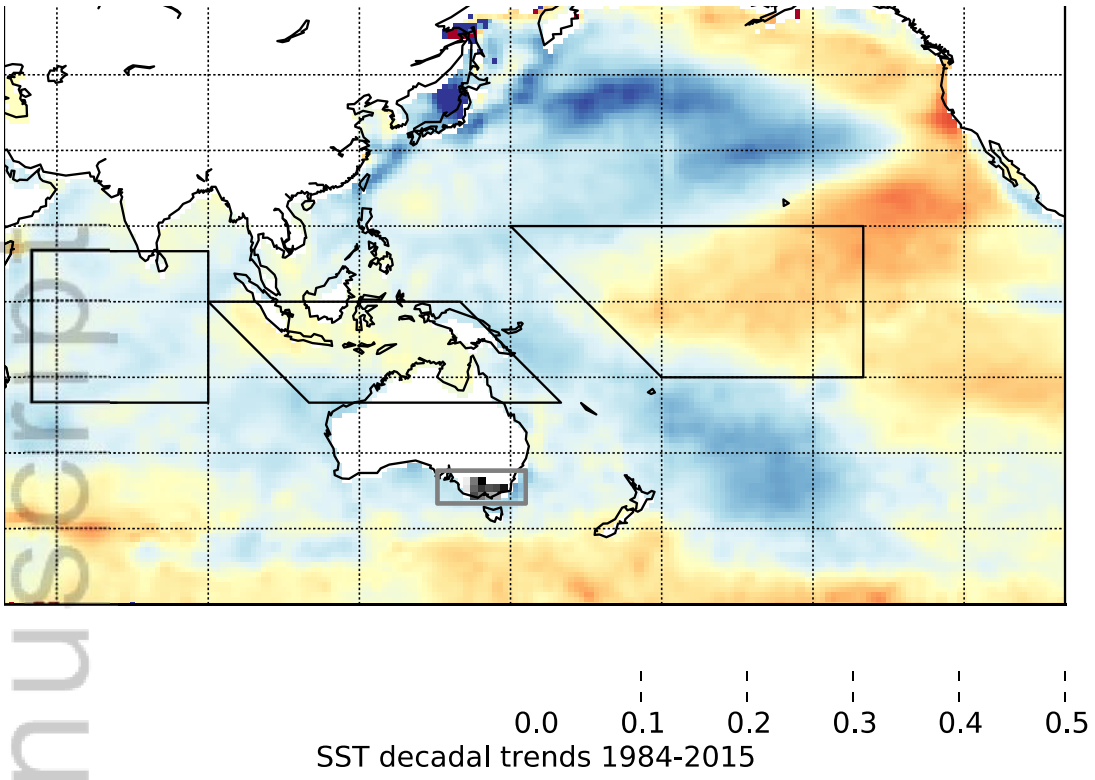

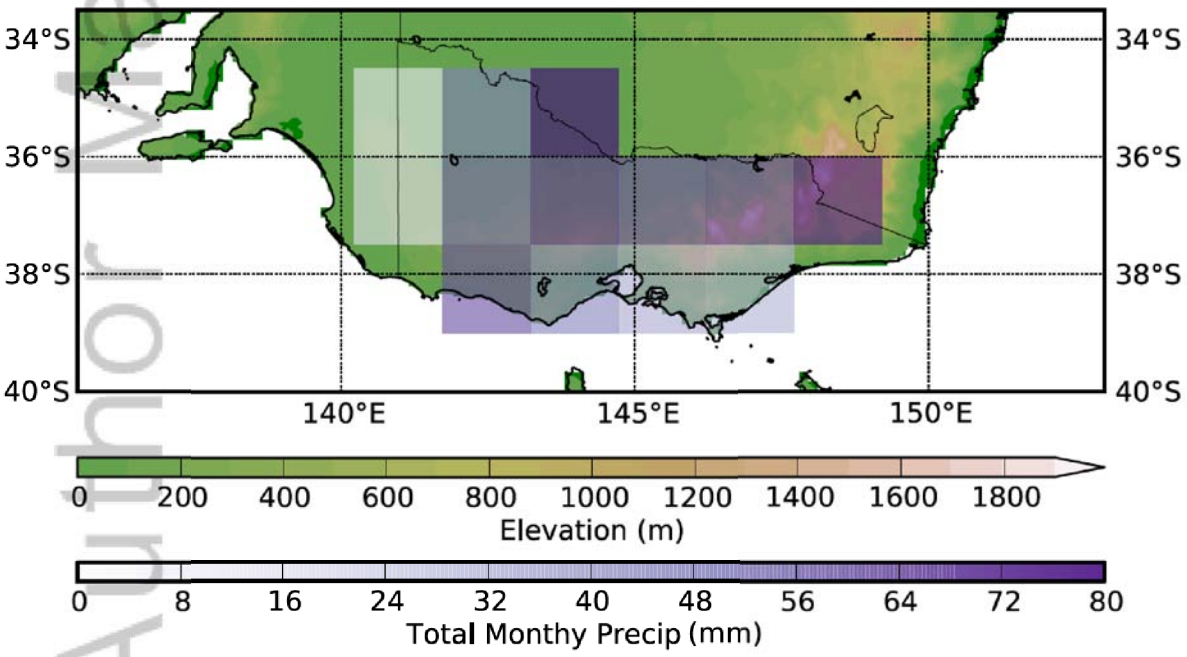

Figure 1: *Global map of mean Sea Surface Temperature linear trends from 1986 to 2014 (in °C) (top) with overlay the area used to construct the Tripole index, (central box minus the average of the other two boxes); also shown by the grey box and enlarged in the lower panel is the area considered as South-East Australia used to define observed rainfall and the model grid boxes considered to construct the South-Eastern Australia average rainfall. The topography of South East Australia is also shown in the lower panel.*

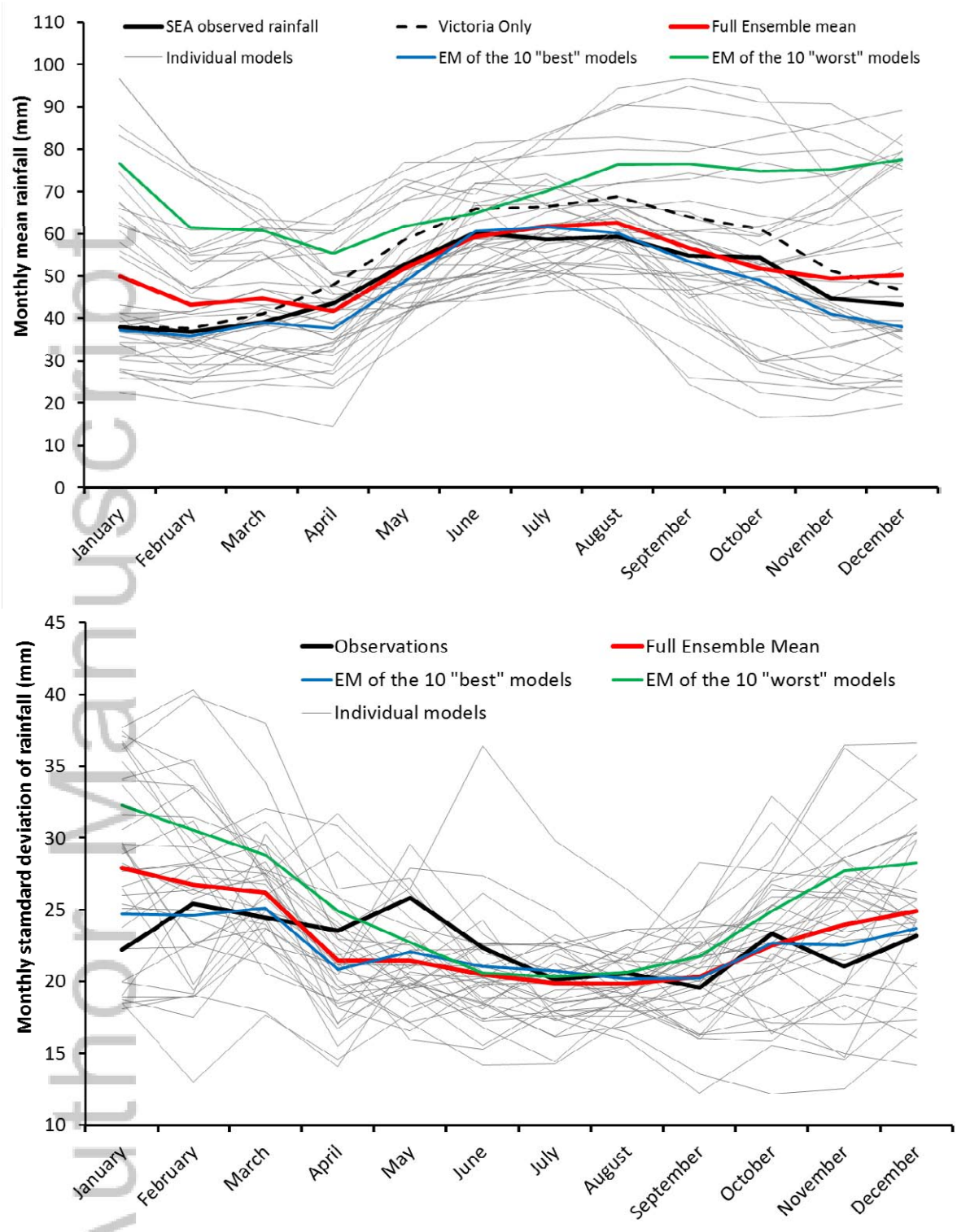

Figure 2: *Annual cycle of monthly mean (top) and standard deviation (bottom) of South-Eastern Australia rainfall (in mm) averaged from 1900 to 2005 for the observations (BoM operational 0.05 degree gridded rainfall), the ensemble mean of the 37 CMIP5 models considered; a selection of the 10 "best" and "worst" CMIP5 GCMs (defined using Euclidean distance), and all individual models. NB: on the top diagram "Victoria only" observed rainfall show the observed rainfall when only gridded data within the boundary of the State of Victoria are used in contrast with SEA rainfall which cover a wider box (displayed in Figure 1b).*

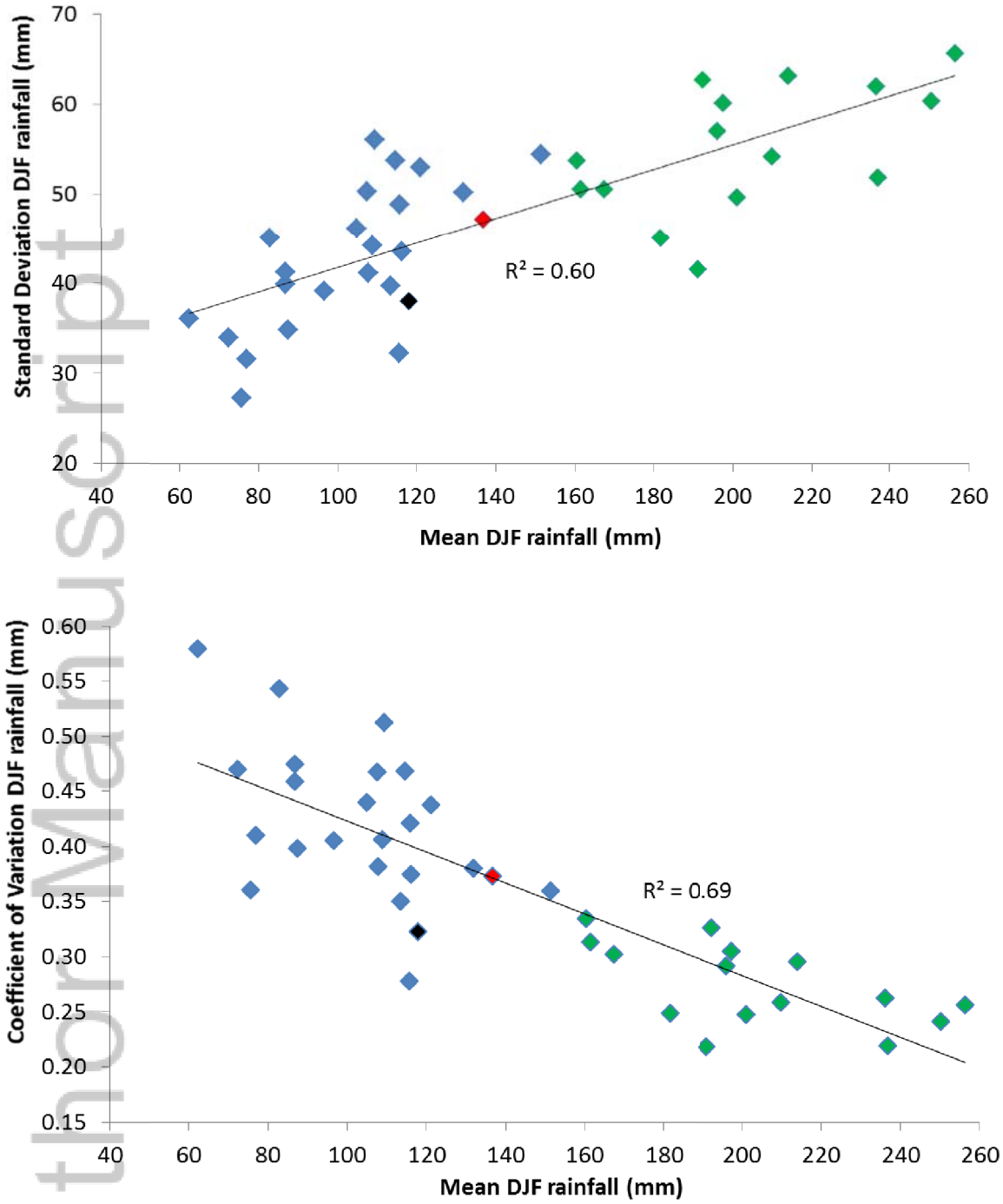

Figure 3: *Relationship between each model's DJF (austral summer) mean rainfall and its year-to-year variability (top panel), computed using values from 1900 to 2005 across the 37 CMIP5 models (the ensemble mean is shown with a red symbol and the observations with a black symbol), lines of best fit and explained variance are displayed. The bottom panel shows the relationship with the coefficient of variation.*

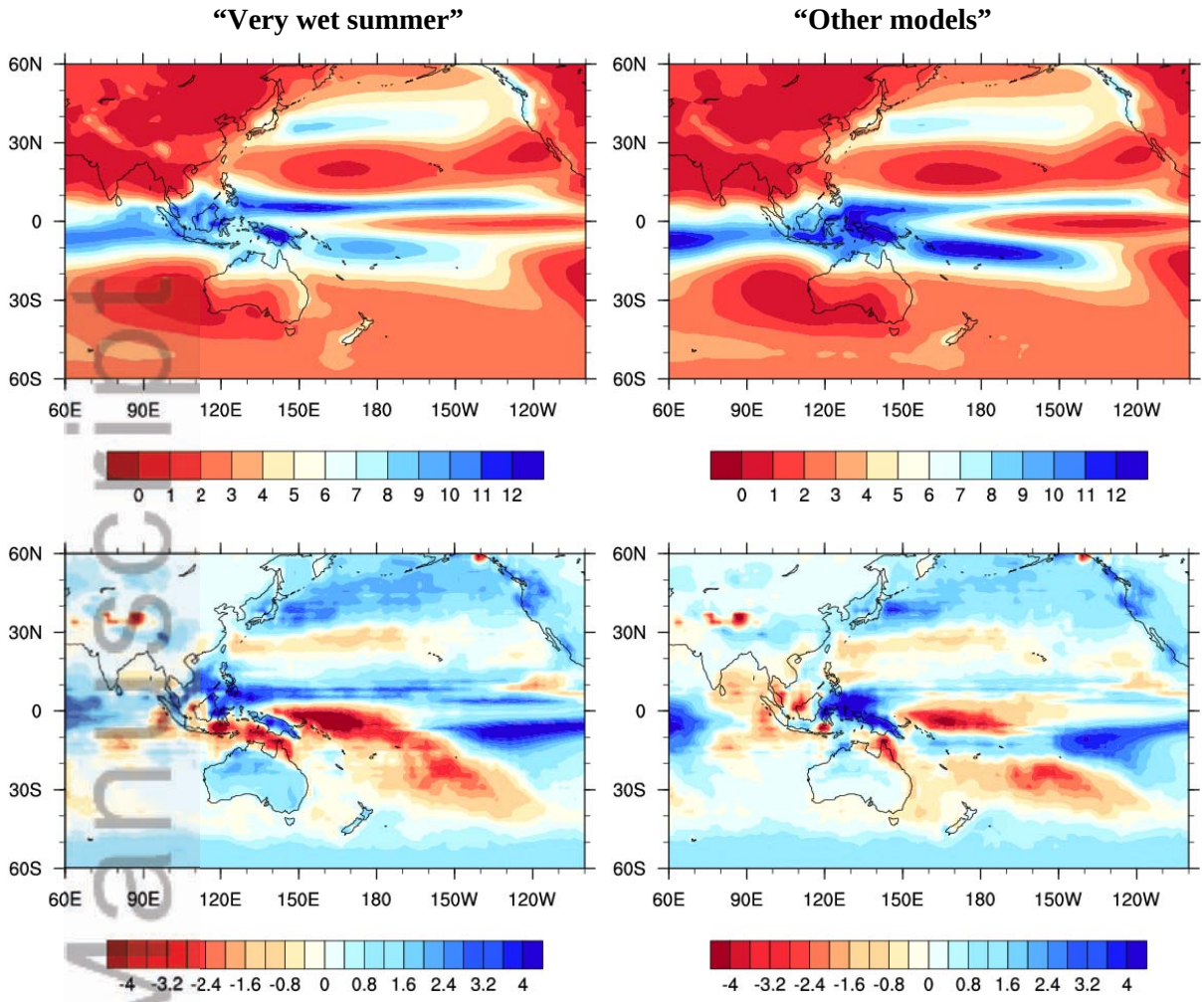

Figure 4: *Maps of global DJF (austral summer) rainfall climatologies (top row) from the 2 groups of CMIP5 models ("very wet summer" on the left, "other" on the right) in mm.day^{-1} and anomalies from the CMAP climatology averaged from 1980-2005 period (bottom row also in mm.day^{-1}).* N.B. scales differ between top and bottom rows.

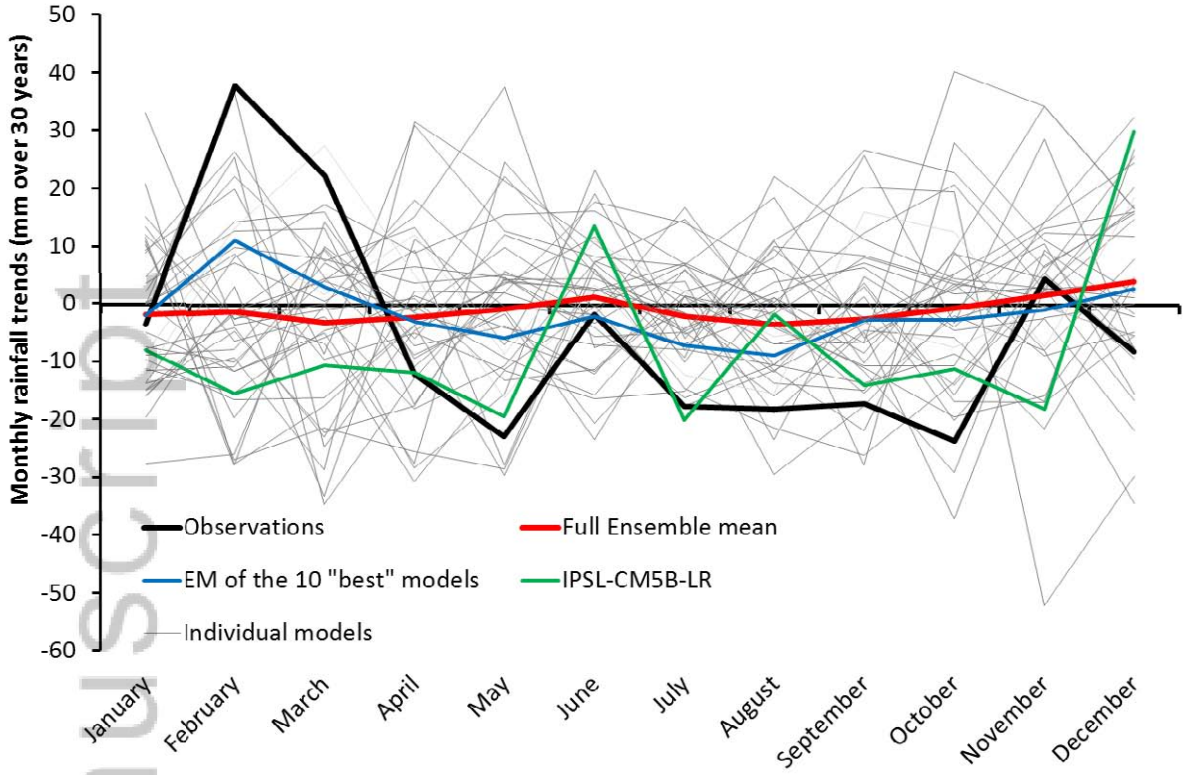

Figure 5: *Annual cycle of linear trends of SEA rainfall (in mm) from 1985 to 2014, for the observations (BoM operational 0.05 degree gridded rainfall), the ensemble mean of the 37 CMIP5 models considered, a selection of the 10 "best" models (defined using Euclidean distance from the black line), all individual models, including the model identified as the closest to the observations (green line). N.B: for the CMIP5 simulations, the historical simulations are used until 2005 and the simulations forced with the RCP 8.5 concentration pathways from 2006.*

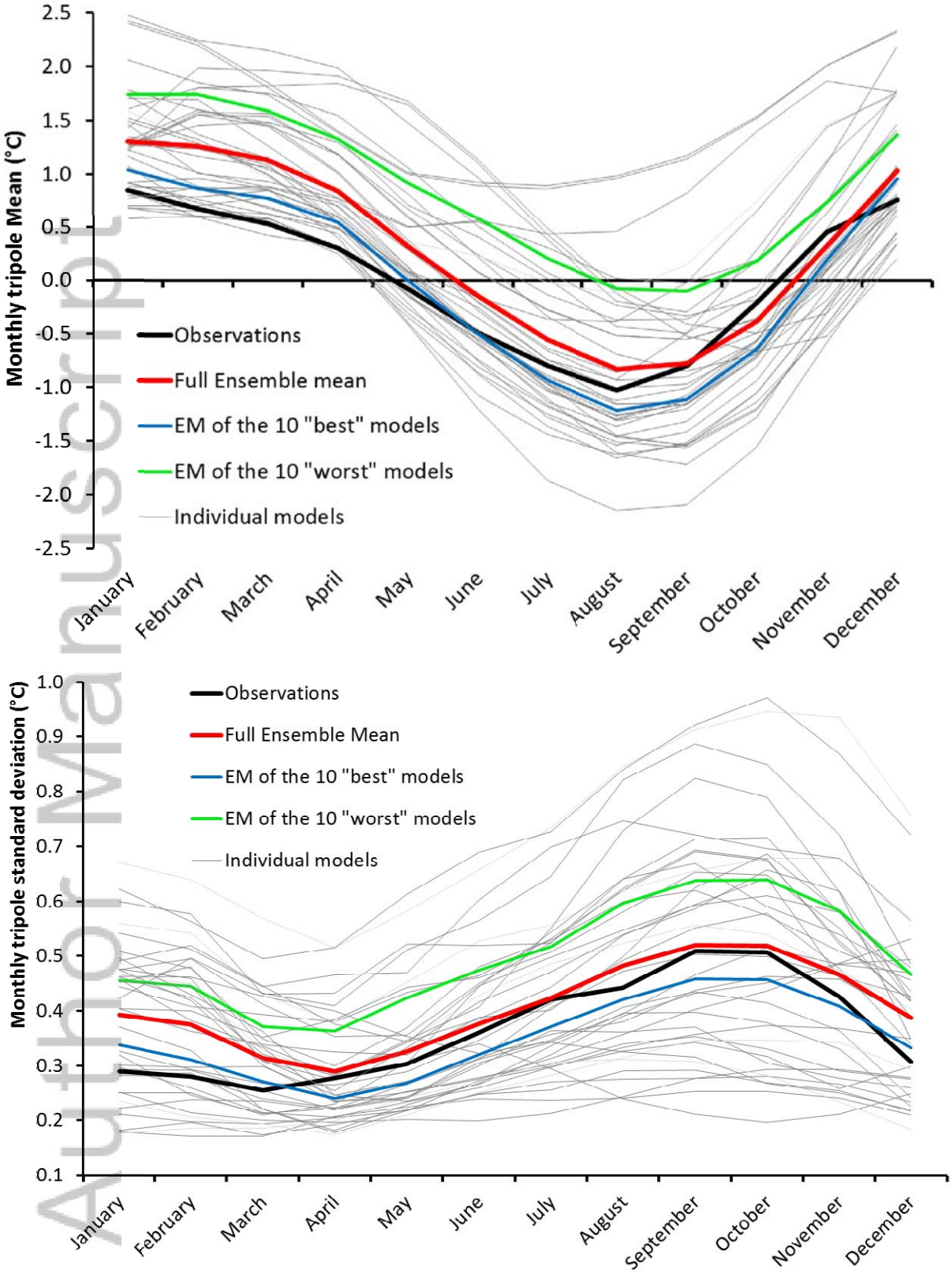

Figure 6: *Annual cycle of the tropical Tripole index mean (top) and year to year variability (standard deviation, bottom) computed from 1900 to 2005 for the observations (HadISST dataset), the ensemble mean of the 37 CMIP5 models considered; a selection of the 10 "best" and "worst" models (defined using Euclidean distance) and all individual model.*

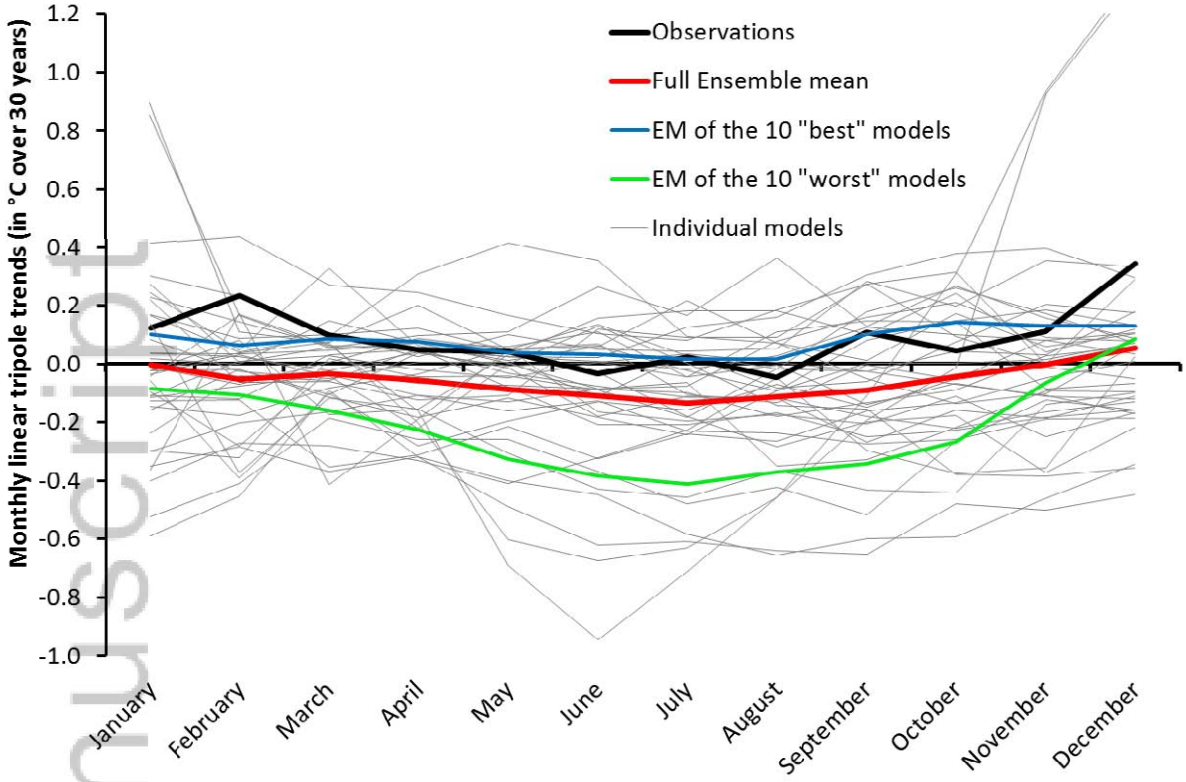

Figure 7: *Annual cycle of linear trends of the tropical Tripole index (in degree Celsius per 30 years) from 1985 to 2014, for the observations (HadISST dataset), the ensemble mean of the 37 CMIP5 models considered, a selection of the 10 "best" and "worst" models (defined using Euclidean distance) and all individual models.*

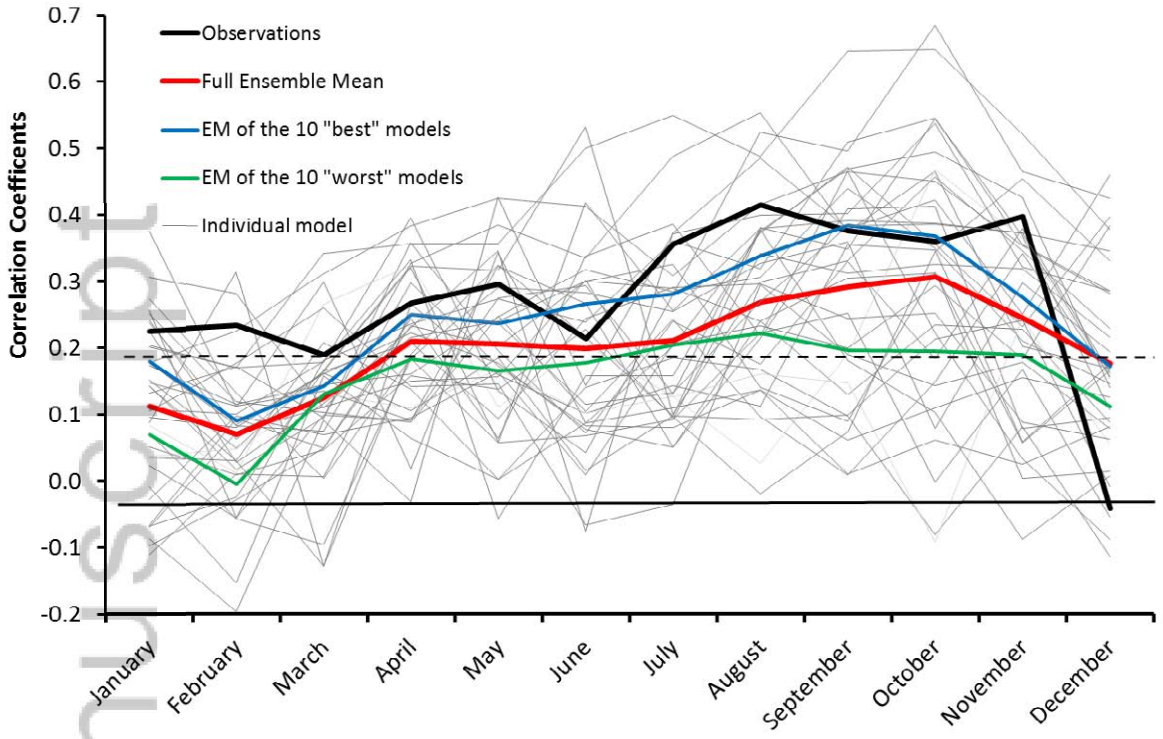

Figure 8: *Annual cycle of the correlation coefficients between the tropical Tripole index and SEA rainfall, computed form 1900 to 2005: for the observations, the ensemble mean of the 37 CMIP5 models considered; a selection of the 10 "best" and "worst" models (defined using Euclidean distance) and all individual models. Correlation above the dashed line are significant at the 95% confidence level.*

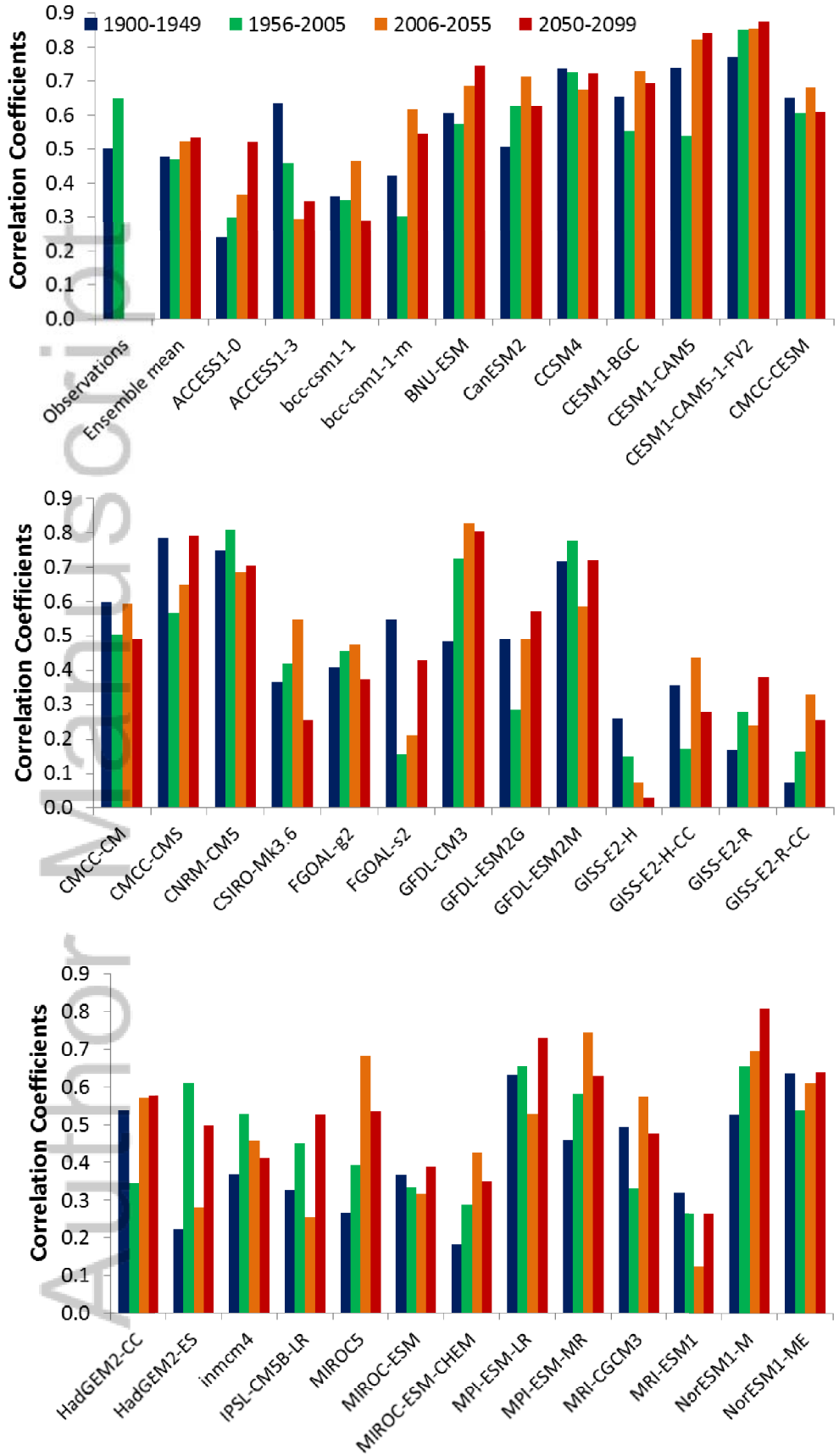

Figure 9: Correlation coefficients between July to November mean Tripole index and SEA rainfall computed on 50-year periods for the observations (past climate only), the ensemble mean of the 37 CMIP5 models considered and the individual models.

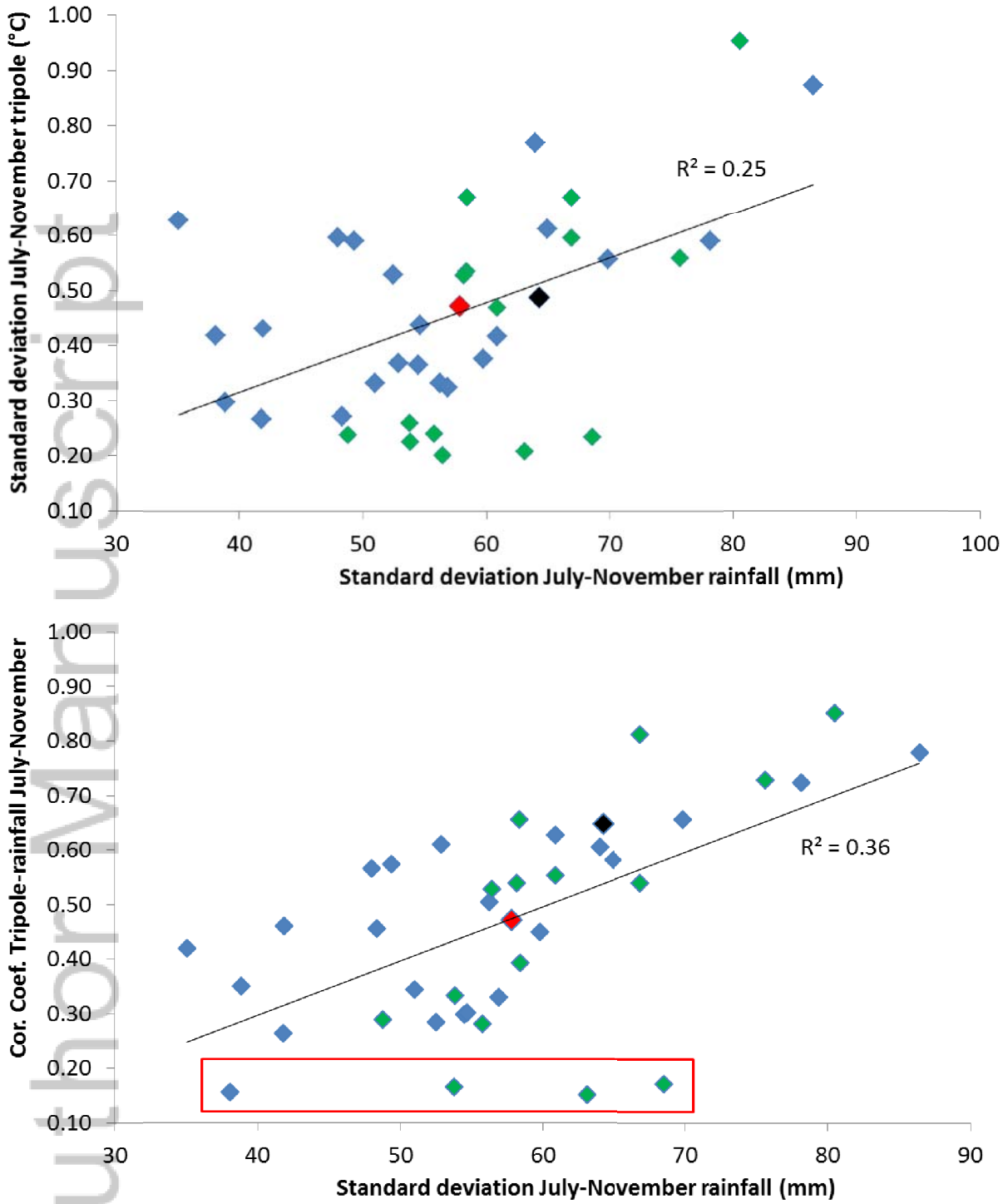

Figure 10: *Scatter plots across metrics computed for 37 individual CMIP5 models: standard deviation of July to November of SEA rainfall versus tropical Tripole index (top panel) and standard deviation of July to November SEA rainfall versus the strength of the SEA rainfall-Tripole relationship (lower panel). All quantities are computed on the last 50 years of the current climate simulations (1956-2005). In all panels, the ensemble mean is shown with a red symbol and the observations with a black symbol, models with very wet summer are identified as green symbols; lines of best fit and square correlation for the whole ensemble are displayed. The four models from the GISS family are outlined by a red box.*

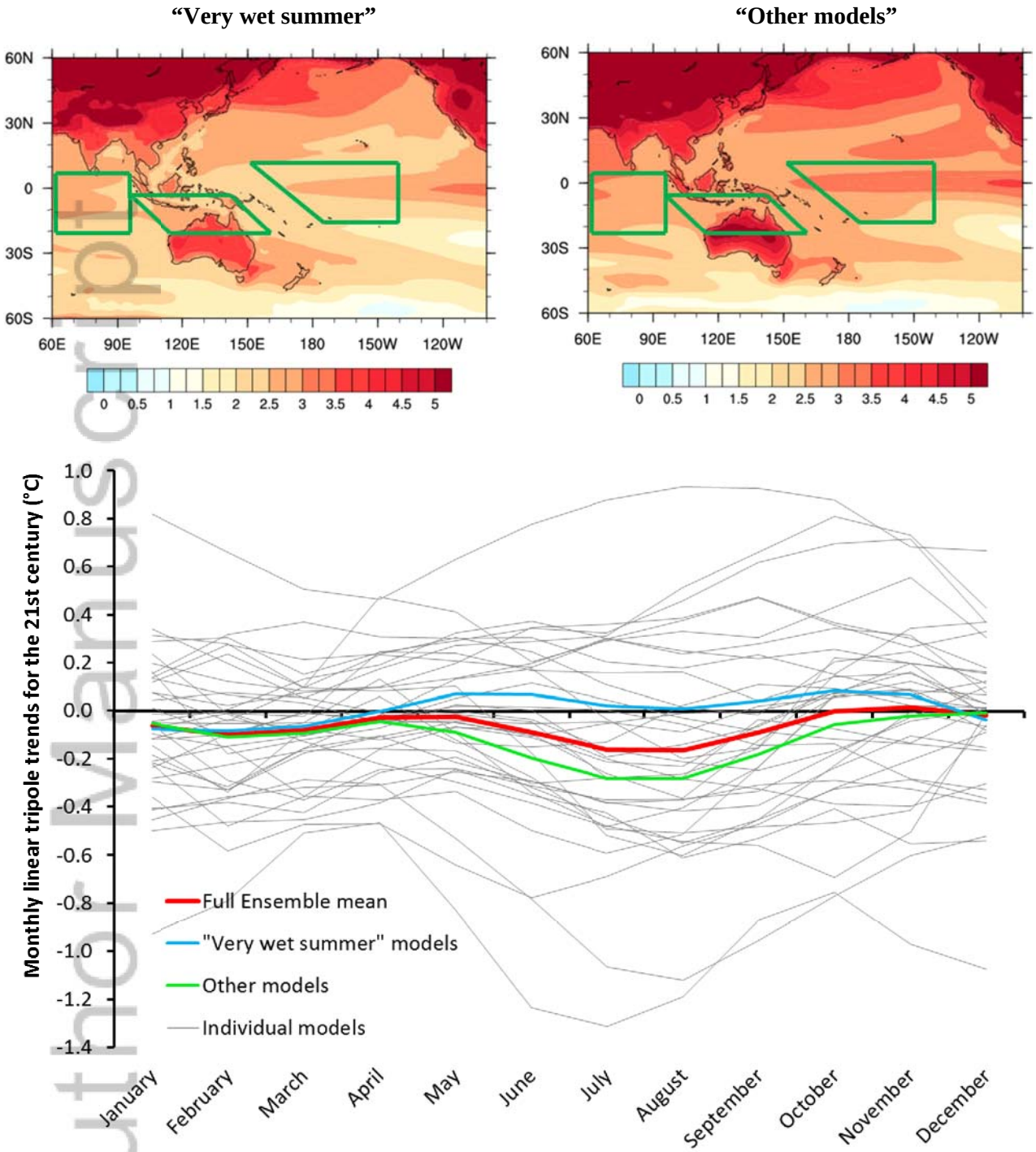

Figure 11: *Maps of global surface temperature change (in °C, annual mean) from the 2 groups of CMIP5 models ("very wet summer" on the left, other on the right). Anomalies are computed between the last 30 years of the 21st century (RCP 8.5) and 20th century (historical) simulations. Bottom panel shows the annual cycles of the mean monthly trends in Tripole index computed from 2006 to 2099: for the ensemble mean of the 37 CMIP5 models considered and the individual model; ensemble mean of the 15 models with "very wet summer" as well as the ensemble mean of the other 22 models are identified.*

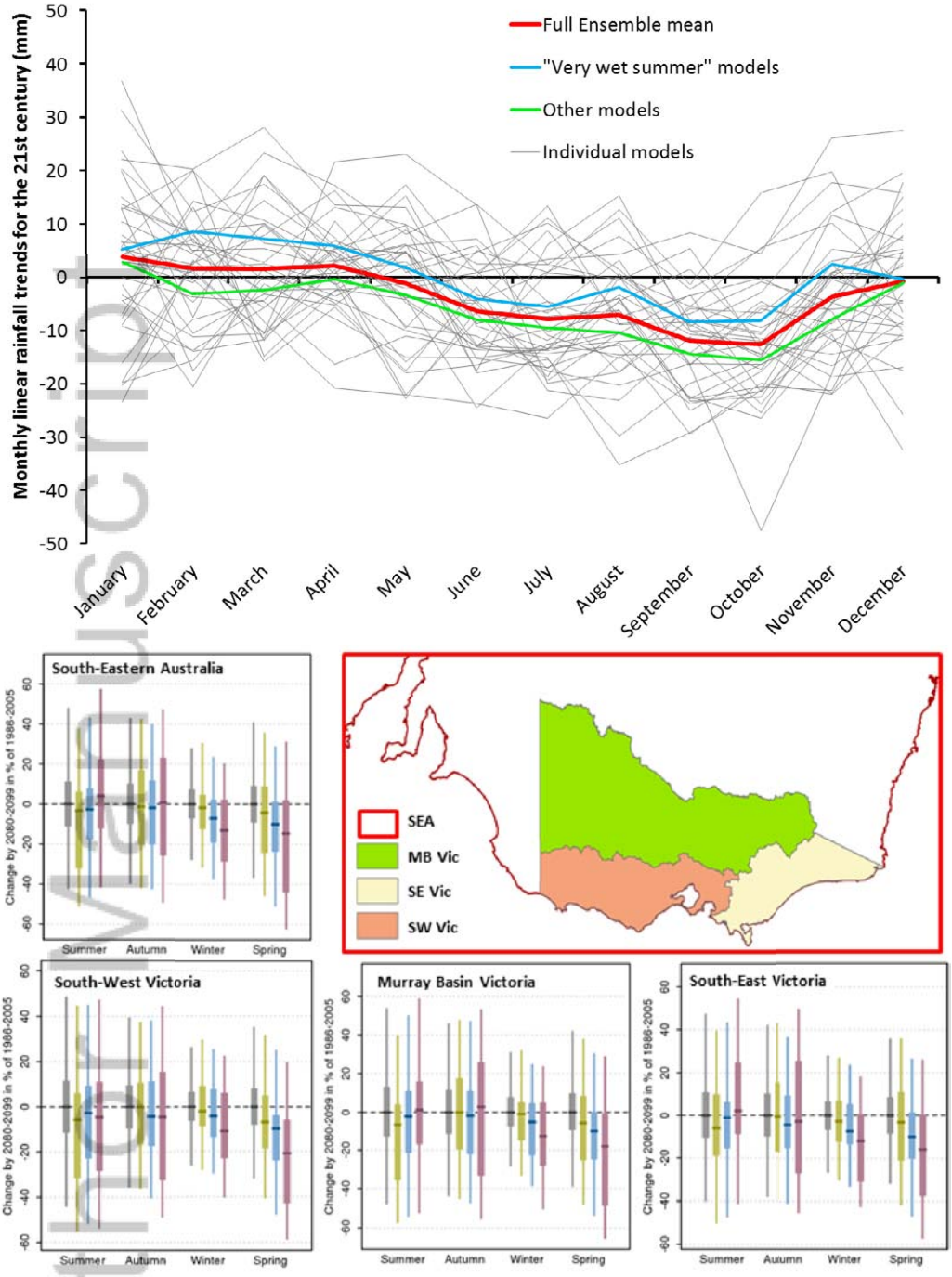

Figure 12: Annual cycle of the *projected rainfall trends in mm over 2006-2099 for the entire South-Eastern Australia box following the RCP8.5 pathway for the ensemble mean of the 37 CMIP5 models considered and individual models (top panel); comparison between various sub-regions across SEA (lower panels): (top left, continental point within the red rectangular in the top right map) and for three Victorian sub-region (South-West, bottom left, Murray basin side of Victoria, bottom middle panel, and South-East Victoria, bottom right panel). Rainfall anomalies are given in per cent with respect to the 1986-2005 mean, for the four calendar seasons, under RCP 2.6 (green), RCP 4.5 (blue) and RCP 8.5 (purple) for 2090. Natural climate variability is represented by the grey bars. For each bar plot, the box shows the median, 10th and 90th percentiles of the 20-year average while line segments indicates changes in the 20-year average of the 10th and 90th percentile, as calculated from individual years.*

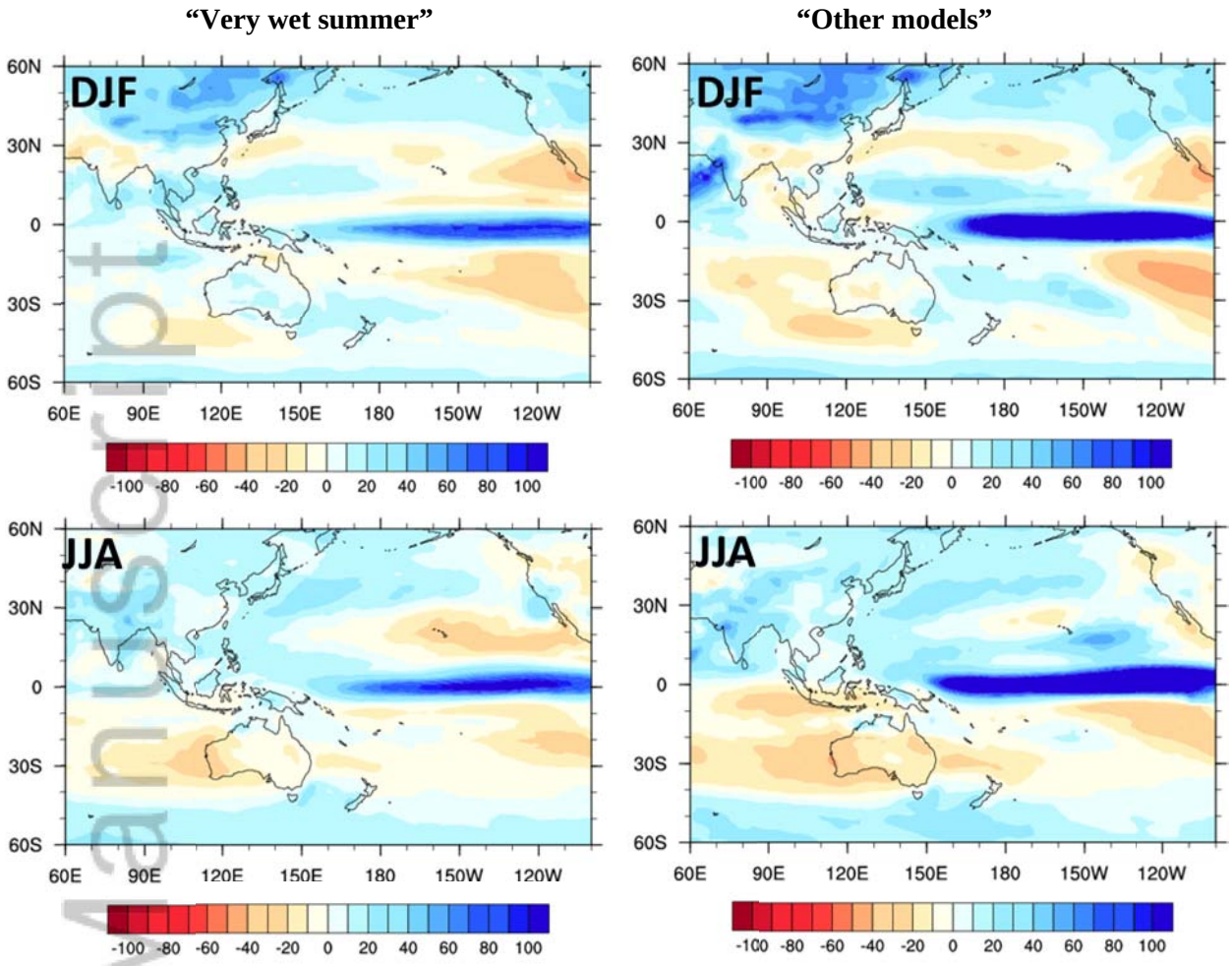

Figure 13: *Maps of Pacific/Indian region change in precipitation (%) in DJF (austral summer: top row) and JJA (austral winter: bottom row) from the 2 groups of CMIP5 models (very wet summer models on the left, other models on the right). Anomalies are computed between the last 30 years of the 21st century (RCP 8.5) and 20th century (historical) simulations.*

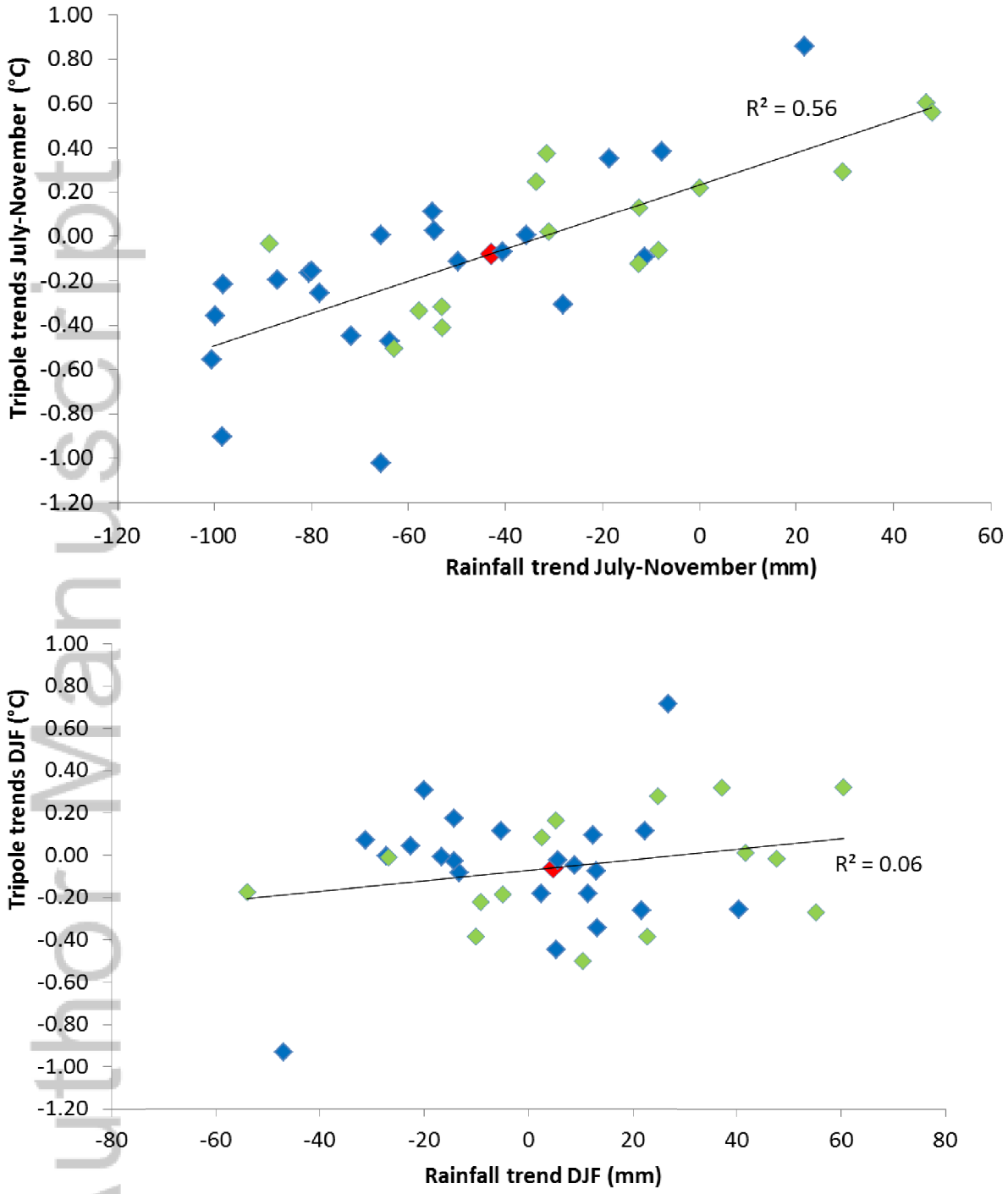

Figure 14: *Scatter plots across metrics computed for 37 individual CMIP5 models: trends in July to November SEA rainfall from 2006 to 2099 using the RCP8.5 pathway versus the tropical Tripole index for the same seasons (top panel); same quantities for the austral summer (DJF: lower panel). In all panels, the ensemble mean is shown with a red symbol and models with very wet summer are shown as green symbols, lines of best fit and square correlation are displayed.*